Structural and biochemical investigations of the late enzymes of (bacterio)chlorophyll *a* biosynthesis

Von der Fakultät für Lebenswissenschaften

der Technischen Universität Carolo-Wilhelmina

zu Braunschweig

zur Erlangung des Grades einer

Doktorin der Naturwissenschaften

(Dr. rer. nat.)

genehmigte

D i s s e r t a t i o n

von Christiane Violeta Lange
aus Kassel

1. Referent: Prof. Dr. Dieter Jahn
2. Referent: Prof. Dr. Wulf Blankenfeldt
eingereicht am: 16.11.2015
mündliche Prüfung (Disputation) am: 18.02.2016

Druckjahr 2016

Vorveröffentlichungen der Dissertation

Teilergebnisse aus dieser Arbeit wurden mit Genehmigung der Fakultät für Lebenswissenschaften, vertreten durch den Mentor der Arbeit, in folgenden Beiträgen vorab veröffentlicht:

Publikationen

Moser, J., Lange, C., Krausze, J., Rebelein, J., Schubert, W.-D., Ribbe, M. W., Heinz, D. W. & Jahn, D. Structure of ADP-aluminium fluoride-stabilized protochlorophyllide oxidoreductase complex. Proc. Natl. Acad. Sci. U.S.A. 110: 2094–2098 (2013).

Lange, C., Kiesel, S., Peters, S., Virus, S., Scheer, H., Jahn, D. & Moser, J. Broadened substrate specificity of 3-hydroxyethyl bacteriochlorophyllide *a* dehydrogenase (BchC) indicates a new route for the biosynthesis of bacteriochlorophyll *a*. J. Biol. Chem. 290: 19697–19709 (2015).

Tagungsbeiträge

Lange, C., Krausze, J., Rebelein, J., Schubert, W.-D., Ribbe, M. W., Heinz, D. W., Moser, J. & Jahn, D.: Biosynthesis of chlorophylls: Three-dimensional structure of ADP•AlF_3-stabilized protochlorophyllide oxidoreductase complex. (Vortrag) VAAM Jahrestagung, Bremen (2013).

Lange, C., Peters, S., Virus, S., Jahn, D. & Moser, J.: Late enzymatic steps of bacteriochlorophyll *a* biosynthesis. (Vortrag) Tetrapyrrole Discussion Group Meeting, University of Kent, Canterbury, UK (2013).

Table of contents

Abbreviations

A_{260}	absorption at 260 nm
AMPPCP	adenosine-5'(βγ-methylene)-triphosphate
AP	alkaline phosphatase
A-PGS	alanyl-phosphatidylglycerol synthase
Ap^r	ampicillin resistance
BChl	bacteriochlorophyll
3^1-OH-BChl *a*	3-Hydroxyethyl-bacteriochlorophyll *a*
BChlide	bacteriochlorophyllide *a*
BCIP	5-Bromo-4-chloro-3-indolyl phosphate
BLAST	basic local alignment search tool
BPheide	bacteriopheophorbide
3^1-OH-BPheide *a*	3-Hydroxyethyl-bacteriopheophorbide *a*
CD	circular dichroism
Chl	chlorophyll
Chlide	chlorophyllide *a*
3^1-OH-Chlide	3-Hydroxyethyl-chlorophyllide *a*
Cm^r	chloramphenicol resistance
COR	chlorophyllide *a* oxidoreductase
CV	column volume(s)
dH_2O	deionized water
DMSO	dimethyl sulfoxide
dNTP	desoxynucleoside triphosphate
DPOR	dark-operative protochlorophyllide *a* oxidoreductase
DTT	1,4-dithiothreitol
EDTA	ethylenediaminetetraacetic acid
EGTA	ethyleneglycol bis(2-aminoethylether)-N,N,N′,N′-tetraacetic acid
EPR	electron paramagnetic resonance
et al.	lat. *et alteri* (and others)
Far	farnesyl
GST	glutathione S-transferase
HEPES	N-2-hydroxyethyl piperazine-N'-2-ethane sulfonic acid
HMM	Hidden Markov Model
HPLC	high performance liquid chromatography
ICP-MS	inductively coupled plasma mass spectrometry
IPTG	isopropyl *β*-D-thiogalactopyranoside
Km^r	kanamycin resistance
LB	Luria Bertani
LPOR	light-dependent protochlorophyllide *a* oxidoreductase
LTB_4 12-HD/PGR	leukotriene B_4 12-hydroxydehydrogenase/15-oxo-prostaglandin 13-reductase
MCS	multiple cloning site
MDR	medium-chain dehydrogenase/reductase
MPE	Mg-protoporphyrin IX monomethyl ester
NBT	Nitro blue tetrazolium
NMR	nuclear magnetic resonance
NMWL	nominal molecular weight limit
OD_{578}	optical density at 578 nm
orf	open reading frame
PAGE	polyacrylamide gelelectrophoresis
PBS	phosphate-buffered saline
Pchlide	protochlorophyllide *a*

PDB	protein data bank, maintained by the Research Collaboratory for Structural Bioinformatics
PDB ID	protein data bank identifier
Pd-BPheide *a*	Palladium-bacteriopheophorbide *a*
Pheide	pheophorbide
Phy	phytyl
PISA	Proteins, Interfaces, Structures and Assemblies
ppm	parts per million
PS	photosystem
p.s.i.	pounds per square inch
PVDF	polyvinylidene difluoride
rmsd	root mean square deviation
RT	room temperature
SDS	sodium dodecyl sulfate
SDT	sodium dithionite
Tris	Tris(hydroxymethyl)-aminomethane
U	units
v/v	volume per volume
w/v	weight per volume
Zn-3-acetyl-Pheide *a*	Zinc-3-acetyl-pheophorbide *a*
Zn-BPheide *a*	Zinc-bacteriopheophorbide *a*
Zn-3^1-13^2-di-OH-Pheide *a*	Zinc-3^1-13^2-di-hydroxy-pheophorbide *a*

Glossary

FeMoco	The complex [Mo-7Fe-9S-C]-homocitrate metallocluster bound to the nitrogenase NifD subunit.
3^1-OH	Abbreviation for the 3-[(1-hydroxy)-ethyl] substituent of (bacterio)chlorophyll derivatives. It is also often referred to as 3-hydroxyethyl in the present literature.
λ_{Em}	Emission wavelength
λ_{Ex}	Excitation wavelength
P cluster	The [8Fe-7S] cluster ligated by the nitrogenase NifD and NifK subunits.
P-loop	The phosphate binding loop which is conserved in a variety of nucleotide-binding proteins
Q_x	Designation of the additional absorption peak of bacteriochlorins in the visible light region (blue-shifted relative to the Q_y peak).
Q_y	Designation of the red-most absorption peak of (bacterio)chlorophylls and their derivatives.

1 Introduction

1.1 Photosynthesis

Photosynthesis is the process in which light energy is converted into chemical energy. Photons are absorbed by light-harvesting structures within the cells, and the energy is used to drive an electron transport chain, generating redox equivalents and forming an electrochemical potential across a membrane for the synthesis of ATP. Moreover, photoautotrophic organisms have the ability to fix carbon dioxide (Blankenship, 2014).

Photosynthesis can be found among eukaryotes (e.g. higher plants and algae) and prokaryotes (bacteria). Six bacterial phyla comprise phototrophic species, which can be divided into purple bacteria (phylum *Proteobacteria*), green sulfur bacteria (*Chlorobi*), heliobacteria (*Firmicutes*), filamentous anoxygenic phototrophs (*Chloroflexi*), chloroacidobacteria (*Acidobacteria*) and cyanobacteria (Blankenship, 2014; Bryant and Frigaard, 2006). They all rely on the presence of light-absorbing pigments, the chlorophylls (Chls) or bacteriochlorophylls (BChls). The (bacterio)chlorophyll molecules are located in light-harvesting antenna complexes and the photosynthetic reaction center. The antenna pigments capture most of the light energy and transfer it to the reaction centers, where distinct pigment molecules are excited and subsequently oxidized.

In eukaryotic phototrophs and *Cyanobacteria*, the sites of the photochemical reactions, Photosystems I and II (PSI and II), are located in the thylakoid membrane of the chloroplasts or the inner bacterial membrane, respectively, and contain numerous chlorophyll molecules (Barber, 2002; Blankenship, 2014; Croce and van Amerongen, 2013). PSII has the ability to oxidize water, so that molecular oxygen is formed (oxygenic photosynthesis). Electrons are transferred *via* an electron transport chain from PSII to PSI, where $NADP^+$ is reduced. In phototrophic bacteria other than cyanobacteria, BChls are the major photosynthetic pigments and anoxygenic photosynthesis is performed, which does not lead to the formation of oxygen. These organisms possess a single

reaction center located in the inner bacterial membrane. Best studied is the reaction center of purple bacteria. Under photosynthetic conditions, a cyclic electron transport pathway leads to the formation of a transmembrane electrochemical potential (Blankenship, 2014). The formation of redox equivalents is indirectly coupled to this gradient. In photoautotrophic organisms, the fixation of carbon dioxide occurs *via* the Calvin cycle, the reverse tricarboxylic acid cycle (*Chlorobi*) or the 3-hydroxypropionate cycle (*Chloroflexi*) (Blankenship, 2014; Overmann and Garcia-Pichel, 2006).

1.2 Photosynthetic organisms

In this study, enzymes from members of the phyla *Cyanobacteria* and *Chlorobi* have been investigated.

1.2.1 *Cyanobacteria*

Cyanobacteria are almost exclusively photoautotrophs, performing oxygenic photosynthesis and inhabiting freshwater, marine and terrestrial environments (Blankenship, 2014). Although *Cyanobacteria* usually contain Chl *a*, a subgroup called prochlorophytes shows the presence of Chl *b* as light-harvesting pigment in addition to Chl *a* (Scheer, 2006). The genus *Prochlorococcus* is an exception within the prochlorophytes because its members contain the unique pigments divinyl Chl *a* and divinyl Chl *b* and synthesize only a single phycobiliprotein (Partensky *et al.,* 1999; Wiethaus *et al.,* 2010). Other members of the *Cyanobacteria* contain Chls *d* and *f* (Chen, 2014; Chen *et al.,* 2010).

1.2.2 Green sulfur bacteria (*Chlorobi*)

The members of the green sulfur bacteria are obligate anaerobic photoautotrophs and occur e.g. in the anaerobic zone at the bottom of lakes or hot springs (Blankenship, 2014; Overmann and Garcia-Pichel, 2006). Their representative *Chlorobaculum tepidum* has developed as a model organism for this group of phototrophs (Bryant and Frigaard, 2006; Eisen *et al.,* 2002). Green sulfur bacteria possess a single BChl *a* and Chl *a*-containing reaction center and extensive light-harvesting structures, called chlorosomes, which enable them to grow under very low light conditions. In these structures, BChl *c*, *d* or *e* molecules self-assemble by pigment-pigment interactions and form tubular structures attached to the inside of the cytoplasmic membrane (Bryant and Frigaard, 2006; Ganapathy *et al.,* 2012; Ganapathy *et al.,* 2009). Interestingly, Chl *a* is esterified with Δ2,6-phytadienol in green sulfur bacteria (Liu and Bryant, 2012).

1.3 Structure, function and occurrence of tetrapyrroles

(Bacterio)chlorophylls belong to the large group of molecules called tetrapyrroles. Tetrapyrroles are widespread and are involved in many essential cellular functions, such as photosynthesis and respiration. The basic structure of tetrapyrroles is formed by aromatic pyrrole rings, four of which are covalently linked by methine bridges. In the case of the bilins, the chromophores of the cyanobacterial phycobiliproteins, a linear tetrapyrrole is formed (Frankenberg and Lagarias, 2003). In other cases, a cyclic structure called porphyrin is formed (Figure 1 **A**), which is able to chelate certain divalent metal ions (e.g. Mg^{2+}, Fe^{2+}, Ni^{2+}, Co^{2+}) *via* the nitrogen atoms. Variants of the porphyrin ring are the chlorin and the bacteriochlorin ring structures (Figure 1 **B** and **C**), which possess a reduced D or D and B ring, respectively (Moss, 1988).

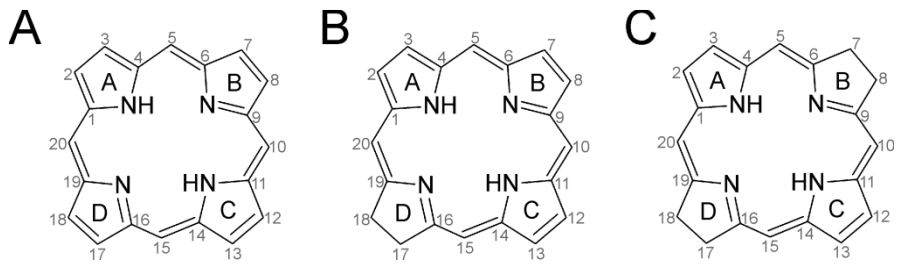

Figure 1: Basic ring structures of cyclic tetrapyrroles. A, Porphyrin; **B**, Chlorin; **C**, Bacteriochlorin. Carbon atoms are numbered according to IUPAC-IUB (Moss, 1988) and rings are numbered A - D. The chlorin ring (17,18-dihydroporphyrin) shows a reduced D ring. The bacteriochlorin ring (7,8,17,18-tetrahydroporphyrin) shows reduced D and B rings.

These ring structures are the basis for the variety of (bacterio)chlorophylls. Apart from those, the cyclic tetrapyrroles comprise the large group of hemes as well as coenzyme F_{430}, vitamin B_{12} (corrinoids), siroheme and heme d_1 (Battersby, 2000). The cyclic tetrapyrroles differ in the oxidation states of the ring system, the nature of the ring substituents and the central metal ion (Jahn *et al.,* 1996). Due to their extended cyclic system of alternating double and single bonds, cyclic tetrapyrroles possess aromatic character and absorb light in the range from near ultraviolet to near infrared (Scheer, 2006; Senge *et al.*, 2006). The oxidation state and the substituents of the ring system and the metal ion influence the absorption properties (Kobayashi *et al.*, 2006).

Figure 2 depicts the large variety of naturally occurring (bacterio)chlorophyll molecules.

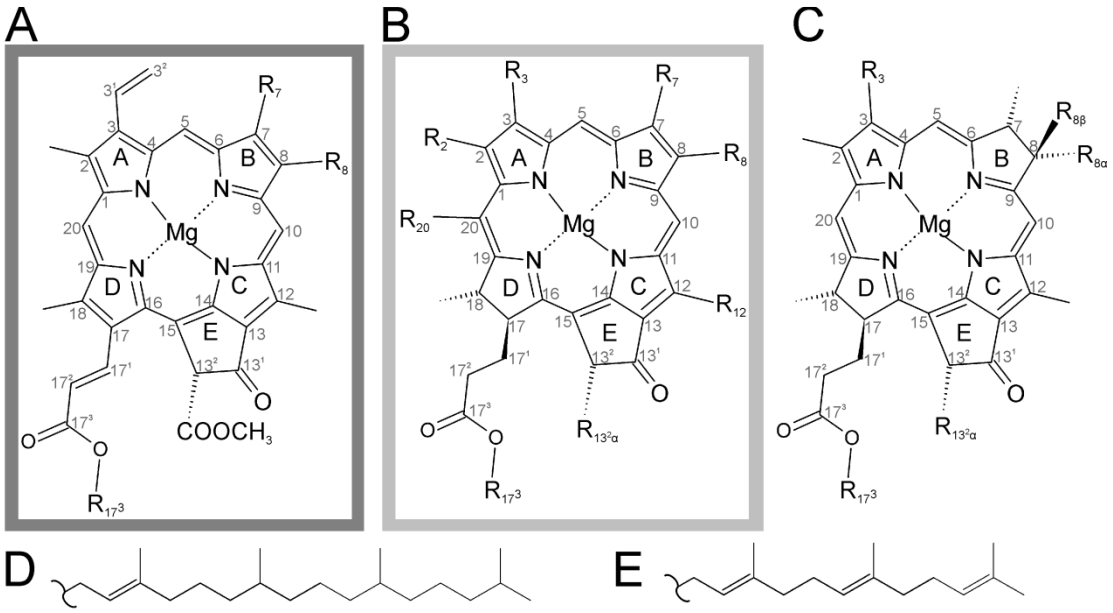

Pigment	R_2	R_3	R_7	R_8 ($R_{8\alpha}$/$R_{8\beta}$)	R_{12}	$R_{13^2\alpha}$	R_{17^3}	R_{20}
Chl c_1/ Chl c_2/ Chl c_3	-	-	CH_3/ CH_3/ $COOCH_3$	CH_2-CH_3/ CH=CH_2/ CH=CH_2	-	-	H	H
Chl *a*	CH_3	CH=CH_2	CH_3	CH_2-CH_3	CH_3	$COOCH_3$	Phy	H
Chl *b*	CH_3	CH=CH_2	CHO	CH_2-CH_3	CH_3	$COOCH_3$	Phy	H
Chl *d*	CH_3	CHO	CH_3	CH_2-CH_3	CH_3	$COOCH_3$	Phy	H
Chl *f*	CHO	CH=CH_2	CH_3	CH_2-CH_3	CH_3	$COOCH_3$	Phy	H
Divinyl Chl *a*	CH_3	CH=CH_2	CH_3	CH=CH_2	CH_3	$COOCH_3$	Phy	H
Divinyl Chl *b*	CH_3	CH=CH_2	CHO	CH=CH_2	CH_3	$COOCH_3$	Phy	H
8^1-OH-Chl *a*	CH_3	CH=CH_2	CH_3	CHOH-CH_3	CH_3	$COOCH_3$	Far	H
BChl *c*	CH_3	CHOH-CH_3	CH_3	$CH_2CH_n(CH_3)_{3-n}$	CH_3/CH_2-CH_3	H	Far/ other	CH_3
BChl *d*	CH_3	CHOH-CH_3	CH_3	$CH_2CH_n(CH_3)_{3-n}$	CH_3/CH_2-CH_3	H	Far/ other	H
BChl *e*	CH_3	CHOH-CH_3	CHO	$CH_2CH_n(CH_3)_{3-n}$	CH_3/CH_2-CH_3	H	Far/ other	CH_3
BChl *a*	-	$COCH_3$	-	H/CH_2-CH_3	-	$COOCH_3$	Phy	-
BChl *b*	-	$COCH_3$	-	=CH-CH_3	-	$COOCH_3$	Phy	-
BChl *g*	-	CH=CH_2	-	=CH-CH_3	-	$COOCH_3$	Far	-

Figure 2: Structures of naturally occurring (bacterio)chlorophylls (based on: Blankenship, 2014; Scheer, 2006). Panels **A** - **C** show the core structures of a porphyrin (**A**), chlorin (**B**) and bacteriochlorin (**C**) ring with the additional isocyclic ring common to all (bacterio)chlorophylls and the central magnesium ion. Carbon atoms are numbered according to IUPAC-IUB (Moss, 1988) and rings are numbered A - E. The individual ring substituents are designated "R" and specified in the table. Pigments based on a porphyrin or chlorin ring structure are highlighted in dark and light gray, respectively. All other pigments possess a bacteriochlorin ring structure (white). BChls *c*, *d* and *e* are mixtures of molecules with differently methylated groups at C8 and C12, with varying hydrophobic chains at $C17^3$ and different absolute configurations at $C3^1$. Other, minor variants of naturally occurring (bacterio)chlorophylls exist which are not included in the table. **D**, Structure of the phytyl side chain (Phy); **E**, Structure of the farnesyl side chain (Far).

Almost all naturally occurring (bacterio)chlorophylls possess a chelated magnesium ion, as well as an additional fifth ring, called ring E or isocyclic ring. The hydrophobic long-chain alcohol esterified to the carboxylic group of C17[3] serves as an anchor, fixing the molecule in its natural environment. In most cases, a phytyl or farnesyl side chain is present (Figure 2, **D** and **E**), but Δ2,6-phytadienyl and other moieties have been observed in green sulfur bacteria (Liu and Bryant, 2012). A high degree of variety among (bacterio)chlorophylls occurs with regard to the oxidation state of the ring system and its substituents.

Due to these variations, each pigment displays a specific absorption spectrum, so that a combination of pigments allows the absorption of a broad range of electromagnetic radiation. Pigments based on a chlorin ring structure have a major absorption peak in the blue light range around 440 nm (designated as Soret or B-band) and a red-most absorption peak around 660 nm (Q_y peak) in organic solvents (Scheer, 2006). Bacteriochlorin-type molecules absorb in the near ultraviolet range of 350 - 400 nm. Their Q_y peak lies between 750 and 800 nm and an additional Q_x peak is present between 500 and 600 nm (Scheer, 2006). *In vivo*, the photosynthetic pigments are arranged in large pigment-protein complexes, which additionally influence their absorption properties.

Chl *a* is the major photosynthetic pigment in eukaryotic phototrophs and cyanobacteria, where it is present in antenna structures and reaction centers. Antenna structures are used to broaden the range of light that can be absorbed. Chl *b* is the major antenna pigment in most eukaryotic phototrophs and prochlorophytes (see section 1.2.1). Other pigments used in oxygenic photosynthesis are Chls c_1, c_2, c_3, *d* and *f*, as well as divinyl Chl *a* and divinyl Chl *b* (Chen, 2014). In anoxygenic photosynthesis, BChl *a* is present in the reaction centers and antenna structures of most anoxygenic bacteria. Other pigments used in anoxygenic photosynthesis are BChls *b*, *c*, *d*, *e* and *g* (Blankenship, 2014; Chew and Bryant, 2007). Purple bacteria contain BChls *a* or *b*, whereas green sulfur bacteria produce BChls *c*, *d* or *e* in addition to BChl *a* and Chl *a* (see section 1.2.2). BChl *g* is only found in heliobacteria, which additionally produce 8-hydroxyethyl-Chl *a*. Filamentous anoxygenic phototrophs produce BChls *a* and *c*. Chloroacidobacteria produce BChls *a* and *c*, Chl *a* and

the unusual pigment Zn-BChl *a* (Garcia Costas *et al.,* 2012; Tsukatani *et al.,* 2012).

A crucial feature of the antenna structures is the ability to transfer the absorbed energy to the reaction center by radiationless transfer. In the reaction center, a pair of (bacterio)chlorophylls is excited by energy absorption to a higher energy level and reduces a primary acceptor pigment by electron transfer. The electron is further transported along the electron transport chain. Thus, in the reaction center, (bacterio)chlorophylls are subjected to oxidation/reduction events. Moreover, (bacterio)chlorophyll precursors have been assigned a feedback regulatory role in their biosynthetic pathways (Masuda and Fujita, 2008).

1.4 Biosynthesis of chlorophylls and bacteriochlorophylls

The variety of (bacterio)chlorophylls is formed by various enzymatic steps starting from the "hub" intermediate chlorophyllide *a* (Chlide; Chl *a* not esterified at C17[3], but carrying a free carboxylic acid side chain), which appears to be the precursor for all BChls and certain Chls (Chen, 2014; Chew and Bryant, 2007). All chlorophototrophs share the enzymatic steps that lead to the formation of Chlide, however, for some reactions, more than one enzyme has been identified.

1.4.1 The common steps: from 5-aminolevulinic acid to chlorophyllide *a*

The common precursor of all tetrapyrroles is 5-aminolevulinic acid. Two 5-aminolevulinic acid molecules are enzymatically condensated to form porphobilinogen, which is then further converted *via* pre-uroporphyrinogen to uroporphyrinogen III. In the consecutive steps, protoporphyrin IX is formed *via* the intermediates coproporphyrinogen III and protoporphyrinogen IX. At the point of uroporphyrinogen III, the biosynthetic pathways to the cyclic tetrapyrroles siroheme, heme d_1, coenzyme F_{430} and the corrinoids separate (Figure 3).

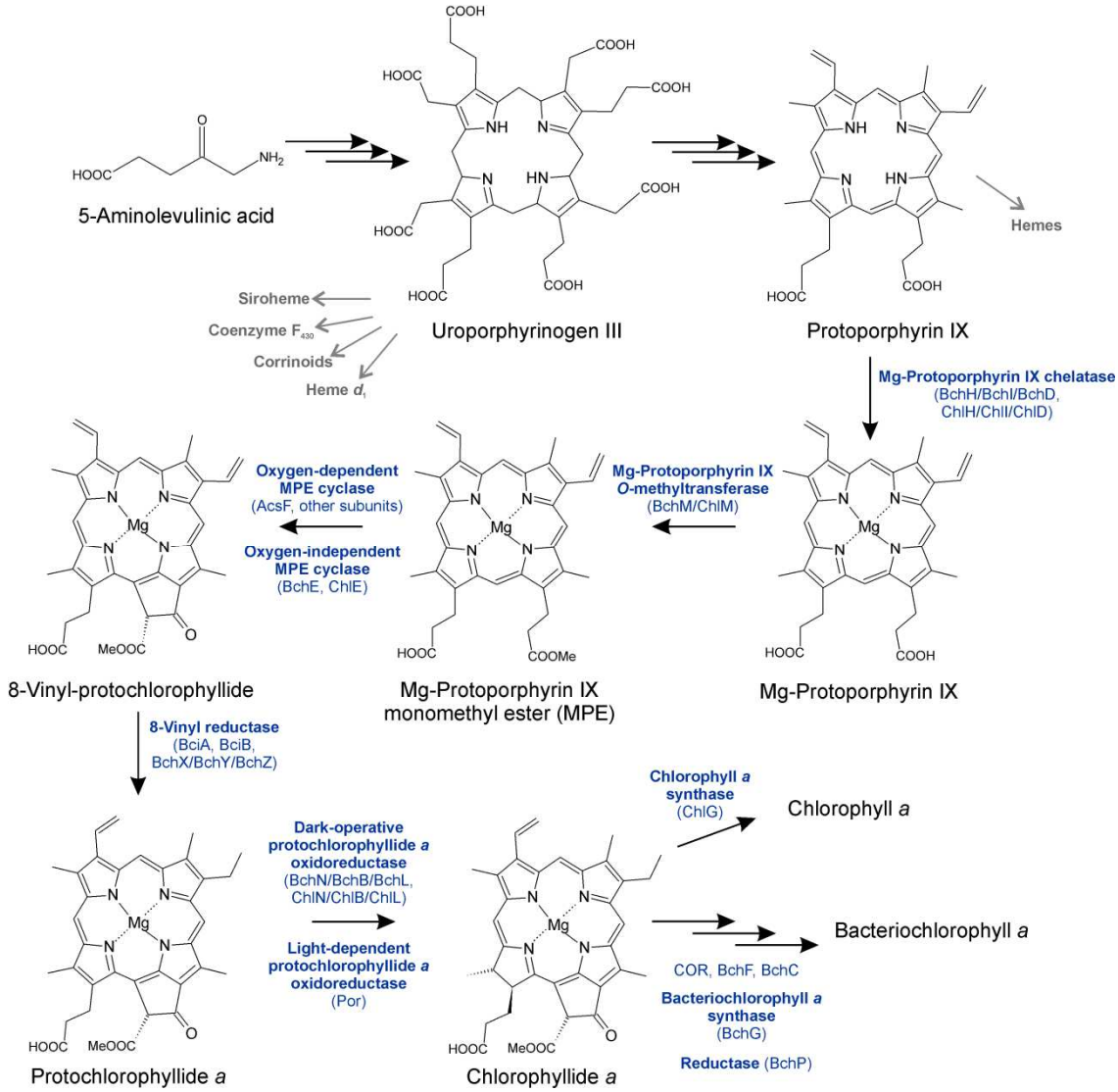

Figure 3: Overview of the common steps of (bacterio)chlorophyll biosynthesis. All tetrapyrroles are derived from 5-aminolevulinic acid. Multiple enzymatic steps lead to uroporphyrinogen III and further to protoporphyrin IX. At the point of uroporphyrinogen III, the biosynthesis pathways leading to siroheme, coenzyme F_{430}, corronoids and heme d_1 diverge (depicted in gray). Similarly, the biosynthesis of hemes diverges at the protoporphyrin IX branching point. The enzymes specific for (bacterio)chlorophyll biosynthesis are highlighted in blue and their individual subunits are given in brackets. The "Bch" nomenclature is used for BChl-synthesizing organisms, whereas the respective proteins in Chl-synthesizing phototrophs are named "Chl". The biosynthetic pathway is depicted in a linear way, although there is evidence that the C8 vinyl reduction can occur at different stages of the pathway in some organisms (Bröcker *et al.*, 2012; Canniffe *et al.,* 2014). Some species code for more than one type of 8-vinyl reductase, whereas other species contain only a single type (BciA, BciB or BchX/BchY/BchZ; Canniffe *et al.,* 2014; Harada *et al.,* 2014). The steps specific for BChl *a* biosynthesis comprising the enzymes COR, BchF and BchC are specified in Figure 4.

Protoporphyrin IX is the last common precursor of hemes and (bacterio)chlorophylls. By the insertion of iron into this molecule by the enzyme ferrochelatase (Dailey, 2002), the biosynthetic pathway for hemes is pursued.

The multisubunit ATP-dependent enzyme Mg-protoporphyrin IX chelatase is responsible for the insertion of Mg^{2+} into protoporphyrin IX, representing the first committed step of (bacterio)chlorophyll biosynthesis (Jensen *et al.,* 1999; Masuda, 2008). The product Mg-protoporphyrin IX is methylated by the *S*-adenosylmethionine-dependent Mg-protoporphyrin IX *O*-methyltransferase (ChlM/BchM) to Mg-protoporphyrin IX monomethyl ester (MPE; Chen *et al.,* 2014; Masuda, 2008). Next, the isocyclic ring is formed. Two unrelated enzymes have been discovered, which are able to catalyze the cyclization: the oxygen-independent Mg-protoporphyrin IX monomethyl ester cyclase (BchE), present in all anoxygenic phototrophs and some cyanobacteria (ChlE, Yamanashi *et al.,* 2015), and the oxygen-dependent cyclase (AcsF and homologs), present in all oxygenic phototrophs (Bröcker *et al.*, 2012). It has been shown that at least AcsF comprises additional subunits (Bollivar *et al.,* 2014; Bröcker *et al.*, 2012; Hollingshead *et al.,* 2012). However, both enzymes remain to be fully characterized.

As both Chl *a* and BChl *a* carry an ethyl group at C8 (Figure 2), the C8 vinyl group of the precursors has to be reduced. Multiple types of vinyl reductases have been identified which accomplish the 8-vinyl reduction in different phototrophs (Bröcker *et al.*, 2012; Harada *et al.,* 2014; Tsukatani *et al.,* 2013a). Some species code for more than one type of vinyl reductase, whereas other species contain only a single type (Canniffe *et al.,* 2014; Harada *et al.,* 2014). Although the (bacterio)chlorophyll biosynthetic pathway is usually depicted in a linear way, there is evidence that the C8 vinyl reduction can occur at different stages of the pathway (Bröcker *et al.*, 2012; Canniffe *et al.,* 2014).

For the reduction of protochlorophyllide *a* (Pchlide) to chlorophyllide *a* (Chlide) two unrelated enzymes have been identified: dark-operative protochlorophyllide *a* oxidoreductase (DPOR) and light-dependent protochlorophyllide *a* oxidoreductase (LPOR), described in more detail in section 1.5. The biosynthesis of Chl *a* is completed by the esterification of the $C17^3$ carboxylic acid side chain of Chlide with phytol, catalyzed by chlorophyll *a* synthase (ChlG). The synthesis of BChl *a* from the precursor bacteriochlorophyllide *a* (BChlide) is accomplished by the enzymes BchG and BchP. The former esterifies BChlide with the isoprenoid alcohol geranylgeraniol,

preceding the reduction of three double bonds to form a phytyl side chain by BchP (Bröcker *et al.*, 2012).

Additional enzymatic steps are required to produce the variety of (bacterio)chlorophylls (Figure 2), but not all enzymes have been identified yet (Chen, 2014; Chew and Bryant, 2007).

1.4.2 Enzymatic steps specific for bacteriochlorophyll *a*

The biosynthesis of BChl *a* requires several additional enzymatic steps. Following the reduction of Pchlide to Chlide (Figure 3), three enzymatic steps lead to the formation of BChlide, the last intermediate before the esterification of the carboxylic acid side chain of $C17^3$ by BchG: the enzyme chlorophyllide *a* oxidoreductase (COR, subunits BchX/BchY/BchZ) reduces the B ring of the chlorin ring system, so that a bacteriochlorin ring system is formed (Nomata *et al.,* 2006b). COR has a high sequence similarity to the enzymes DPOR and nitrogenase and contains [4Fe-4S] clusters which accomplish the two-electron reduction of the chlorin substrate in an ATP-dependent manner (Kiesel *et al.,* 2015; Kim *et al.,* 2008; Nomata *et al.,* 2006b; Wätzlich *et al.,* 2009). Recently, it was shown that COR from various organisms is a bifunctional enzyme which is also capable of the 8-vinyl reduction (Figure 3, Harada *et al.,* 2014; Tsukatani *et al.,* 2013a) and that the enzyme from *Heliobacterium modesticaldum* catalyzes the 8-ethylidene group formation in BChl *g* biosynthesis (Tsukatani *et al.,* 2013b). The enzyme 3-vinyl bacteriochlorophyllide *a* hydratase (BchF) catalyzes the hydroxylation of the 3-vinyl group and subsequently, 3-hydroxyethyl bacteriochlorophyllide *a* dehydrogenase (BchC) oxidizes the 3-hydroxyethyl group to a 3-acetyl side chain (Figure 4). Both BchF and BchC will be described in more detail in sections 1.6 and 1.7, respectively.

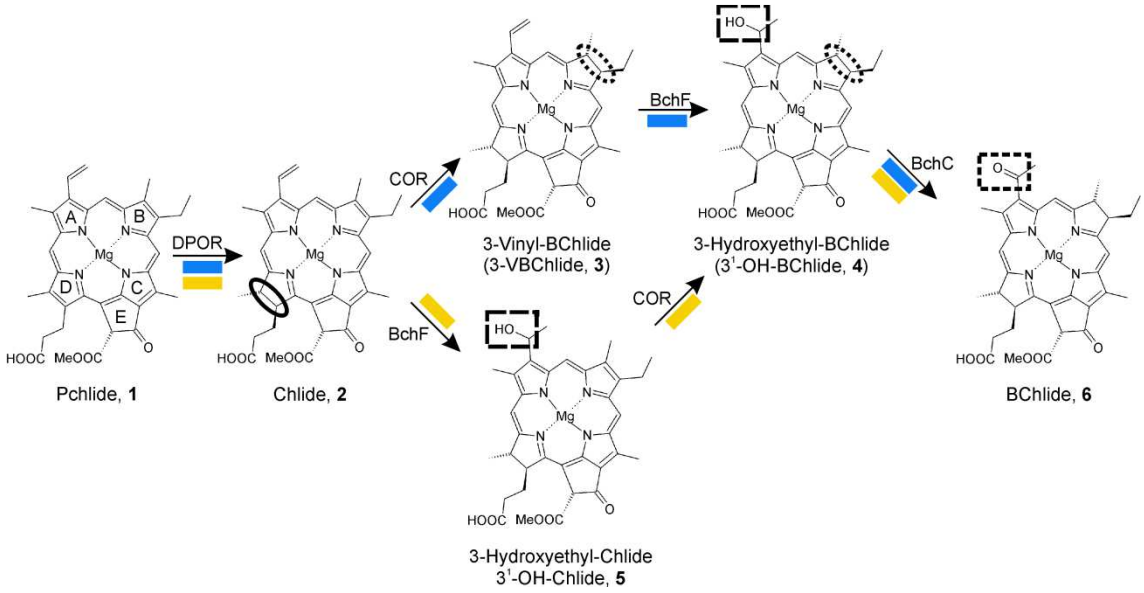

Figure 4: The branched pathway of BChl *a* biosynthesis from Pchlide. Following the reduction of Pchlide (**1**) to Chlide (**2**), the enzymes COR, BchF and BchC lead to the formation of BChlide (**6**). The two possible reaction sequences described in the literature are depicted and labeled with blue and yellow markings. Catalyzed modifications by the respective enzymes are indicated by boxes and ovals.

In the literature, the order of the biosynthetic steps involving the enzymes COR, BchF and BchC is not unambiguously clear. The spectroscopic analyses of several *Rhodobacter capsulatus bchF* mutant strains (Bollivar *et al.,* 1994a; Burke *et al.,* 1993) as well as *R. capsulatus* and *Rhodobacter sphaeroides bchC* mutants (Coomber *et al.,* 1990; Hunter and Coomber, 1988; Wellington and Beatty, 1989) showed that these mutants accumulate different BChl *a* precursors, so that two possible reaction sequences can be derived (Figure 4): the first possible reaction sequence comprises the DPOR reduction, followed by the reduction of the tetrapyrrole B ring (COR), and proceeds *via* the BchF and BchC reactions (blue markings). In the second variant, the DPOR reaction is followed by BchF catalysis. Subsequently, the BchF reaction product 3-hydroxyethyl-chlorophyllide *a* (3^1-OH-Chlide, **5**) is reduced by COR, followed by the BchC catalyzed oxidation (yellow markings). Thus, the metabolite Chlide (**2**) marks a branching point of the BChl *a* biosynthesis pathway and is a substrate for both COR and BchF.

1.5 Protochlorophyllide *a* oxidoreductases and homologs

The stereospecific two-electron reduction of the C17-C18 double bond of the tetrapyrrole D ring (Figure 4) is challenging because the aromatic system of the porphyrin ring has to be modified. This task is accomplished by two unrelated enzymatic systems. In anoxygenic phototrophs, the multi-subunit enzyme DPOR is present. On the other hand, the single subunit enzyme LPOR exclusively functions in angiosperms. In cyanobacteria, algae, mosses, ferns and gymnosperms, both LPOR and DPOR are encoded (Fujita, 1996). Recently, LPOR activity was also shown in the aerobic anoxygenic phototrophic α-proteobacterium *Dinoroseobacter shibae* DFL12^T (Kaschner *et al.,* 2014). LPOR is a light-dependent enzyme, whereas DPOR enables the respective organisms to perform Chl biosynthesis in the dark.

1.5.1 Light-dependent protochlorophyllide *a* oxidoreductase

LPOR is a single subunit enzyme belonging to the superfamily of short-chain dehydrogenases/reductases, showing a conserved cofactor binding region and the active site motif YxxxK (Baker, 1994; Kavanagh *et al.,* 2008; Wilks and Timko, 1995). In the dark, LPOR forms a ternary complex with its substrate Pchlide and the cosubstrate NADPH. The catalytic mechanism is triggered by light absorption and proceeds *via* several light-driven steps followed by light-independent steps (Reinbothe *et al.,* 2010). Upon illumination, the Pchlide molecule acts as a photoreceptor, is transferred to an excited state by light energy absorption, and thus facilitates hydride transfer from the *pro-S* face of NADPH to C17 of Pchlide (Scrutton *et al.,* 2012). Subsequent protonation of C18 is probably mediated by the tyrosine residue of the active site motif, whereas the proximate lysine residue is thought to lower the pK_a value of the tyrosine (Reinbothe *et al.,* 2010).

1.5.2 Dark-operative protochlorophyllide *a* oxidoreductase - a nitrogenase-like enzyme

DPOR is comprised of subunits BchL, BchN and BchB (BChl-producing organisms) or ChlL, ChlN and ChlB (Chl-producing organisms), respectively (Bollivar *et al.,* 1994a; Burke *et al.,* 1993; Fujita, 2000; Yang and Bauer, 1990). In the following, the DPOR subunits will be designated L, N and B only, in order to account for the different nomenclature in Chl and BChl producing organisms. The DPOR subunits share a high degree of structural and sequential identity with the molybdenum-dependent nitrogenase subunits NifH, NifD and NifK, respectively (about 35 % amino acid sequence identity for NifH and L and about 15 % for NifD and N and NifK and B, Fujita *et al.,* 1993; Wätzlich *et al.,* 2009). Nitrogenase is the enzyme capable of reducing dinitrogen to ammonia, thus making it available for organisms that cannot fix nitrogen themselves. The nitrogenase subunits are found in microorganisms called diazotrophs, and form a holoenzyme composed of two subcomplexes, a $NifH_2$ homodimer and a $(NifD/NifK)_2$ heterotetramer. By hydrolyzing sixteen ATP molecules, the enzyme accomplishes the eight-electron reduction of dinitrogen, producing two molecules of ammonia and molecular hydrogen (Seefeldt *et al.,* 2009).

DPOR is a two-component protein: in solution, recombinantly produced L protein forms homodimers, which bind a redox-active [4Fe-4S] cluster *via* two cysteine residues from each monomer (Bröcker *et al.,* 2008a; Nomata *et al.,* 2006a; Sarma *et al.,* 2008). The crystal structure of L_2 from *R. sphaeroides* reflected the high degree of similarity to $NifH_2$ of nitrogenase (Sarma *et al.,* 2008), which similarly coordinates a [4Fe-4S] cluster *via* two cysteine residues from each monomer and possesses two nucleotide binding sites (Jang *et al.,* 2000). The latter comprise three amino acid sequence regions highly conserved among a variety of nucleotide-binding proteins: the phosphate binding loop (P-loop) as well as the so-called switch I and switch II regions. All three regions interact with the phosphate groups of the nucleotide, so that switch I and II can trigger a conformational rearrangement of the entire protein depending on the bound nucleotide (Sablin and Fletterick, 2001; Vetter and Wittinghofer, 2001). These sequence features and the respective biochemical characterizations of the L_2 homodimer from *Prochlorococcus marinus* characterize the protein as a

nucleotide-dependent switch protein: in circular dichroism (CD) spectroscopy experiments in the visible light region it was shown that the conformation of the dimer changed depending on the presence of a nucleotide (MgATP or MgADP). It was suggested that ATP hydrolysis enables the tight interaction of L_2 and $(NB)_2$ (Bröcker *et al.,* 2010b) and thus drives the enzymatic DPOR activity. The same characterization had been performed before for $NifH_2$ (Lanzilotta *et al.,* 1997; Ryle and Seefeldt, 1996; Schindelin *et al.,* 1997).

DPOR subunits N and B interact tightly with each other and form a $(NB)_2$ heterotetramer (Bröcker *et al.,* 2008a; Bröcker *et al.,* 2008b; Fujita, 2000; Nomata *et al.,* 2005). Each heterotetramer ligates two [4Fe-4S] clusters, each *via* three cysteine residues from subunit N and an unusual aspartate ligand from subunit B (Bröcker *et al.,* 2010a; Muraki *et al.,* 2010). It has been suggested that the aspartate ligand serves to lower the redox potential of the NB-bound [4Fe-4S] cluster in order to accomplish the reduction of the stable porphyrin ring of Pchlide (Kondo *et al.,* 2011). The [4Fe-4S] clusters render the enzyme sensitive to oxygen, whereas the $(NB)_2$-bound clusters seem to be more oxygen-tolerant than the L_2-bound cluster in the *R. capsulatus* enzyme (Bröcker *et al.,* 2008b; Nomata *et al.,* 2006a; Nomata *et al.,* 2008). The crystal structure of the Pchlide-bound *R. capsulatus* $(NB)_2$ complex showed that the ring system of Pchlide binds in a cavity formed by both subunits (Muraki *et al.,* 2010). This supported biochemical studies indicating that NB is the site of substrate binding and reduction (Bröcker *et al.,* 2008b; Nomata *et al.,* 2008). The highly oxygen-sensitive nitrogenase enzyme differs from DPOR with regard to the heterotetramer-bound metalloclusters: instead of the DPOR NB [4Fe-4S] cluster, NifD/NifK contains a special [8Fe-7S] cluster (P cluster) ligated by residues from both NifD and NifK (Seefeldt *et al.,* 2009). The site of nitrogen reduction is a complex cofactor with the composition [Mo-7Fe-9S-C]-homocitrate (FeMoco; Spatzal, 2015) which occupies a similar position in the enzyme as the Pchlide binding cavity in DPOR (Bröcker *et al.,* 2010a; Muraki *et al.,* 2010).

A schematic representation of the DPOR and nitrogenase holoenzymes is depicted in Figure 5.

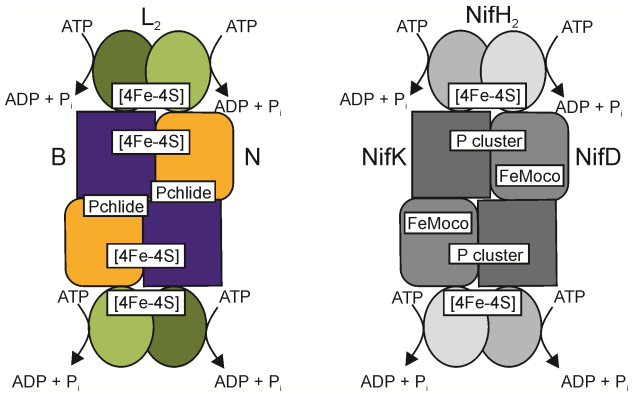

Figure 5: Schematic representation of DPOR (left) and nitrogenase (right) octameric complexes. During catalysis, both enzymes form transient complexes consisting of two L_2 or $NifH_2$ homodimers and one $(NB)_2$ or $(NifD/NifK)_2$ heterotetramer. The subunit-bridging [4Fe-4S] clusters are shown for DPOR and $NifH_2$. In place of the [4Fe-4S] cluster bound by DPOR subunits N and B, nitrogenase contains a special [8Fe-7S] cluster (P cluster). The DPOR substrate binding site for Pchlide is indicated, whereas nitrogenase binds a complex iron and molybdenum containing cofactor (FeMoco), where nitrogen reduction takes place. The ATPase activity of subunits L and NifH is shown. The DPOR subunits are labeled "N", "B" and "L" to account for the different nomenclature in Chl and BChl producing organisms.

Size exclusion chromatography experiments showed that the three DPOR subunits L, N and B from *P. marinus* form a heterooctameric complex during catalysis, consisting of two homodimers and one heterotetramer (Bröcker *et al.,* 2010b; Figure 5). Label-transfer experiments indicated that L_2 interacts with both subunits N and B (Wätzlich *et al.,* 2009). During DPOR catalysis, single electrons are transferred from an external electron donor *via* the redox-active [4Fe-4S] clusters of L_2 and $(NB)_2$ to the substrate Pchlide. *In vivo*, the initial electron donors for DPOR are probably ferredoxins (Bröcker *et al.,* 2008a; Nomata *et al.,* 2005), which reduce the L_2-bound $[4Fe\text{-}4S]^{2+}$ cluster. In *in vitro* experiments, the artificial electron donor dithionite is used instead (Bröcker *et al.,* 2008a; Fujita, 2000). Details of the DPOR redox cycle (Figure 6) were inferred from electron paramagnetic resonance (EPR) investigations of different redox stages within the cycle (Bröcker *et al.,* 2010b). Moreover, the transient octameric DPOR complex could be stabilized by binding analogs of different stages of ATP hydrolysis, adenosine-5'(γ-thio)-triphosphate, adenosine-5'(βγ-imido)-triphosphate or $MgADP{\bullet}AlF_4^-$ in the same work.

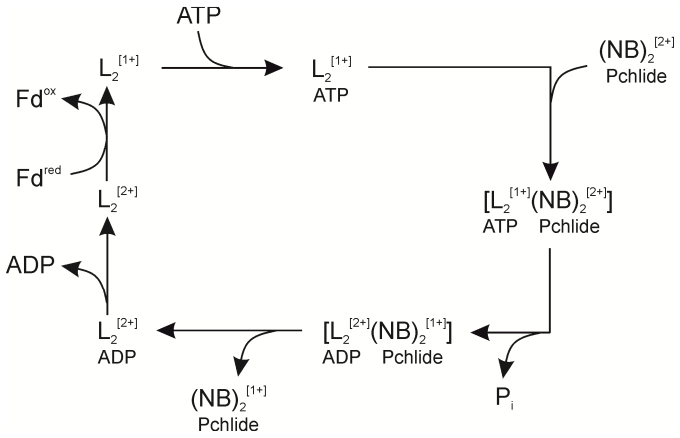

Figure 6: Suggested redox cycle of DPOR (modified from Bröcker *et al.,* 2010b). *In vivo*, a ferredoxin (Fd) is the likely electron donor for the $[4Fe\text{-}4S]^{2+}$ cluster bound to L_2. After the subsequent binding of ATP, the transient DPOR complex is assembled. Simultaneous with ATP hydrolysis, electron transfer from the L_2-bound $[4Fe\text{-}4S]^{1+}$ cluster to the NB-bound $[4Fe\text{-}4S]^{2+}$ cluster takes place. Next, the complex dissociates and after the dissociation of ADP, $L_2^{[2+]}$ can be re-reduced. The DPOR subunits are labeled "N", "B" and "L" to account for the different nomenclature in Chl and BChl producing organisms. Superscript numbers indicate the oxidation states of the protein-bound [4Fe-4S] clusters; only one of the two NB-bound clusters is considered. For simplicity, only one of the two L_2 dimers of the transient DPOR complex is shown.

After the first reduction step yielding $L_2^{[1+]}$, two molecules of ATP are bound and the transient octameric DPOR complex is assembled by the association of ATP-bound reduced L_2 and Pchlide-bound oxidized $(NB)_2$. Preliminary binding of Pchlide to $(NB)_2$ is required for efficient complex formation. Because of the tight interaction of the subcomplexes, one electron can be transferred from the L_2-bound $[4Fe\text{-}4S]^{1+}$ cluster to the NB-bound $[4Fe\text{-}4S]^{2+}$ cluster. Simultaneously, ATP hydrolysis takes place. It was shown that a complete ATP hydrolysis is necessary for electron transfer (Bröcker *et al.,* 2010b). Next, the octameric complex disassembles and after the dissociation of ADP, $L_2^{[2+]}$ can be re-reduced. As the transformation of Pchlide to Chlide is a two-electron reduction, the stepwise electron transfer from the NB-bound [4Fe-4S] cluster to Pchlide probably proceeds *via* radical intermediates, as deduced from absorption and EPR spectroscopy investigations of combinations of mutant proteins and the DPOR inhibitors nicotinamide and Chl *c* (Nomata *et al.,* 2013; Nomata *et al.,* 2014). By the first electron transfer a Pchlide anion radical is formed, which is transformed to an intermediate neutral radical by stereospecific protonation. The second electron transfer generates an anion intermediate which is protonated to form the product Chlide.

The DPOR enzyme from the prochlorophyte *P. marinus* has been investigated with regard to its substrate specificity, using chemically modified pigments (Bröcker *et al.,* 2008b). Polarity changes of the substituents at C3, C7 and C8 (Figure 2) were tolerated, whereas bulky side chains at C3 and C7 did not facilitate substrate turnover. Moreover, ring E was found to be involved in substrate recognition and no modification of the C17 propionate side chain was tolerated (Bröcker *et al.,* 2008b).

In the literature, the structures of the DPOR subcomplexes from different organisms are described (Table 1). Additionally, the structure of the octameric nitrogenase complex and its subcomplexes has been solved in many variations (Table 1), allowing a detailed analysis of the subcomplex interactions.

Table 1: Summary of the X-ray crystallographic structures of DPOR subcomplexes and selected nitrogenase variants described in the literature. The protein data bank (PDB) entry with the identifier (PDB ID) 2KRU is an exception as this structure was solved by nuclear magnetic resonance (NMR) spectroscopy. In all structures, the redox-active metalloclusters are visible (except for 2KRU); additional structural features are listed („Remarks"). Nitrogenase structures were selected because of their relevance for the present work. Note that in the PDB, entry 4WZB now supercedes 2AFK. MgAMPPCP = Mg-adenosine-5'(βγ-methylene)-triphosphate; *T. elongatus* = *Thermosynechococcus elongatus*; *A. vinelandii* = *Azotobacter vinelandii*.

PDB ID	Protein complex	Organism	Remarks	Reference
	DPOR			
3FWY	$BchL_2$	*R. sphaeroides*	MgADP-bound	Sarma *et al.,* 2008
2XDQ	$(ChlN/ChlB)_2$	*T. elongatus*	-	Bröcker *et al.,* 2010a
3AEK	$(BchN/BchB)_2$	*R. capsulatus*	Pchlide-bound	Muraki *et al.,* 2010
2AER	$(BchN/BchB)_2$	*R. capsulatus*	Pchlide-free	Muraki *et al.,* 2010
2KRU	C-terminal domain of BchB	*C. tepidum*	Solution NMR structure	Pulavarti *et al.,* 2013
	Nitrogenase			
1N2C	$(NifH_2)_2(NifD/NifK)_2$	*A. vinelandii*	MgADP•AlF_4^--bound	Schindelin *et al.,* 1997
1FP6	$NifH_2$	*A. vinelandii*	MgADP-bound	Jang *et al.,* 2000
1M34	$(NifH_2)_2(NifD/NifK)_2$	*A. vinelandii*	MgADP•AlF_4^--bound	Schmid *et al.,* 2002
2AFK	$(NifH_2)_2(NifD/NifK)_2$	*A. vinelandii*	MgAMPPCP-bound	Tezcan *et al.,* 2005
2AFH	$(NifH_2)_2(NifD/NifK)_2$	*A. vinelandii*	nucleotide-free	Tezcan *et al.,* 2005
2AFI	$(NifH_2)_2(NifD/NifK)_2$	*A. vinelandii*	MgADP-bound	Tezcan *et al.,* 2005
4WZA	$(NifH_2)_2(NifD/NifK)_2$	*A. vinelandii*	MgAMPPCP- and MgADP-bound	Tezcan *et al.,* 2015
4WZB	$(NifH_2)_2(NifD/NifK)_2$	*A. vinelandii*	MgAMPPCP-bound	Tezcan *et al.,* 2015

1.6 3-Vinyl bacteriochlorophyllide *a* hydratase (BchF)

The 3-vinyl bacteriochlorophyllide *a* hydratase activity of the *bchF* gene product was first derived from substrate accumulation studies with *Rhodobacter* mutants, which accumulated different BChl *a* precursors: the spectroscopic analysis of the *bchF* mutant strains MB1003 and KZR8G9 showed the accumulation of Chlide and 3-vinyl BChlide (Burke *et al.,* 1993; Taylor *et al.,* 1983; Zsebo and Hearst, 1984), whereas the *bchF* and *bchZ*-disrupted mutant CB1200 accumulated Chlide (Bollivar *et al.,* 1994a). Moreover, whole cell isotope labeling experiments showed that the oxygen atom at $C3^1$ was provided by a water molecule in the purple bacteria *R. sphaeroides*, *Roseobacter denitrificans* and *Rhodovulum sulfidophilum* (Porra *et al.,* 1996; Porra *et al.,* 1998). Later, a complementation study showed that *bchF* from the green sulfur bacterium *C. tepidum* can complement a *bchF*-deficient *Rhodobacter* mutant (Xiong, 2000). Apart from that, BchF had not been characterized further.

In green sulfur bacteria, the biosynthesis of BChl *a* as well as BChls *c*, *d* and *e* requires the hydratation of the 3-vinyl group (Figure 2). In the genome of *C. tepidum*, BchF is encoded by the open reading frame (orf) CT1421, but a *bchF* paralog, termed *bchV* (orf CT1776), can be found (Eisen *et al.,* 2002). By the enzymatic addition of water to the 3-vinyl group, a chiral center at $C3^1$ is formed. It was observed that both *R* and *S* epimers of BChls *c*, *d* and *e* are present in various species of green phototrophic bacteria (Frigaard *et al.*, 2006; Senge and Smith, 1995). Interestingly, the stereochemistry at $C3^1$ seems to correlate with the degree of methylation at C8 and C12 of BChls *c*, *d* and *e* in *Chlorobium* species (Figure 2): the majority of pigments with a higher degree of methylation shows *S*-stereochemistry, whereas less methylated pigments rather have *R*-stereochemistry at $C3^1$ (Frigaard *et al.*, 2006; Senge and Smith, 1995). Smith *et al.* suggested that the bulky side chains at C8 of the more methylated pigments enable a 180° rotation of the 3-vinyl side chain before hydratation, so that the *S*-stereoisomer is favored (Smith *et al.,* 1983). From the substrate accumulation studies of a *C. tepidum bchV* mutant it was inferred that BchV rather acts on the higher methylated substrates, whereas the optimal substrates for BchF are the less methylated pigments (Frigaard *et al.*, 2006; Liu and Bryant, 2012). With regard to the stereospecificity of BchF catalysis, a

study of the photosynthetic pigments in the green bacterium *Chloroflexus aurantiacus* showed that both *R* and *S* epimers of BChl *c* are present (Fages *et al.,* 1990), although this organism codes for BchF, but not BchV (Liu and Bryant, 2012). Furthermore, Liu and Bryant describe that in a *C. tepidum bchV* mutant, BChl *c* molecules with both *R* and *S* chirality can be detected (Liu and Bryant, 2012).

1.7 3-Hydroxyethyl bacteriochlorophyllide *a* dehydrogenase (BchC)

As described for BchF, the 3-hydroxyethyl bacteriochlorophyllide *a* dehydrogenase activity of the *bchC* gene product was derived from substrate accumulation studies: spectroscopic analysis of the *bchC* mutants *R. capsulatus* CW100 (Wellington and Beatty, 1989) and *R. sphaeroides* T127 and TB34 (Coomber *et al.,* 1990; Hunter and Coomber, 1988) showed the accumulation of 3^1-OH-BChlide (Figure 4). Thus, BchC was said to oxidize the 3-hydroxyethyl group of 3^1-OH-BChlide to a 3-acetyl side chain, forming BChlide. In *C. tepidum*, BchC is encoded by orf CT1422 (Eisen *et al.,* 2002).

1.8 Medium-chain dehydrogenases/reductases

The superfamily of medium-chain dehydrogenases/reductases (MDRs) comprises a large number of dehydrogenases and reductases in eukaryotes, bacteria and archaea with a variety of cellular functions (Persson *et al.,* 2008). Well-known MDR enzymes are the alcohol dehydrogenase ADH I from *Saccharomyces cerevisiae* or horse liver alcohol dehydrogenase (Eklund and Ramaswamy, 2008; Leskovac *et al.,* 2002). MDRs are about 350 amino acids in length and typically consist of two domains: the N-terminal substrate binding domain with distant similarity to GroES, and the C-terminal domain comprising the cofactor binding site (Hedlund *et al.,* 2010). MDRs use either NAD(H) or NADP(H) as redox cofactor and can be further subdivided into zinc-dependent and zinc-independent enzymes (Hedlund *et al.,* 2010). The zinc-dependent enzymes bind either one or two zinc ions which either directly participate in catalysis or own an important structural function

(Auld and Bergman, 2008). Based on the amino acid sequences, the MDR superfamily can be divided into numerous subfamilies, e.g. the prostaglandin reductase or the polyol dehydrogenase family (Hedlund *et al.,* 2010).

1.9 Aim of this study

In the literature, the structures of the components of the multimeric DPOR enzyme from different bacteria are described. Moreover, the structure of the enzyme nitrogenase is well-known, to which DPOR has a high degree of structural and sequence identity. However, it remained to be investigated by structural analysis, how the DPOR subcomplexes interact with each other and accomplish the two-electron reduction of the tetrapyrrole D ring. Thus, the first aim of this study was to crystallize the MgADP•AlF_4^- and Pchlide-bound octameric DPOR complex from *P. marinus* in order to solve its three-dimensional structure. On the basis of the available structures, differences and/or similarities of DPOR and nitrogenase should be analyzed.

Following the DPOR-catalyzed reduction of Pchlide to Chlide, additional enzymatic steps are necessary for the formation of BChl *a*. Two of the involved enzymes, BchF and BchC, have been identified, but are only marginally characterized to date. Therefore, the second aim of this study was to heterologously produce BchF and BchC from *C. tepidum* in *E. coli* in order to characterize both enzymes further. Activity assays using the recombinantly produced enzymes were to be established: a coupled activity assay based on the DPOR reaction as well as a BchC activity assay using artificial, chemically modified substrates. With regard to the coupled activity assay, the use of absorption and fluorescence spectroscopy for product detection was to be elucidated. Regarding the BchC activity assay, the artificial substrates were to be used for the investigation of BchC substrate specificity. Moreover, the biochemical characterization of BchC concerning its metal requirement, cofactor specificity and amino acid residues necessary for enzymatic activity was object of this work.

2 Materials and Methods

2.1 Instruments, accessories, chemicals and enzymes

Table 2: Instruments used in the present study.

Instrument / Device	Model	Manufacturer
Agarose gel electrophoresis chamber	Agagel Mini	Biometra
Agarose gel chamber power supply	Standard Power Pack P25	Biometra
Agarose gel documentation device	DeVision DBox	Decon DC Science Tec
Anaerobic work stations	MACS-MG-1000 Vinyl anaerobic chamber	DW Scientific Coy Laboratory Products Inc.
Amicon® stirred cell	Model 8050	Merck Millipore
Autoclaves	LVSA 50/70	Zirbus Technology
Blotting device	Trans-Blot® SD	Bio-Rad
Blue-light transilluminator	Flu-O-Blu	Biozym
Digital microscope (anaerobic work station)	VHX-500F Objective: VHZ20R, 20-200x magnification	KEYENCE
Centrifuges	Minispin Centrifuge 5804 Optima™ L-90K Avanti® J-26 XP Avanti® J-E Avanti® J-30 I Biofuge fresco Megafuge 1.0R	Eppendorf Eppendorf Beckman-Coulter Beckman-Coulter Beckman-Coulter Beckman-Coulter Heraeus Heraeus
Cryo holder (fluorimeter)	PMU-830	Jasco
Filtration/degassing system	Refrigerated Vapor Trap RVT400 Vacuum pump Ultrasonic bath	Savant vacuubrand Merck Eurolab
Fluorimeter	FP-8500	Jasco
French® Press	French® Pressure Cell French® Pressure Cell Press	SLM Aminco Polytec
HPLC	Jasco HPLC system with FP-1520 multi-wavelength fluorescence detector, UltraSep ES RP18 column, 5 µm, 250 × 4 mm	Jasco SEPSERV
Magnetic stirrer	VS-C7 Electronicrührer Multipoint HP15 IKAMAG REO	VWR Variomag® IKA
Microplate reader	iMark™ Microplate Absobance Reader	Bio-Rad
N_2-saturation device for buffers	-	self-construction working group of D. Jahn
pH determination	CG 842	Schott

Instrument / Device	Model	Manufacturer
Pipettes	Reference (100-1000 µL, 50-200 µL, 2-20 µL, 0.5-10 µL) Research (10-100 µL) Discovery Comfort (1-10 mL)	Eppendorf HTL
Rotating evaporator	VV2000 with water bath WB2000	Heidolph
Rotating incubator	OV5	Biometra
Spectrophotometer	V-650 Ultrospec 2000 NanoDrop® ND-1000	Jasco Biochrom Peqlab Biotechnologie GmbH
Scales	SBA52 BP61S BL1500	Scaltec Sartorius Sartorius
SDS-PAGE system	Mini-PROTEAN® 3 system	Bio-Rad
SDS-PAGE power supply	Power Pac 300 Power Pac 3000	Bio-Rad Bio-Rad
Shaker	3020 TR-150	GFL Infors AG
Thermocycler	T personal	Biometra
Thermomixer	Thermomixer Compact	Eppendorf
Vortex	Vortex Genie® 2	Scientific Industries
Water-bath shaker	Aquatron	Infors AG

Table 3 lists the accessories used in this study.

Table 3: Accessories used in the present study.

Application	Accessory	Manufacturer
Kits	Crystallization Screens	QIAGEN
	QIAquick® PCR Purification Kit	QIAGEN
	QIAquick® Gel Extraction Kit	QIAGEN
	QuikChange™ II Site-directed Mutagenesis Kit	Stratagene
Pigment analysis	CM Sepharose CL-6B	Pharmacia Fine Chemicals AB
	Cuvettes: 115-QS micro cuvette with lid 115F-QS micro cuvette with lid semi-micro cuvettes polystyrene	 Hellma Analytics Hellma Analytics Sarstedt
	NMR sample tubes: Thin Wall Precision NMR sample tubes, 5 mm Ø, 300 MHz, 7 or 8 inches NMR sample tubes 178 mm Economic with cap	 Wilmad-LabGlass Glasgerätebau Ochs Laborfachhandel e.K.
Protein biochemical methods	Amicon® polyethersulfone ultrafiltration disc (Ø 44.5 mm, 30'000 NMWL)	Millipore
	Amicon® Ultra-0.5 Centrifugal Filter Devices, 10'000 NMWL/30'000 NMWL	Merck Millipore
	'illustra' NAP-5 columns	GE Healthcare
	Protino® Glutathione Agarose 4B	Macherey-Nagel
	Poly-Prep® Chromatography Columns 0.8 x 4 cm and 25 mL	Bio-Rad
	Immobilon®-P polyvinylidene difluoride (PVDF) membrane, 0.45 µm pore size	Merck Millipore
Others	Sterile filter Filtropur S 0.2	Sarstedt

Table 4 lists chemicals, enzymes, markers and proteins used in this study. Chemicals which are not explicitly listed here were purchased from Merck, Fluka, Carl Roth, Sigma-Aldrich, Gerbu and VWR.

Table 4: Chemicals, enzymes, markers and proteins used in the present study.

Chemical / Enzyme / Protein		Manufacturer
Chemicals	Acetone	VWR
	$AlCl_3$	Sigma-Aldrich
	ATP	Sigma
	Bradford reagent	Sigma-Aldrich
	Phosphocreatine disodium salt hydrate	Sigma-Aldrich
	Dimethyl sulfoxide (DMSO)	Roth
	Ethylenediaminetetraacetic acid (EDTA)	Roth
	Ethyleneglycol bis(2-aminoethylether)-N,N,N′,N′-tetraacetic acid (EGTA)	Roth
	Fe(III) citrate monohydrate	Fluka
	GelStar™ Nucleic Acid Gel Stain	Lonza
	L-cysteine hydrochloride monohydrate	Roth
	NaADP	Sigma
	NAD^+: β-Nicotinamide adenine dinucleotide hydrate and β-Nicotinamide adenine dinucleotide (10 mg per vial)	Sigma-Aldrich
	NADH: β-Nicotinamide adenine dinucleotide, reduced disodium salt hydrate	Sigma-Aldrich
	$NADP^+$: β-Nicotinamide adenine dinucleotide phosphate hydrate	Sigma-Aldrich
	NaF	Fluka
	Sodium dithionite (SDT)	Sigma-Aldrich
	Triton™ X-100	Sigma-Aldrich
	Tween® 80	Roth
	Zinc acetate dihydrate	Fluka
Enzymes and proteins	Benzonase®	Merck Millipore
	Bovine serum albumin	Roth
	Creatine Phosphokinase from rabbit muscle	Sigma-Aldrich
	T4 DNA ligase	New England Biolabs
	PreScission protease	GE Healthcare
	Restriction endonucleases	New England Biolabs
	Penta-His antibody, Mouse Monoclonal IgG_1	QIAGEN
	Anti-Mouse IgG (F_c specific) Alkaline Phosphatase produced in goat	Sigma-Aldrich
Markers	GeneRuler™ DNA Ladder Mix	Thermo Fisher Scientific
	Unstained protein molecular weight marker	Thermo Fisher Scientific
	PageRuler™ Prestained Protein Ladder	Thermo Fisher Scientific

2.2 Bacterial strains, plasmids and oligonucleotide primers

Table 5: Bacterial strains used in the present study.

Strain	Genotype	Reference/Source
E. coli BL21-CodonPlus (DE3)-RIL	*E. coli* B F^{-} *ompT hsdS*(r_B^{-} m_B^{-}) *dcm*$^{+}$ Tet^r *gal* λ(DE3) *endA* Hte [*argU ileY leuW* Cam^r]	Stratagene
E. coli BL21 (DE3)	*E. coli* B F^{-} *dcm ompT hsdS*(r_B^{-} m_B^{-}) *gal* λ(DE3)	Stratagene, Studier and Moffatt, 1986
E. coli BL21 (DE3) pGEX-6P-1/ PA0920Δaa1-542	*E. coli* BL21 (DE3) containing the following expression vector: pGEX-6P-1 carrying base pairs 1627 - 2643 of ORF PA0920 from *P. aeruginosa* cloned into *Bam*HI/*Xho*I sites, Ap^r	Hebecker *et al.,* 2011
E. coli DH10B	F^{-} *mcrA* Δ(*mrr-hsdRMS-mcrBC*) Φ80*lacZ*ΔM15 Δ*lacX*74 *recA1 endA1 araD*139 Δ(*ara*, *leu*)7697 *galU galK* λ^{-} *rpsL nupG*	Invitrogen
R. capsulatus ZY5	derived from the wild-type strain SB1003 (Yen and Marrs, 1976), relevant characteristics: *F108*::Km^r *rif-10*; contains a kanamycin resistance (Km^r) cassette disrupting the *bchL* gene and thus accumulates Pchlide	Yang and Bauer, 1990
R. capsulatus CB1200	derived from the wild-type strain SB1003 (Yen and Marrs, 1976), relevant characteristics: *bchF bchZ*::Ω*Sp*^{r} *rif10*; contains a point mutation in the *bchF* gene and a directed disruption of the *bchZ* gene and thus accumulates Chlide	Bollivar *et al.,* 1994a

Table 6: Plasmids used in the present study.

Plasmid	Description	Reference/Source
pGEX_*chlL*	Expression vector carrying the *P. marinus chlL* gene cloned into the *Bam*HI/*Sal*I sites of pGEX6P-1, N-terminal glutathione S-transferase (GST) tag and PreScission protease cleavage site, Ap^r	Bröcker *et al.,* 2008b; Uliczka, 2007
pGEX_*chlNB*	Expression vector carrying the *P. marinus chlN* and *chlB* genes cloned into the *Eco*RI/*Sal*I and *Sal*I/*Not*I sites of pGEX6P-1 and an implemented *E. coli*-specific rbs upstream of *chlB*, N-terminal GST-tag and PreScission protease cleavage site fused to ChlN, Ap^r	Bröcker *et al.,* 2008b; Uliczka, 2007
pGEX6P-1 PmNB R48A	Derived from pGEX_*chlNB* by site-directed mutagenesis; amino acid Arg-48 of subunit B changed to alanine, Ap^r	This work
pGEX6P-1 PmNB D290A	Derived from pGEX_*chlNB* by site-directed mutagenesis; amino acid Asp-290 of subunit B changed to alanine, Ap^r	This work
pGEX6P-1 PmNB H394A	Derived from pGEX_*chlNB* by site-directed mutagenesis; amino acid His-394 of subunit B changed to alanine, Ap^r	This work
pGEX-*bchNBL**	Expression vector carrying the *C. tepidum bchN-bchB-bchL* operon cloned into the *Bam*HI/*Not*I sites of pGEX6P-1 and *E. coli*-optimized rbs of *bchB* and *bchL*, N-terminal GST-tag and PreScission protease cleavage site fused to BchN, Ap^r	Bröcker *et al.,* 2008a
pGEX6P-1_bchC	Expression vector carrying the *C. tepidum bchC* gene cloned into the *Bam*HI/*Sal*I sites of pGEX6P-1, N-terminal GST-tag and PreScission protease cleavage site, Ap^r	Kindly provided by Simone Virus
pACYCDuet™-1	Expression vector containing two multiple cloning sites (MCS) with preceeding T7 promotors/*lac* operators and ribosome binding sites (rbs), coding for N-terminal His_6-tag (MCS1) and C-terminal S-tag (MCS2), P15A replicon, *lacI*, Cm^r	Merck Millipore Novagen®
pACYCDuet-1_bchF	pACYCDuet™-1 carrying the *C. tepidum bchF* gene cloned into the *Bam*HI/*Sal*I sites (MCS1), N-terminal His_6-tag fused to BchF, Cm^r	This work
pACYCDuet-1_FC	pACYCDuet™-1 carrying the *C. tepidum bchF* gene (*Bam*HI/*Sal*I sites, MCS1) and the *C. tepidum bchC* gene (*Nde*I/*Xho*I sites, MCS2), N-terminal His_6-tag fused to BchF, C-terminal S-tag fused to BchC, Cm^r	Kindly provided by Simone Virus
pACYCDuet-1_bchC	pACYCDuet™-1 carrying the *C. tepidum bchC* gene (*Nde*I/*Xho*I sites, MCS2), C-terminal S-tag fused to BchC, Cm^r	Peters, 2013

Plasmid	Description	Reference/Source
pGEX6P-1 Ct BchC S39A	Derived from pGEX6P-1_bchC by site-directed mutagenesis; amino acid Ser-39 changed to alanine, Ap^r	This work
pGEX6P-1 Ct BchC S42A	Derived from pGEX6P-1_bchC by site-directed mutagenesis; amino acid Ser-42 changed to alanine, Ap^r	This work
pGEX6P-1 Ct BchC E46A	Derived from pGEX6P-1_bchC by site-directed mutagenesis; amino acid Glu-46 changed to alanine, Ap^r	This work
pGEX6P-1 Ct BchC Y67A	Derived from pGEX6P-1_bchC by site-directed mutagenesis; amino acid Tyr-67 changed to alanine, Ap^r	This work
pGEX6P-1 Ct BchC E68A	Derived from pGEX6P-1_bchC by site-directed mutagenesis; amino acid Glu-68 changed to alanine, Ap^r	This work
pGEX6P-1 Ct BchC H141A	Derived from pGEX6P-1_bchC by site-directed mutagenesis; amino acid His-141 changed to alanine, Ap^r	This work

Table 7 lists the oligonucleotide primers used in this study. Site-directed mutagenesis primers were purchased from biomers.net GmbH, dissolved in deionized water (dH_2O) to a concentration of 100 pmol/µL and stored at -20 °C.

Table 7: Oligonucleotides used in the present study. For site-directed mutagenesis primers, exchanged nucleotides are shown in bold.

Primer name	Sequence (5' - 3')	Source
Site-directed mutagenesis primers		
PmB_R48A_Fwd	CAATGATTGAG**GC**T**C**GAGGCAGTAGAC	this work
PmB_R48A_Rev	GTCTACTGCCTC**G**A**GC**CTCAATCATTG	this work
PmB_D290A_Fwd	CAAAATCAGTCG**CTAG**CAATTACTTGACAGG	this work
PmB_D290A_Rev	CCTGTCAAGTAATTG**CTAG**CGACTGATTTTG	this work
PmB_H394A_Fwd	GTAATAAGCACACC**C**ATG**GC**TGTTCAAGATG	this work
PmB_H394A_Rev	CATCTTGAACA**GC**CAT**G**GGTGTGCTTATTAC	this work
CtBchC_S39A_Fwd	CGAAACCTGGTGG**G**CGTCCATCAGTACC	this work
CtBchC_S39A_Rev	GGTACTGATGGACG**C**CCACCAGGTTTCG	this work
CtBchC_S42A_Fwd	GTGGTCGTCCATC**GCT**ACCGGCACAG	this work
CtBchC_S42A_Rev	CTGTGCCGGT**AGC**GATGGACGACCAC	this work
CtBchC_E46A_Fwd	CATCAGTACCGGCACAG**C**GAAAATGGCCCT CAAC	this work
CtBchC_E46A_Rev	GTTGAGGGCCATTTTC**G**CTGTGCCGGTACT GATG	this work
CtBchC_Y67A_Fwd	CTTCATTCCCGGC**GCT**GAAACCGTTG	this work
CtBchC_Y67A_Rev	CAACGGTTTC**AGC**GCCGGGAATGAAG	this work
CtBchC_E68A_Fwd	CTTCATTCCCGGCTATG**CC**ACCGTTGGGCG CATC	this work
CtBchC_E68A_Rev	GATGCGCCCAACGGT**GG**CATAGCCGGGAAT GAAG	this work
CtBchC_H141A_Fwd	GACGGCGCTG**GC**TATCGTCGATCTC	this work
CtBchC_H141A_Rev	GAGATCGACGATA**GC**CAGCGCCGTC	this work
Sequencing primers		
pGEX6P1rev	CACCGTCATCACCGAAAC	Collection AG Jahn
pGEX3'seq	CCGGGAGCTGCAGTTGTCAGAGG	Collection AG Jahn
pGEX5'seq	GGGCTGGCAAGCCACGTTTGGTG	Collection AG Jahn
pACYCDuetDown1	GATTATGCGGCCGTGTACAA	Collection AG Jahn
pACYCDuetUP2	TTGTACACGGCCGCATAATC	Collection AG Jahn
pGEX-5	CTGGCAAGCCACGTTTGG	GATC Biotech AG
pET-RP	CTAGTTATTGCTCAGCGG	GATC Biotech AG
P.m.bchB1inSeq_rev	GTTTCAGAAGCTCCCCAG	Uliczka, 2007
P.m.bchB2inSeq_rev	CCATCTCCCGACTGTAAG	Uliczka, 2007

2.3 Growth media and media additives

2.3.1 Sterilization of media

If not otherwise indicated, growth media were sterilized by autoclaving prior to use (121 °C, 1 bar excess pressure, 20 min). Due to their heat sensitivity, certain media additives were filter-sterilized through a 0.2 µm pore-sized filter.

2.3.2 Growth media

All *E. coli* strains were grown in Luria Bertani (LB) medium (Sambrook and Russell, 2001). For cultures of *Rhodobacter capsulatus* ZY5, PY medium (Young *et al.,* 1989) supplemented with 1 mM $MgSO_4$, 1 mM $CaCl_2$, 5 µg/mL kanamycin was used (section 2.4.1). *R. capsulatus* CB1200 was grown in RCV 2/3 PY medium. To obtain solid media of LB and PY medium, 1.5 % (w/v) agar-agar was added before sterilization.

LB medium	Yeast extract	5 g/L
	Tryptone/Peptone	10 g/L
	NaCl	5 g/L
PY medium	Yeast extract	3 g/L
	Peptone from casein	3 g/L
RCV 2/3 PY medium	Yeast extract	2 g/L
	Peptone	2 g/L
	in RCV medium	
RCV medium	DL-malic acid	4 g/L
	$(NH_4)_2SO_4$	1 g/L
	D-biotin	15 µg/L
	KH_2PO_4	600 mg/L
	K_2HPO_4	900 mg/L
	Super salts	50 mL/L
	Trace elements	1 mL/L
	adjusted to pH 6.8 with NaOH	
Super salts	EDTA	400 mg/L
	Mg_2SO_4	4 g/L
	$CaCl_2$	1.5 g/L
	$FeSO_4$	240 mg/L
	Thiamine hydrochloride	2 mg/L
Trace elements	$MnSO_4 \times H_2O$	1.59 g/L
	H_3BO_3	2.8 g/L
	$Cu(NO_3)_2 \times 3\ H_2O$	40 mg/L
	$ZnSO_4 \times 7\ H_2O$	240 mg/L
	$NaMoO_4 \times 2\ H_2O$	750 mg/L

2.3.3 Additives

Media additives were prepared as concentrated stock solutions, sterilized and added to the sterile media immediately before use. Because of their heat sensitivity, antibiotics and L-cysteine stock solutions were filter-sterilized through a 0.2 µm pore-sized filter. All other media additive stock solutions were sterilized by autoclaving (121 °C, 1 bar excess pressure, 20 min). Antibiotics stock solutions were stored at -20 °C. L-cysteine stock solutions were prepared directly before use.

Additive	**Solvent**	**Stock concentration**	**Final concentration**
Ampicillin	dH_2O	100 mg/mL	100 µg/mL
Chloramphenicol	70 % (v/v) ethanol	34 mg/mL	34 µg/mL
Kanamycin sulfate	dH_2O	50 mg/mL	5 µg/mL
$CaCl_2$	dH_2O	1 M	1 mM
$MgSO_4$	dH_2O	1 M	1 mM
Fe(III)-citrate	dH_2O	100 mM	1 mM
L-cysteine hydrochloride	dH_2O	100 mM	1 mM

2.4 Microbiological methods

2.4.1 Cultivation of bacteria

Cultivation of E. coli

All *E. coli* cultures were grown in LB medium or LB agar plates (section 2.3.2) supplemented with the appropriate antibiotics. Liquid cultures were prepared for plasmid preparation (5 mL in a test tube) or as pre-cultures (for the inoculation of main cultures for protein production or preparation of competent cells) with volumes up to 30 mL in 100 mL baffled Erlenmeyer flasks by inoculating the respective medium with cells from a glycerol stock or a single colony from an agar plate. Liquid cultures were cultivated over night (37 °C, 200 rpm). For protein production or preparation of competent cells, main cultures were inoculated with the pre-culture (ratio 1:100) and incubated as described in section 2.5.1, 0 and 2.6.1.

Cultivation of R. capsulatus *ZY5*

From a glycerol stock, *R. capsulatus* ZY5 was plated onto a PY agar plate (supplemented with 1 mM $MgSO_4$, 1 mM $CaCl_2$ and 5 µg/mL kanamycin) and was grown at 30 °C for 5 days in the dark. For a liquid culture, 50 mL PY medium with the given additives (section 2.3.2) was inoculated with colonies from the plate and incubated in a 50 mL-Falcon tube in a rotating incubator (agitation, 34 °C, darkness) for four days. For the production of Pchlide, 600 mL PY medium with the above mentioned additives (section 2.3.2) was inoculated

with the pre-culture (ratio 1:30) and incubated in a non-baffled Erlenmeyer flask (34 °C, 3 days, 130 rpm) in a water-bath shaker in the dark. To the main culture, twelve pieces of sterile foam bungs were added, which adsorbed the secreted pigment molecules.

Cultivation of R. capsulatus *CB1200*

The cultivation was kindly performed by S. Virus according to a method described before (Müller *et al.,* 2011) with some modifications. *R. capsulatus* CB1200 cells grown on a RCV 2/3 PY plate were suspended in 100 mL RCV 2/3 PY medium by vortexing. 5 mL of the suspension were incubated (32 °C, 200 rpm, 24 h, darkness). 45 mL of the same medium supplemented with 0.2 % (w/v) Tween® 80 were added and the culture was incubated for another 24 h under the same conditions.

2.4.2 Determination of cell density

Cell growth was monitored by measuring the optical density at 578 nm (OD_{578}) in a spectrophotometer. In cases of high cell density, the culture was diluted with the respective medium, so that values between 0.05 and 1.0 could be measured.

2.4.3 Storage of bacterial cells

Bacterial cells were stored as glycerol stocks at -80 °C. For glycerol stock preparation, a liquid over night culture was carefully mixed with sterile 80 % (w/v) glycerol to a final concentration of 20 % (w/v) glycerol.

2.5 Molecular biological methods

In this study, the *C. tepidum bchF* gene was cloned into the first multiple cloning site (MCS) of pACYCDuet-1, fusing BchF to an N-terminal His_6-tag. The resulting plasmid (pACYCDuet-1_bchF) was used for the heterologous production of His_6-BchF (section 2.6.1).

2.5.1 Preparation of chemically competent *E. coli* cells

Preparation of $CaCl_2$ competent E. coli *cells*

For plasmid propagation, chemically competent *E. coli* DH10B cells were prepared. For recombinant protein production (section 2.6.1), the strains *E. coli* BL21-CodonPlus (DE3)-RIL or *E. coli* BL21 (DE3) were used (section 2.2).

From a pre-culture containing the respective antibiotic if necessary, 100 mL of a main culture was prepared in 500 mL baffled Erlenmeyer flasks. Cultures were grown to an OD_{578} of 0.6 - 0.8 (37 °C, 200 rpm), placed on ice for 10 min and harvested (4 °C, 10 min, 3'220 g). The cell pellet from 50 mL culture was resuspended in 10 ml ice-cold calcium chloride solution, placed on ice for 15 min and sedimented again (4 °C, 10 min, 3'220 g). The resulting cell pellet was resuspended in 1 mL calcium chloride solution and stored in aliquots of 100 µL at -80 °C.

Calcium chloride solution	$CaCl_2$	100 mM
	Glycerol	10 % (w/v)

Preparation of RbCl competent E. coli *cells*

From a pre-culture containing the respective antibiotic if necessary, a main culture was prepared in baffled Erlenmeyer flasks. Cultures were grown to an OD_{578} of 0.5 - 0.6 (37 °C, 180 rpm) and harvested (4 °C, 15 min, 3'830 g). Buffers TFB-I and TFB-II were sterilized by passing through a 0.2 µm pore-sized filter. The pellet from 250 mL culture was resuspended in 50 mL cold TFB-I and sedimented again (4 °C, 10 min, 3'220 g). Subsequently, each pellet was resuspended in 1.5 mL TFB-II and placed on ice for 45 min. Competent cells were stored in aliquots of 200 µL at -80 °C.

TFB-I	Potassium acetate	30 mM
	$CaCl_2$	10 mM
	$MnCl_2$	50 mM
	RbCl	100 mM
	Glycerol	15 % (w/v)
	adjusted to pH 5.8 with acetic acid	
TFB-II	Piperazine-N,N'-bis-(2-ethanesulphonic acid) (PIPES)-HCl pH 6.5	10 mM
	$CaCl_2$	75 mM
	RbCl	10 mM
	Glycerol	15 % (w/v)
	adjusted to pH 6.5 with KOH	

2.5.2 Transformation of chemically competent *E. coli* cells

For plasmid propagation or recombinant protein production, 1 µL plasmid DNA (section 2.5.3), 10 µL of a ligation reaction (section 2.5.8) or 12.5 µL of a site-directed mutagenesis reaction was mixed with 50 - 100 µL (100 µL for ligation

or mutagenesis reactions) competent cells which had been thawed on ice. After incubation (10 - 25 min on ice), cells were subjected to a heat shock (45 sec - 2 min, 42 °C) and subsequently incubated on ice for 2 min. After addition of 250 - 1000 µL LB medium, cells were incubated (37 °C, 35 - 90 min, 500 - 700 rpm). When plasmids from a ligation or mutagenesis reaction were transformed, 100 or 200 µL of the cell suspension was plated on LB agar plates containing the respective antibiotics. Subsequently, the cell suspension was centrifuged (RT, 2 min, 2400 g), the supernatant was discarded and the residual cell suspension was plated out. When intact plasmids were transformed, volumes between 2 and 100 µL were applied.

2.5.3 Preparation of plasmid DNA ("Mini-Prep")

For the preparation of plasmid DNA from *E. coli* DH10B, 4 mL of a pre-culture (section 2.4.1) were centrifuged (room temperature (RT), 2 or 10 min, 12'100 g) and the cell pellet was resuspended in 300 µL P1 (RNAse A added directly before use). In the next step, 300 µL P2 were added and tubes were inverted carefully. After a short incubation (RT, 2 min), 300 µL P3 were added and tubes were inverted again. Precipitated proteins and other insoluble cell components were sedimented (RT, 15 min, 12'100 g), the supernatant containing the soluble plasmid DNA was transferred to a new tube containing 600 µL isopropanol and the sample was mixed thoroughly by vortexing. After a centrifugation step sedimenting the plasmid DNA (RT, 15 min, 12'100 g), the pellet was washed with 400 µL 70 % (v/v) ethanol. After another centrifugation step (RT, 5 min, 12'100 g), pellets were dried (37 °C, 300 rpm) until transparent and dissolved in 50 µL dH_2O.

When the prepared plasmid DNA was used for DNA sequence determination (section 2.5.9), further purification of the plasmids was necessary. For this, 20 µL of a plasmid preparation were applied to the QIAquick® PCR Purification Kit according to the manufacturer's instructions. Elution of the DNA from the columns occurred with 50 µL dH_2O (70 °C) after 10 min incubation on the column.

P1	Tris(hydroxymethyl)-aminomethane (Tris)-HCl pH 8.0	50 mM
	Ethylenediaminetetraacetic acid (EDTA)	10 mM
	RNAse A	100 µg/mL
P2	NaOH	200 mM
	Sodium dodecyl sulfate (SDS)	1 % (w/v)
P3	Potassium acetate adjusted to pH 5.5 with acetic acid	3 M
RNAse A stock	10 mg/mL in 50 % (w/v) glycerol	

2.5.4 Determination of DNA concentration

DNA concentration of prepared plasmids (section 2.5.3) was determined by UV-visible light absorption spectroscopy using the NanoDrop® spectrophotometer. The method is based on the absorption of the aromatic bases at 260 nm (A_{260}). For double-stranded DNA, a concentration of 50 µg/mL has an A_{260} of 1 (Sambrook and Russell, 2001)

2.5.5 Restriction digest of DNA

For the construction of plasmid pACYCDuet-1_bchF, the *bchF* insert (484 bp) was excised from plasmid pACYCDuet-1_FC with the restriction endonucleases *Bam*HI and *Sal*I and ligated into the empty pACYCDuet-1 vector, which was treated with the same enzymes (resulting fragment of 3977 bp). The recommended reaction buffer P3, restriction endonucleases and bovine serum albumin were purchased from New England Biolabs. The reaction was set up according to the manufacturer's instructions in a total volume of 50 µL, using 15 µL plasmid DNA. The restriction digest was performed at 37 °C for 2 h. Subsequently, the whole sample was subjected to agarose gel electrophoresis.

For the newly constructed plasmid pACYCDuet-1_bchF, a control restriction digest was set up after plasmid DNA preparation (section 2.5.3) to screen for positive clones. 2 µL plasmid DNA was used and the reaction was performed in a total volume of 10 µL. The whole sample was subjected to agarose gel electrophoresis. On the basis of the restriction digest, two positive clones were chosen for DNA sequence determination (section 2.5.9).

2.5.6 Agarose gel electrophoresis and visualization of DNA bands

In order to purify the digested DNA or to analyze the outcome of the control restriction digest (section 2.5.5) or gel extraction (section 2.5.7), agarose gel electrophoresis was performed. For this, samples were supplemented with 5x DNA loading dye. Agarose gels were prepared by dissolving agarose in TAE buffer to a concentration of 1 % (w/v). The complete sample volume was applied to the gel and electrophoresis was performed at 80 - 100 V with TAE buffer as running buffer. The DNA standard GeneRuler™ DNA Ladder Mix was used. For DNA preparation from the gel, the gel was stained with GelStar™ by preparing a 10'000x dilution in TAE buffer and incubation the gel for 1.5 h in the dark. The DNA bands (*bchF* insert: 484 bp, open pACYCDuet-1 vector: 3977 bp) were visible upon excitation of the intercalating dye with a blue-light transilluminator and could be excised from the gel. The excised gel pieces were weighed and stored at -20 °C over night or processed immediately. Analytical agarose gels were stained with ethidium bromide solution and detection occurred with UV light.

TAE buffer	Tris	40 mM
	Acetic acid	20 mM
	EDTA pH 8.0	1 mM
DNA loading dye (5x)	Bromophenol blue	350 µM
	Xylen Cyanol FF	450 µM
	Glycerol	50 % (w/v)
Ethidium bromide solution	Ethidium bromide	10 µg/mL

2.5.7 Gel extraction of DNA fragments

Extraction of the DNA fragments from the excised gel pieces (section 2.5.6) was performed using the QIAquick® Gel Extraction Kit according to the manufacturer's instructions. Elution of the DNA from the columns occurred with 30 µL dH_2O (70 °C). To assess the success of the gel extraction, agarose gel electrophoresis was performed using 2 µL sample (section 2.5.6).

2.5.8 Ligation

Ligation of DNA fragments was performed using the T4 DNA ligase according to the manufacturer's instructions. Reactions were set up in a total volume of 20 µL and were incubated at RT for 1.5 h. Three different volume ratios of the open vector and the insert were applied (1, 2 or 2.5 µL vector DNA and 2, 1 or 2.5 µL insert DNA). A control reaction lacking the insert was prepared. After ligation, transformation into competent *E. coli* cells was performed (section 2.5.2).

2.5.9 DNA sequencing

DNA sequence determination was performed by the GATC Biotech AG according to the method described by Sanger *et al.,* 1977, using the oligonucleotide primers given in Table 7. Plasmid DNA and primers were provided within the concentration range suggested by the company. The resulting sequences were analyzed with the Lasergene software package (DNASTAR® Inc.).

2.5.10 Site-directed mutagenesis

For the site-directed mutagenesis of DPOR subunits ChlB from *P marinus* (based on plasmid pGEX_*chlNB*, ~8 ng/µL) and BchC (based on plasmid pGEX6P-1_bchC, 18 ng/µL), the QuikChange™ Site-directed Mutagenesis Kit was used according to the manufacturer's instructions, employing the oligonucleotide primers listed in Table 7. The primers carry the desired mutated DNA sequences. During the PCR employed for mutagenesis, *PfuTurbo*® DNA

polymerase replicates the entire plasmid, thus incorporating the mutated primers. Subsequently, samples are treated with the restriction endonuclease *Dpn*I which is specific for methylated DNA and thus digests the non-mutated template plasmid (methylated by the *E. coli* host strain). The mutated plasmids are discriminated from the templates by the lack of the DNA methylation pattern.

12.5 µL of the *Dpn*I-treated PCR reaction were transformed into *E. coli* DH10B cells (section 2.5.2).

Component	**Volume**
Reaction buffer (10x)	2.5 µL
Template DNA	1 µL
Forward primer	62.5 ng
Reverse primer	62.5 ng
Desoxynucleoside triphosphate (dNTP) mix	0.5 µL
PfuTurbo® DNA polymerase (2.5 U/µL)	0.5 µL
dH_2O	add to 25 µL

2.6 Protein biochemical methods

The enzymes DPOR (from *P. marinus* and *C. tepidum*), BchF and BchC (both from *C. tepidum*) were recombinantly produced in *E. coli* host strains. Subsequently, the proteins were purified and subjected to activity assays or solubilization experiments. Mutant proteins of *P. marinus* DPOR and *C. tepidum* BchC were produced and purified analogously to the respective wild-type proteins.

2.6.1 Recombinant protein production in *E. coli*

In the following sections, the production of recombinant proteins in *E. coli* is described. All buffers were prepared from concentrated stock solutions, which were sterilized by autoclaving for long-term storage. Stock solutions and final buffers were prepared with dH_2O unless indicated otherwise and the pH of buffer-1 and buffer-2 was adjusted after dilution of the stock solutions. In the case of buffer-3, the pH was not adjusted after dilution. As buffer-3 was used for the recombinant protein production of the oxygen-sensitive DPOR enzyme, it was stored in gas-tight bottles and subjected to repeated cycles of vacuum and flushing with dinitrogen gas in order to remove dissolved oxygen from the solution before use.

Buffer-1	Tris-HCl pH 8.0	50 mM
	adjusted to pH 8.0 with HCl	
Buffer-2	Tris-HCl pH 8.0	50 mM
	NaCl	500 mM
	adjusted to pH 8.0 with HCl	
Buffer-3	N-2-hydroxyethyl piperazine-N'-2-ethane sulfonic acid (HEPES)-NaOH pH 7.5	100 mM
	NaCl	150 mM
	$MgCl_2$	10 mM

Production of DPOR subunits from P. marinus

The production of subunits L, N and B from *P. marinus* was adopted from Bröcker *et al.,* 2008b: plasmids pGEX_*chlL* and pGEX_*chlNB* were transformed into *E. coli* BL21-CodonPlus (DE3)-RIL cells (section 2.5.2). 500 mL LB medium containing ampicillin, chloramphenicol, L-cysteine and Fe(III)-citrate (section 2.3.3) were inoculated with an overnight *E. coli* culture (section 2.4.1). Cells were grown aerobically to an OD_{578} of approx. 0.5 (37 °C, 200 rpm). Subsequently, cells were shifted to 25 °C and incubated for 40 - 45 min without agitation before protein production was induced with 25 µM isopropyl *β*-D-thiogalactopyranoside (IPTG). In the case of pGEX_*chlL* produced for activity assays, additional 250 µL ampicillin were added to each culture. Cultivation was continued over night (15 - 19 h, 25 °C, 160 or 170 rpm). Subsequently, 1.7 mM sodium dithionite (SDT) was added to the cultures, cells were transferred to an anaerobic chamber (95 % N_2, 5 % H_2, <1 parts per million (ppm) O_2) and

incubated for 1 - 3 h without agitation at 17 or 20 °C. Cell harvesting was performed in gas-tight tubes (15 min, 4 °C, 3'000 g or 1'860 g for the crystallization experiments). Under anoxic conditions, the pellet from 1 L culture was resuspended in 15 mL (for crystallization experiments, section 2.6.2) or 20 mL (for activity assay experiments, section 2.6.2) anoxic buffer-3 and stored at -20 °C.

Production of DPOR subunits from C. tepidum

The production of the DPOR subunits N, B and L from *C. tepidum* occurred in *E. coli* BL21-CodonPlus (DE3)-RIL cells carrying plasmid pGEX-*bchNBL** based on Bröcker *et al.,* 2008a: 500 mL LB medium containing ampicillin, chloramphenicol, L-cysteine and Fe(III)-citrate (section 2.3.3) were inoculated with an overnight *E. coli* culture (section 2.4.1). Cells were grown aerobically to an OD_{578} of 0.5 - 0.6 (37 °C, 200 rpm) before protein expression was induced with 50 µM IPTG. Cultivation was continued over night (15 - 16 h, 17 °C, 160 - 170 rpm). Subsequently, 1.7 mM SDT was added to the cultures, cells were transferred to an anaerobic chamber (95 % N_2, 5 % H_2, <1 ppm O_2, Coy Laboratories) and incubated for 1 - 2.5 h without agitation at 17 or 20 °C. Cell harvesting was performed in gas-tight tubes (15 min, 4 °C, 4'000 g). Under anoxic conditions, the pellet from 500 mL culture was resuspended in 10 mL anoxic buffer-3 and stored at -20 °C.

Production of BchF and BchC from C. tepidum

The production of His_6-BchF (plasmid pACYCDuet-1_bchF), BchC-S (plasmid pACYCDuet-1_bchC) and both His_6-BchF and BchC-S (co-expressed from plasmid pACYCDuet-1_FC) or GST-BchC (plasmid pGEX6P-1_bchC) occurred in *E. coli* BL21 (DE3). The pGEX6P-1_bchC construct was chosen for the production and subsequent purification of BchC because the GST fusion tag can easily been removed from the protein of interest. In an earlier work, the optimal conditions for protein production and affinity chromatography had already been elucidated (Peters, 2013) and were retained throughout this study with minor modifications. 500 mL LB medium containing chloramphenicol (pACYC-constructs) or ampicillin (pGEX-construct) were inoculated with the respective overnight pre-culture (section 2.4.1). Cells were grown aerobically to an OD_{578} of approx. 0.5 at (37 °C, 200 rpm) before protein expression was induced with 300 µM IPTG for the pACYC constructs (50 µM for pGEX6P-1_bchC). After 3 h (14 h) of cultivation at 37 °C (17 °C) and 200 rpm (180 rpm), cells were harvested by centrifugation (20 min, 4 °C, 2'000 g for the pACYC constructs or 15 min, 4 °C, 3'000 g for pGEX6P-1_bchC), cell pellets were kept on ice, resuspended in 10 mL ice-cold buffer-1 per 500 mL culture (20 mL per liter culture of buffer-2) and stored at -20 °C.

2.6.2 Further processing of recombinantly produced proteins

All further steps involving cells overexpressing DPOR subunits were performed in an anaerobic chamber (95 % N_2, 5 % H_2, <1 ppm O_2). Cell pellets containing recombinantly produced proteins (section 2.6.1) were thawed on ice over night and cell disruption was performed by a single passage through a French® Press (16'000 pounds per square inch (p.s.i.) working pressure).

DPOR from P. marinus

DPOR subunits were either prepared for crystallization experiments (section 2.6.10) or for the use in activity assays (section 2.8.1). The preparations were based on the descriptions by Bröcker *et al.,* 2010b; Bröcker *et al.,* 2008b; Moser and Bröcker, 2011.

Preparation for crystallization experiments - First, subunits N and B were purified *via* affinity chromatography using the N-terminal GST fusion tag of subunit N. Subunit B, which had been co-expressed from the same plasmid (section 2.6.1), was co-purified with subunit N due to the tight interaction of the two proteins. For this, the resuspended cells from 10 L of *E. coli* culture were supplemented with 20 µL Benzonase® prior to cell disruption, disrupted by French Press treatment and subjected to ultracentrifugation (4 °C, 90 min, 167'000 g). The supernatant of this centrifugation was applied to 3x 7 mL Protino® Glutathione Agarose 4B equilibrated with buffer-3 at 17 °C. The first column flow-through was applied to the column once more to increase protein binding. After washing with 7 column volumes (CV) of buffer-3, the column was closed and 600 U PreScission protease were added to each column together with 1 CV of buffer-3. After repeated careful mixing with the resin for about 1 h, incubation was continued over night. Subsequently, the protein was drained from the column, and remaining protein was washed out with 2x 1 CV of buffer-3 per column. Because the columns retained a brownish color, additional 200 U of PreScission protease were added, incubation was continued for 4 h, the protein was drained from the column and washed out with 5 mL additional buffer-3. The combined eluates were concentrated to 9.2 mg/mL (section 2.6.9), frozen in liquid nitrogen and stored at -80 °C.

For the subsequent purification of subunit L *via* its N-terminal GST-tag, the resuspended cells from 10 L of *E. coli* culture were supplemented with 20 µL Benzonase® prior to cell disruption, disrupted by French Press treatment and subjected to ultracentrifugation (4 °C, 90 min, 167'000 g). The supernatant of this centrifugation was applied to 3x 7 mL Protino® Glutathione Agarose 4B equilibrated with buffer-3 at 17 °C. The first column flow-through was applied to the column once more and the column was washed with 7 CV of buffer-3. Subsequently, the amount of column-bound protein was determined using 10 µL resin from each column (section 2.6.3). A total of 51 mg (431 nmol) of $(GST\text{-}L)_2$ protein was purified and immobilized on the columns.

Next, the formation of the DPOR complex was initiated. For this, the purified DPOR subunits N and B, the DPOR substrate Pchlide and an analog of the

transition state of ATP hydrolysis ($MgADP•AlF_4^-$) were added to the L_2-binding columns.

The analog $MgADP•AlF_4^-$ was prepared *in situ* in complex buffer containing 10 mM NaADP (100 mM stock in buffer-3, freshly prepared), 2 mM $AlCl_3$ (50 mM stock in buffer-3) and 50 mM NaF (200 mM stock in dH_2O), which was incubated for 30 min. 24 mL of this solution was supplemented with 54 mg (259 nmol) purified $(NB)_2$ and 1.3 µmol Pchlide. The DPOR complex formation was initiated by adding a total of 10 mL of the resulting solution to each L-loaded column (each column was loaded with about 17 mg (144 nmol) of $(GST-L)_2$). These 10 mL were slowly soaked into the column material in portions of 3 - 4 mL and a 10 - 15 min incubation after each portion. When the column material was completely green, i.e. completely soaked with the solution, the column was closed and incubated for 1 h. After the application of 7 CV complex washing buffer, 600 U PreScission protease were added to each column. After repeated careful mixing with the resin for about 1 h, incubation was continued over night. Subsequently, the green colored protein was washed from the colums with 3x 1 CV of complex washing buffer per column. Because the columns retained a green color, additional 200 U of PreScission protease were added, incubation was continued for 4 h and the protein was eluted with 1 CV complex washing buffer. The combined eluates were concentrated to 9.5 mg/mL (section 2.6.9) and stored at 4 °C.

Complex buffer	HEPES-NaOH pH 7.5	100 mM
	NaCl	150 mM
	$MgCl_2$	10 mM
	NaF	50 mM
	$AlCl_3$	2 mM
	NaADP	10 mM
Complex washing buffer	HEPES-NaOH pH 7.5	100 mM
	NaCl	150 mM
	$MgCl_2$	10 mM
	NaF	50 mM
	$AlCl_3$	2 mM

Preparation for activity assays - When the protein subunits were processed for the use in *in vitro* activity assays, 5 mM dithiothreitol (DTT) were added to the cell suspension before cell disruption. Also, buffer-4 was used for protein preparation, which was freshly prepared by adding 5 mM DTT to buffer-3. After cell disruption, 2.5 µL Benzonase® were added to 20 mL of the crude cellular extract containing subunits N and B, because it was used for subsequent affinity chromatography. The disrupted cells containing subunits N and B or L were subjected to ultracentrifugation (4 °C, 65 min, 130'000 g).

The resulting cell-free extract from 500 mL *E. coli* culture containing subunit L was stored at 4 °C for several hours until used for activity assays (section 2.8.1).

The resulting cell-free extract from 1 L *E. coli* culture containing subunits N and B was subjected to affinity chromatography, purifying subunit N *via* its N-terminal GST fusion tag and co-purifying subunit B with subunit N. For this, it

was applied to 1 mL Protino® Glutathione Agarose 4B equilibrated with buffer-4 at 17 or 20 °C. The first column flow-through was applied to the column once more and the resin was repeatedly carefully mixed to increase protein binding. After washing with 10 CV of buffer-4, the column was closed and 1.2 CV of buffer-4 and 60 U PreScission protease were added to the column. After repeated careful mixing with the resin, incubation was continued over night. Subsequently, the resin was mixed again, incubation was continued for 1 h and the protein was drained from the column. Remaining protein was washed out with 2 x 1 CV of buffer-4. The protein solution was stored at 4 °C until used for activity assays (section 2.8.1).

Buffer-4	HEPES-NaOH pH 7.5	100 mM
	NaCl	150 mM
	$MgCl_2$	10 mM
	DTT	5 mM

DPOR from C. tepidum

Crude cellular extract containing all three DPOR subunits from *C. tepidum* (produced from plasmid pGEX-*bchNBL**) was subjected to ultracentrifugation (4 °C, 65 min, 130'000 g) to yield cell-free extract containing the soluble proteins. This extract was stored in 500 µL aliquots in anaerobic bottles at -20 °C for up to three months.

BchF and BchC from C. tepidum *expressed from pACYCDuet vectors*

Crude cellular extracts of cultures overproducing His_6-BchF (plasmid pACYCDuet-1_bchF), BchC-S (plasmid pACYCDuet-1_bchC) and both His_6-BchF and BchC-S (plasmid pACYCDuet-1_FC) were stored on ice for up to 6 h for use in activity assays (section 2.8.3). Alternatively, the crude cellular extract containing His_6-BchF was used for solubilization experiments.

In order to solubilize the His_6-BchF fusion protein (produced from pACYCDuet-1_bchF) from the total *E. coli* membrane fraction, the latter was prepared by differential centrifugation. This method is based on the separation of particles due to their different sedimentation velocities. A drawback of the method is the contamination of fast sedimenting particles with slow sedimenting particles close to the bottom of the centrifugation tube. The procedure was based on the description of the preparation of the total *P. aeruginosa* membrane fraction (Arendt *et al.,* 2013). First, 10 mL of the crude cellular extract was centrifuged with low speed (4 °C, 60 min, 4'000 g) to sediment remaining unbroken cells and potential inclusion bodies. The resulting supernatant was subjected to ultracentrifugation (4 °C, 60 min, 146'000 g) to sediment the total membrane fraction. The supernatant from this centrifugation step was discarded, the membrane pellet was washed twice with 3 mL ice-cold buffer-5 and subsequently, membrane proteins were solubilized by stirring at 4 °C for 2 h in 7 mL solubilization buffer (Klein *et al.,* 2009). A subsequent ultracentrifugation step (4 °C, 60 min, 146'000 g) yielded the solubilized membrane proteins in the supernatant, which were stored on ice until further use.

Buffer-5	Tris-HCl pH 8.0	50 mM
	$MgCl_2$	20 mM
	adjusted to pH 8.0 with HCl	
Solubilization buffer	Tris-HCl pH 8.0	50 mM
	$MgCl_2$	20 mM
	adjusted to pH 8.0 with HCl	
	Triton™ X-100	0.6 % (v/v)

BchC from C. tepidum *equipped with N-terminal GST-tag*

When cells overproducing GST-BchC from *C. tepidum* were processed, 2 µL Benzonase® was added to the resuspended cells from 1 L of *E. coli* culture before disruption. The crude cellular extract was subjected to ultracentrifugation (4 °C, 65 min, 130'000 g) to yield a cell-free extract containing the soluble proteins, as described before by Peters, 2013. The cell-free BchC-containing extract was subjected to affinity chromatography *via* its N-terminal GST fusion tag, using 1 mL Protino® Glutathione Agarose 4B equilibrated with buffer-2 at RT. The first column flow-through was applied to the column once more to increase protein binding. After washing with 10 CV of buffer-2, the column was closed and 1.5 CV of buffer-2 and 60 U PreScission protease were added to the column. After repeated careful mixing with the resin over 60 – 90 min, the protein was drained from the column, and remaining protein was washed out with 2x 1 CV of buffer-2. The protein solution was stored at 4 °C.

2.6.3 Determination of protein concentration

The concentration of affinity-purified proteins was determined using the Bradford Reagent according to the manufacturer's instructions. The method is based on the complex formation of the dye Coomassie Brilliant Blue G with the protein, which is accompanied by an absorption shift of the dye from 465 to 595 nm (Bradford, 1976). Thus, from the absorption at 595 nm the protein concentration can be calculated after calibration with a standard. If necessary, protein samples were diluted with their respective buffer before the assay. As a standard, bovine serum albumin was used, dissolved in the respective protein buffer. The absorption of the samples was either measured in polystyrene cuvettes or in a 96-well plate. During the preparation of the octameric DPOR complex, the amount of column-bound L protein was determined using 10 µL resin. The resin was suspended in 20 µL of the respective buffer and applied to the colorimetric assay.

2.6.4 Discontinuous SDS polyacrylamide gelelectrophoresis

Discontinuous SDS-polyacrylamide gelelectrophoresis (SDS-PAGE) was used to analyze protein samples by separating the denatured proteins in a polyacrylamide gel matrix according to their molecular mass (Laemmli, 1970;

Sambrook and Russell, 2001). For denaturation, protein samples were supplemented with the same volume of 2x SDS-PAGE loading buffer and incubated (10 min, 95 °C). Samples collected during the solubilization of BchF from the total membrane fraction of *E. coli* were treated at 40 °C for 30 min to reduce protein aggregation (Klein *et al.,* 2009). The Unstained protein molecular weight marker was used for gels which were treated with staining solution after gel electrophoresis. The PageRuler™ Prestained Protein Ladder was used for gels subsequently subjected to Western blot analysis (section 0). Gels were run at 45 mA per gel until the bromophenol blue band had passed the gel. Subsequently, the gel was stained and destained with the respective solutions until the protein bands were visible.

Running gel	Rotiphorese® Gel 30	2 mL
(12 % (w/v) acrylamide)	1.5 M Tris-HCl pH 8.8, 0.4 % (w/v) SDS	1.25 mL
	dH_2O	1.75 mL
	10 % (w/v) ammoniumperoxodisulfate	50 µL
	N,N,N',N'-tetramethylethylenediamine	5 µL
Stacking gel	Rotiphorese® Gel 30	0.5 mL
(6 % (w/v) acrylamide)	0.5 M Tris-HCl pH 6.8, 0.4 % (w/v) SDS	0.625 mL
	dH_2O	1.375 mL
	10 % (w/v) ammoniumperoxodisulfate	25 µL
	N,N,N',N'-tetramethylethylenediamine	2.5 µL
2x SDS-PAGE loading buffer	Tris-HCl pH 6.8	100 mM
	Glycerol	40 % (w/v)
	β-Mercaptoethanol	2 % (v/v)
	SDS	3.2 % (w/v)
	Bromophenol blue	0.2 % (w/v)
1x Running buffer	Tris	25 mM
	Glycine	192 mM
	SDS	0.1 % (w/v)
Staining solution	Ethanol	30 % (v/v)
	Acetic acid	10 % (v/v)
	Coomassie Brilliant Blue G250	0.25 % (w/v)
Destaining solution	Ethanol	30 % (v/v)
	Acetic acid	10 % (v/v)

2.6.5 Western Blot analysis

For further analysis, samples from the solubilization experiments (section 2.6.2) were subjected to Western blotting based on the method described by Towbin *et al.,* 1979. The N-terminal His_6-tag fused to BchF provided the possibility to specifically detect the His_6-BchF fusion protein. For this, the samples were subjected to SDS-PAGE (section 2.6.4). Subsequently, the gel was equilibrated in Towbin buffer for 15 min. A piece of PVDF membrane was activated in 100 % methanol for 15 min and equilibrated in Towbin buffer. The separated proteins were transferred from the polyacrylamide gel to the PVDF membrane by semi-dry electroblotting (10 V, 1 h per gel). Subsequently, the membrane was

incubated in blocking buffer (1 h, RT, agitation, then 4 °C over night). After consecutive washing steps with phosphate-buffered saline (PBS)-Tween (3x 5 min, RT, agitation), the primary antibody targeted against the His_6-tag was applied (2'000x dilution in blocking buffer, 1 h, RT, agitation). After consecutive washing steps with washing buffer (3x 10 min, RT, agitation), the secondary antibody fused to the enzyme alkaline phosphatase (AP) was applied (5'000x dilution in washing buffer, 1 h, RT, agitation). AP catalyzes the formation of the dye diformazan from the substrates Nitro blue tetrazolium (NBT) and 5-Bromo-4-chloro-3-indolyl phosphate (BCIP) as described by Blake *et al.,* 1984. For this, the membrane was washed with PBS-Tween (3x 10 min, RT, agitation) and agitated in AP-buffer for 10 min. Next, fresh AP-buffer was applied, supplemented with 660 µg/mL NBT and 82.5 µg/mL BCIP and agitated. The color formation was stopped by rinsing the membrane with water when protein bands were visible. The membrane was dried and stored in the dark.

Towbin buffer	Tris-HCl pH 9.5 Glycin	25 mM 192 mM
1x PBS	NaCl KCl Na_2HPO_4 KH_2PO_4	137 mM 2,7 mM 10 mM 2 mM
PBS-Tween	Tween® 20 in 1x PBS	0.1 % (v/v)
Blocking buffer	Skim milk powder in PBS-Tween	5 % (w/v)
Washing buffer	Skim milk powder in PBS-Tween	0.5 % (w/v)
AP-buffer	Tris-HCl pH 9.5 NaCl $MgCl_2$	100 mM 100 mM 5 mM
NBT solution	NBT in 70 % (v/v) dimethylformamide	100 mg/mL
BCIP solution	BCIP in dimethylformamide	50 mg/mL

2.6.6 N-terminal amino acid sequence determination

The identity of the purified DPOR subunits, BchC and of the solubilized His_6-BchF fusion protein was confirmed by N-terminal amino acid sequencing (Edman degradation). The method is based on the stepwise derivatization of the N-terminus with phenylisothiocyanate and subsequent degradation and identification of the derivatized N-terminal amino acid.

For this, protein samples were subjected to SDS-PAGE (section 2.6.4) and the separated proteins were transferred to a membrane by semi-dry electroblotting

(section 0). After the transfer, the membrane was stained with Ponceau S solution and the background destained with dH_2O. The protein band of interest was excised from the membrane and subjected to Edman degradation, which was kindly performed by Beate Jaschok-Kentner, Helmholtz Centre for Infection Research.

In the case of His_6-BchF, a sample of the solubilized protein mixed with 2x SDS sample buffer (section 2.6.4) was used directly for the N-terminal amino acid sequence determination without preceding SDS-PAGE and electroblotting.

Ponceau S solution	Ponceau S	0.4 % (w/v)
	Trichloroacetic acid	368 mM
	Sulfosalicylic acid	240 mM

2.6.7 Chelator treatment of BchC

In order to remove any putative divalent cations involved in BchC function, the purified protein (combined elution fractions 1 and 2 from a typical protein purification, section 2.6.2) was treated with 10 or 100 mM EDTA or ethyleneglycol bis(2-aminoethylether)-N,N,N′,N′-tetraacetic acid (EGTA) (75 min, 48 °C), which was added to the protein solution. The elevated temperature represents the optimal growth temperature of *C. tepidum* (Eisen *et al.,* 2002) and was chosen based on earlier studies with zinc-dependent MDRs in which their metal dependence was elucidated (Bashir *et al.,* 2009; Machielsen and van der Oost, 2006; Magonet *et al.,* 1992). In these studies, the investigated enzymes were efficiently treated with chelating substances at elevated temperatures to also remove catalytic zinc ions. After incubation, samples were centrifuged (RT, 10 min, 12'100 g) to remove precipitated protein and the remaining protein solution was applied to an 'illustra' NAP-5 column according to the manufacturer's instructions to remove the chelating agents. The protein was eluted with buffer-2, concentrated to about 20 µM with Amicon® Ultra-0.5 Centrifugal Filter Devices (10'000 nominal molecular weight limit (NMWL), section 2.6.9) and stored at 4 °C. Of the chelator-treated protein, 800 pmol were applied to activity assays (section 2.8.4).

2.6.8 Inductively coupled plasma mass spectrometry

The zinc ion (Zn^{2+}) content of the purified BchC protein (section 2.6.2) was determined by inductively coupled plasma mass spectrometry (ICP-MS) (performed by Currenta GmbH & Co OHG, Leverkusen, Germany). As a negative control, the C-terminal domain of zinc-independent alanyl-phosphatidylglycerol synthase (A-$PGS_{543-881}$) from *P. aeruginosa* was used (Hebecker *et al.,* 2011). The C-terminal A-PGS domain was produced with an N-terminal GST-tag as described by Hebecker *et al.,* 2011, using the host strain *E. coli* BL21 (DE3) pGEX-6P-1/PA0920Δaa1-542. BchC was produced as described (section 2.6.1). For both protein productions, 20 mL buffer-6 were used to resuspend the cell pellet from 1 L *E. coli* culture. Subsequently, the suspension was centrifuged again (4 °C, 3'220 g, 10 min) and the pellet was

stored at -20 °C. For protein purification, the pellet was resuspended in 20 mL buffer-6 and protein purification of both proteins was performed as described in section 2.6.2 using buffer-6 instead of buffer-2. 1 mL protein solution was used for the analysis. Production and purification of the two proteins was kindly performed by S. Virus.

Buffer-6	Tris-HCl pH 8.0	50 mM
	NaCl	500 mM
	Glycerol	5 % (w/v)

2.6.9 Protein concentration

If necessary, purified proteins were concentrated by ultrafiltration. For the concentration of the purified DPOR subunits N and B and the octameric DPOR complex (section 2.6.2), an Amicon® 8050 stirred cell equipped with a polyethersulfone ultrafiltration disc (30'000 NMWL) was used. The stirred cell was operated under anoxic conditions. The ultrafiltration disc was equilibrated in the respective protein buffer before use to facilitate the removal of molecular oxygen from the disc. When the volume of the octameric DPOR complex protein solution became too low, Amicon® Ultra-0.5 Centrifugal Filter Devices (30'000 NMWL) were used for further concentration according to the manufacturer's instructions.

Chelator-treated BchC protein solutions (section 2.6.7) were concentrated with Amicon® Ultra-0.5 Centrifugal Filter Devices (10'000 NMWL) according to the manufacturer's instructions.

2.6.10 Protein crystallization

A common method for the production of protein crystals is the vapour diffusion method. For this, a reservoir solution is prepared, which usually contains a buffer and a precipitant (e.g. ammonium sulfate or polyethylene glycols, Rhodes, 2006). Other additives can be added to the solution to vary the crystallization conditions. A small volume of this reservoir is mixed with an equally small volume of the concentrated protein solution and the drop is placed in a sealed compartment together with an excess volume of the reservoir solution. The drop can either be "hanging" from the lid of the compartment or "sitting" in a well above the reservoir. Due to the concentration differences of the solutes between the drop and the reservoir solution, the solvent slowly evaporates from the drop, leading to an increase in protein and precipitant concentration until the system has reached equilibrium. This process goes along with the supersaturation of the protein solution which then facilitates nucleation, i.e. the formation of initial small protein crystals. Subsequently, crystals can grow, lowering the concentration of dissolved protein in the drop.

Preparation of P. marinus *DPOR crystals*

The concentrated DPOR complex (section 2.6.2) was used for sitting drop crystallization trials. The commercially available crystallization screens JCSG Core I, PEG I, PEG II, MPD and PACT were applied, which comprised 96 different reservoir solutions each. The 96-well plates filled with reservoir were obtained from the Helmholtz Centre for Infection Research. The plates were transferred to an anaerobic work station at 17 °C and the sealing tape was carefully removed to facilitate gas exchange between the solutions and the anoxic environment. In total, the plates stood open for about 8 h before crystallization, but they were closed repeatedly in between to prevent evaporation of the reservoir solutions. Each sitting drop was prepared by carefully mixing 1 µL reservoir solution with 1 µL of the DPOR complex solution.

For the preparation of the crystallization experiments, the protein solution was diluted to a concentration of 7.5 mg/mL with complex washing buffer (section 2.6.2) in order to prevent immediate protein precipitation in the crystallization drop.

Plates were sealed and stored in the dark. In regular intervals, wells were checked for protein crystals and photographs were taken with the help of a camera attached to a microscope.

Crystals of sufficient size were removed from the well and soaked in solution-1 for cryoprotection and to stabilize the octameric DPOR complex. Subsequently, crystals were stored in liquid nitrogen.

Solution-1	HEPES-NaOH pH 7.5	142 mM
	NaCl	62 mM
	$MgCl_2$	4 mM
	NaF	10 mM
	$AlCl_3$	208 µM
	Glycerol	15 % (w/v)
	PEG 8000	13 % (w/v)
	DTT	5 mM
	Pchlide	10 µM
	Dimethyl sulfoxide (DMSO)	0.17 % (v/v)

Data collection and structure determination

In a protein crystal, protein molecules are arranged in a three-dimensional crystal lattice. The smallest unit which represents all the properties of the whole crystal is called the unit cell. It is defined by the length of its three edges a, b and c and the angles α, β and γ (Rhodes, 2006). The crystal is formed by the three-dimensional packing of unit cells. Within a unit cell, the asymmetric unit is defined. From this group of atoms, the unit cell is generated by applying the crystallographic symmetry operations (defined by the space group) (Rupp, 2010).

When protein crystals are exposed to X-ray radiation, scattering of the X-ray beams by the electrons of the protein atoms takes place. The three-dimensional

arrangement of the atoms leads to interference of the scattered beams, resulting in a specific scattering pattern. The emerging scattering pattern can also be explained by the idea that the incident X-ray beams are reflected by planes which are formed by the regular arrangement of the unit cells. Therefore, the emerging beams are called “reflections”. The pattern and the intensity of the individual reflections can be detected.

In order to obtain a model of the protein molecule from the X-ray diffraction experiment, the electron density map of the molecule has to be calculated from the recorded reflections. However, the intensity of the reflections does not provide sufficient information to draw conclusions regarding the position of the scattering centers of the protein molecule. Additionally, the phase of each reflection has to be known, however, this information is lost during the X-ray diffraction experiment (“phase problem”). Thus, other methods (i.e. isomorphous replacement, anomalous dispersion, molecular replacement) have been developed to obtain the phase information. Whereas isomorphous replacement and anomalous dispersion are based on the reduction of the number of scattering atoms in the unit cell (by the introduction of heavy metal ions or selenomethionine at defined sites of the protein), the method of molecular replacement is based on the extraction of the phase information from known protein structures which are similar to the structure to be solved. This phase information can be used to calculate initial electron density for the unknown protein structure.

In the present study, data collection and processing up to the final structure was performed by Dr. Jörn Kraußе, Helmholtz Centre for Infection Research. A single crystal was used for the diffraction experiment. X-ray diffraction data were collected at beamline 14.2 of BESSY II (Helmholtz Centre Berlin) at a wavelength of 0.91841 Å at 100 K. Data were processed in space group C2 with XDS and scaled with XSCALE (Kabsch, 2010). The space group describes the symmetry elements of a unit cell: space group C2 implies a monoclinic centered crystal system with a two-fold rotational symmetry axis. The upper resolution limits were assessed through the observation of $I/\sigma I$ (signal-to-noise ratio) and R_{merge}. Both parameters are, apart from completeness and redundancy, means to assess the quality of the recorded diffraction data (Wlodawer *et al.,* 2008). Data were extended to 2.1 Å resolution along a* and c* but only to 2.8 Å along b*. Thus, the initial dataset showed anisotropy and was anisotropy-corrected with the anisotropy correction server (Strong *et al.,* 2006) in order to include reflections from the higher resolution shells. The resulting dataset showed reasonable completeness to 2.6 Å resolution. However, incomplete data to 2.15 Å resolution were included in later calculations to obtain more detailed electron density maps.

Molecular replacement with phenix.auto-mr (Adams *et al.,* 2010) was used for model building based on the anisotropy-corrected dataset, using a subunit L monomer from *R. sphaeroides* (PDB ID 3FWY) and the N and B monomers from *T. elongatus* (PDB ID 2XDQ) as search models after pruning with chainsaw (Collaborative Computational Project, Number 4, 1994). The obtained initial model and electron density was improved using the program phenix.mr_rosetta (DiMaio *et al.,* 2011), manually rebuilt in COOT (Emsley and Cowtan, 2004) and refined with phenix.refine (Adams *et al.,* 2010).

Finally, the structure model of the substrate-bound DPOR complex from *P. marinus* was obtained and the structure was deposited in the protein data bank (PDB ID 2YNM).

2.6.11 Bioinformatic tools

Amino acid sequence alignments were computed with the default settings of the programs ClustalW (version 2.1, Goujon *et al.,* 2010; Larkin *et al.,* 2007) or Clustal Omega (versions 1.2.0 and 1.2.1, Goujon *et al.,* 2010; McWilliam *et al.,* 2013; Sievers *et al.,* 2011). ClustalW was used for the alignment of the DPOR subunits L, N and B, using the protein sequences from the following organisms: *Anabaena variabilis*, *Chlorobaculum parvum*, *C. tepidum*, *Chlorobium chlorochromatii*, *Chlorobium ferrooxidans* (only N alignment), *Chloroflexus aggregans*, *D. shibae*, *Heliobacterium modesticaldum*, *Nostoc punctiforme*, *P. marinus*, *R. capsulatus*, *R. sphaeroides*, *Roseiflexus castenholzii*, *R. denitrificans*, *T. elongatus*. The amino acid sequences of the nitrogenase subunits NifH, NifD and NifK from the following organisms were aligned with ClustalW: *Anabaena variabilis*, *A. vinelandii*, *Bradyrhizobium japonicum*, *C. tepidum*, *Denitrovibrio acetiphilus*, *Desulfitobacterium hafniense*, *Desulfomicrobium baculatum*, *Geobacter bemidjiensis*, *Herbaspirillum seropedicae*, *Klebsiella pneumoniae*, *Leptothrix cholodnii*, *Paludibacter propionicigenes*, *Prosthecochloris aestuarii*, *R. sphaeroides*, *Spirochaeta thermophila*, *Treponema azotonutricium*. The information about conserved residues was implemented into the structure-based amino-acid sequence alignments (see next section).

Clustal Omega was used for the alignment of BchF, BchC and MDR sequences. BchC sequences from the following organisms were used: *Acidiphilum multivorum*, *Bradyrhizobium oligotrophicum*, *Chlorobaculum parvum*, *C. tepidum*, *Chlorobium limicola*, *Chlorobium luteolum*, *Chlorobium phaeobacteroides*, *Chlorobium phaeovibrioides*, *D. shibae*, *Halorhodospira halophila*, *Jannaschia sp.*, *Prosthecochloris aestuarii*, *Pelodictyon phaeoclathratiforme*, *R. sphaeroides*, *Rhodopseudomonas palustris*, *Rhodospirillum photometricum*, *R. denitrificans*, *Thioflavicoccus mobilis*, *Thiocystis violascens*. The following zinc-dependent MDRs were used: liver alcohol dehydrogenase *Equus caballus*, alcohol dehydrogenase 1 *S. cerevisiae*, L-threonine dehydrogenase *Pyrococcus horikoshii*, L-threonine dehydrogenase *Thermcoccus kodakaraensis*, sorbitol dehydrogenase *Homo sapiens*, sorbitol dehydrogenase *Bemisia argentifolii*, L-arabinitol 4-dehydrogenase *Neurospora crassa*, galactitol-1-phosphat dehydrogenase *E. coli*, cinnamyl alcohol dehydrogenase 5 *Arabidopsis thaliana*, L-threonine dehydrogenase *E. coli*, L-threonine dehydrogenase *Bacillus subtilis*. The alignments are deposited in the appendix (Figure 29 and Figure 30). The selected zinc-dependent and zinc-independent MDRs were chosen because they are well-characterized and/or a three-dimensional structure is available in the PDB.

Structure-based sequence alignments of DPOR and nitrogenase subunits were created using default settings of the “MatchMaker” subroutine of the program UCSF Chimera (Meng *et al.,* 2006; Pettersen *et al.,* 2004). The respective

DPOR subunits from *P. marinus* were used as the reference structure. The following peptide chains were used for superposition: *P. marinus* L chain A, *R. sphaeroides* L chain A (PDB ID 3FWY), *A. vinelandii* NifH chain E (PDB ID 1M34), *P. marinus* N chain C, *T. elongatus* N chain A (PDB ID 2XDQ), *R. capsulatus* N chain A (PDB ID 3AEK), *A. vinelandii* NifD chain A, *P. marinus* B chain D, *T. elongatus* B chain B, *R. capsulatus* B chain B, *A. vinelandii* NifK chain B. From these superpositions, multiple sequence alignments were calculated with default settings of "MatchAlign". The implemented structure analysis tool was used for the calculation of MgADP•AlF_3 and peptide contacts.

The docking interfaces of the octameric DPOR complex and the MgADP•AlF_4^--stabilized nitrogenase complex from *A. vinelandii* (Schmid *et al.,* 2002) were analyzed using the "Proteins, Interfaces, Structures and Assemblies" (PISA) server (version 1.37, Krissinel and Henrick, 2007). This tool identifies residues located at the interface of two protein subunits and detects hydrogen bonds and salt bridges between individual residues. A detailed list of all residues involved in the interaction of DPOR and nitrogenase subunits of the aluminum fluoride stabilized complexes is given in the appendix.

Molecular graphics and the superposition of C_α atoms of DPOR and nitrogenase ("align" command) were computed with PyMOL (Schrödinger, 2010).

Identity values of protein sequences were determined with the default settings of the basic local alignment search tool (BLAST) provided by the National Center for Biotechnology Information (versions 2.2.30+ and 2.2.32+, Altschul *et al.,* 1990).

The prediction of membrane-spanning regions of BchF sequences was performed with the TMpred tool (Hofmann and Stoffel, 1993). For each sequence, the "strongly preferred model" for the membrane topology was considered.

The tool InterProScan (version v4.8, Goujon *et al.,* 2010; Zdobnov and Apweiler, 2001) was used to analyze the *C. tepidum* BchC sequence with regard to functional domains.

2.7 Isolation of Pchlide and Chlide

Pchlide was used as substrate for DPOR activity assays as well as for DPOR protein crystallization experiments. The pigment was isolated from *R. capsulatus* strain ZY5 (Yang and Bauer, 1990) which contains a kanamycin resistance cassette disrupting the *bchL* gene, thus abolishing DPOR activity. This leads to the accumulation of the DPOR substrate Pchlide, which is secreted into the medium (Fujita, 2000). The accumulated Pchlide was characterized as a mixture of monovinyl (vinyl group at C3 and an ethyl group at C8) and divinyl (vinyl groups at C3 and C8), with the divinyl pigment being the prevalent species (Heyes *et al.,* 2006; Yang and Bauer, 1990). Pchlide isolation was performed according to a method described before (Heyes *et al.,* 2002) with slight modifications. *R. capsulatus* ZY5 was grown as described in section 2.4.1. To the main culture of 600 mL, twelve pieces of sterile foam bungs were added, which adsorbed the secreted pigment molecules. All subsequent steps were performed under low-light conditions. After 3 days of cultivation, the foam bungs were removed from the cultures, dried and the green pigment was released from the foam bungs with a total of 1 L ice-cold acetone applied in three portions. A column with 50 mL CM Sepharose CL-6B as column material was packed, washed with 10 CV of water and equilibrated with 10 CV acetone. The Pchlide solution was applied to the column and the pigment was adsorbed at the column material. After washing with 5 CV of ice-cold solution-2, elution occurred with 2 CV of ice-cold solution-3. The solvent was evaporated (350 mbar, 55 °C), the dried pigment dissolved in DMSO and stored at -20 °C. The Pchlide concentration was determined by UV-visible light spectroscopy (section 2.8.6).

Solution-2	Methanol	5 % (v/v)
	Acetone	95 % (v/v)
Solution-3	Methanol	25 % (v/v)
	Acetone	75 % (v/v)

Chlide was used as a standard substance for high performance liquid chromatography (HPLC) analyses (section 2.8.8). The preparation of Chlide was kindly performed by S. Virus. Chlide was isolated from *R. capsulatus* strain CB1200 (Bollivar *et al.,* 1994a) according to a method described before (Müller *et al.,* 2011) with some modifications. The employed strain contains a point mutation in the *bchF* gene and a directed disruption of the *bchZ* gene, so that the intermediate Chlide is accumulated (Bollivar *et al.,* 1994a). *R. capsulatus* CB1200 was grown as described in section 2.4.1. After the subsequent centrifugation of the cell suspension (3'000 g, 4°C, 30 min), Chlide was extracted from the supernatant: about 50 mL of a saturated NaCl solution were added to 150 mL culture supernatant and the mixture was extracted three times with about 30 mL diethyl ether each time. The collected diethyl ether phases were washed with a saturated NaCl solution until the turbidity of the mixture had disappeared. Subsequently, a washing step with 5 - 10 mL of water was performed and the solvent was evaporated. The pigment was dissolved in DMSO and stored at -20 °C. The Chlide concentration was determined by UV-visible light spectroscopy (section 2.8.6).

2.8 Enzyme activity assays

To determine the specific activity of *P. marinus* DPOR mutant proteins, *in vitro* activity assays were performed based on the work of Bröcker *et al.,* 2008a; Fujita, 2000 and Bröcker *et al.,* 2008b. Moreover, *C. tepidum* DPOR was used in a coupled *in vitro* activity assay with the enzymes BchF and BchC. All DPOR assays were performed under anoxic conditions. The DPOR substrate Pchlide was prepared as described in section 2.7. All other assay components were prepared as stock solutions in anoxic buffer-3 under anoxic conditions and stored in appropriate aliquots at -20 °C, so that repeated freeze-thaw cycles were avoided. For individual assays, a mastermix was prepared comprising the components creatine phosphate, SDT, DTT, ATP, creatine kinase and Pchlide.

2.8.1 Activity assay of *P. marinus* DPOR

P. marinus DPOR activity assays were performed employing cell-free extract containing subunit L (section 2.6.2) and purified subunits N and B (section 2.6.2). First, the mastermix (see above) was added to the respective volume of buffer-3 provided in the reaction tubes. Then, purified subunits N and B were added and the reaction was started by the addition of cell-free extract containing subunit L. Incubation occurred at 25 °C, 500 rpm and darkness.

In a preliminary assay, the optimal ratio of purified $(NB)_2$ and cell-free L extract was determined. For this, samples containing 10 - 1000 pmol of wild-type $(NB)_2$ and 100 µL cell-free L extract were incubated for 35 min, reactions were stopped by the addition of 500 µL acetone, samples were processed (section 2.8.5) and analyzed by UV-visible light spectroscopy (section 2.8.6). For the main assay, the samples for the analysis of DPOR mutant proteins were set up using the ratio of $(NB)_2$ and L with the highest activity (in all cases 300 pmol $(NB)_2$ and 100 µL cell-free L extract). Because different volumes of the wild-type and mutant proteins were used, buffer-4 was added to some samples to compensate the different DTT concentrations. After selected time points from 1 – 20 min reactions were stopped by the addition of 500 µL acetone, samples were processed (section 2.8.5) and analyzed by UV-visible light spectroscopy (section 2.8.6). Control samples lacking the L protein or both L and NB were prepared.

Specific activities of the wild-type and mutant proteins were calculated by monitoring the absorption of the DPOR product Chlide at 665 nm, using an absorption coefficient of ε_{667} = 74.9 $mM^{-1}cm^{-1}$ (McFeeters *et al.,* 1971). Specific activities were calculated as $pmol_{Chlide}/(min*mg_{NB\ protein})$, the wild-type value was set to 100 % and all other values were related to it.

Table 8: Composition of the main *P. marinus* DPOR activity assay.

Component	Stock concentration	Assay concentration
SDT	1 M	0.72 mM
DTT	500 mM	5 mM
ATP	200 mM	2 mM
Creatine kinase	6.7 U/µL	0.08 U/µL
Creatine phosphate	500 mM	20 mM
Pchlide	1.4 - 10.9 mM	3 - 20 µM
Buffer-4	different volumes	
Purified $(NB)_2$ wild-type/mutant	300 pmol	
Cell-free extract L	100 µL	
Buffer-3	add to 250 µL	

2.8.2 Activity assays of *C. tepidum* DPOR

C. tepidum DPOR activity assays were performed employing the cell-free extract containing all three DPOR subunits (section 2.6.2, Bröcker *et al.,* 2008a). The mastermix (see above) was added to the respective volume of buffer-3 provided in the reaction tubes, the reaction was started by the addition of the cell-free DPOR extract and incubated (34 °C, 600 rpm, 60 min, darkness). Subsequently, samples were subjected to the coupled activity assay using the enzymes BchF and BchC.

Table 9: Composition of the *C. tepidum* DPOR activity assay.

Component	Stock concentration	Assay concentration
SDT	1 M	0.72 mM
DTT	500 mM	5 mM
ATP	200 mM	2 mM
Creatine kinase	6.7 U/µL	0.08 U/µL
Creatine phosphate	500 mM	20 mM
Pchlide	3.9 mM	5 µM
DPOR cell-free extract	40 or 100 µL	
Buffer-3	add to 250 µL	

2.8.3 Coupled activity assays of *C. tepidum* DPOR, BchF and BchC

Initial coupled activity assays involving the enzymes DPOR, BchF and BchC from *C. tepidum* had been performed before (Peters, 2013). Subsequently, control plasmids were constructed: plasmid pACYCDuet_BchC contained only the *bchC* gene in the second MCS (equipped with a C-terminal S-tag, Peters, 2013) and pACYCDuet_BchF containing only *bchF* in the first MCS (N-terminal His_6-tag, section 2.6.2). The proteins were recombinantly produced (section 2.6.1) and used for activity assays.

Coupled activity assays were based on the activity assays of *C. tepidum* DPOR. (section 2.8.2). After incubation, those samples were transferred to aerobic conditions and supplemented with compounds for the coupled activity assay, which were prepared during the DPOR incubation time: the redox cofactors NAD^+ or $NADP^+$ were freshly dissolved at a concentration of 50 mM in buffer-1

and stored on ice until use. Furthermore, for each sample, a mix of the redox cofactor and the enzymes BchF and/or BchC was prepared in a total volume of 250 µL buffer-1. BchF and BchC were either supplied together or separately in the form of crude cellular extracts (100 µL, for preparation of the extracts see section 2.6.2) or separately as solubilized BchF (100 µL, for preparation see section 2.6.2) or purified BchC (1.6 – 3.9 µM assay concentration, for preparation see section 2.6.2). Control reactions were prepared lacking BchF, BchC or both BchF and BchC.

Reactions were incubated for 30 min at 34 °C and 600 rpm in the dark. The redox cofactor was present at the beginning of the reaction at a concentration of 250 µM. After 20 min, additional cofactor was added to the samples resulting in a final concentration of 500 µM. Reactions were stopped by the addition of 1 mL acetone, samples were processed (section 2.8.5) and analyzed by UV-visible light spectroscopy (section 2.8.6).

In the very first experiments, the samples were supplemented with additional DPOR substrate Pchlide to keep the Pchlide concentration at 5 µM after the 2x dilution of the DPOR reaction with the components for the coupled activity assay. However, this was discontinued in later activity assays. Moreover, the initial activity assays contained 5 mM zinc acetate (1 M stock solution in dH_2O) because at the beginning of the experiments, a zinc-dependent BchC catalysis was expected. The addition of zinc acetate was omitted for later activity assays because of increasing experimental evidence for a zinc-independent BchC catalysis.

The analysis of BchC mutant proteins was mainly performed as described above for the wild-type enzyme with minor modifications. 1.8 or 2.0 nmol (3.6 or 4.0 µM) of the wild-type or the mutant proteins were applied. After the compounds for the coupled activity assay were added, incubation was continued for 15 min, 30 min and 3 h. Additional cofactor (NAD^+) was added after 20 min or 1 h.

2.8.4 BchC activity assay in the presence of artificial substrates

In vitro BchC activity assays were performed to characterize the enzyme with regard to its substrate specificity, cofactor occupancy and metal dependence.

Assay samples were set up containing purified BchC protein (3.2 - 8.4 µM), an artificial substrate (750 nM – 23 µM) and NAD^+ or NADH in a total volume of 250 µL buffer-1. The redox cofactors were freshly dissolved at a concentration of 50 mM in buffer-1 and stored on ice until use. For substrates carrying a 3^1-OH group NAD^+ was used as a cofactor. For substrates carrying a 3-acetyl group NADH was used and the reverse BchC reaction was investigated. Reactions were incubated for 30 min or 3 h at 34 °C and 600 rpm in the dark. The redox cofactor was present at the beginning of the reaction at a concentration of 500 µM. After 20 min or 1.5 h, additional cofactor was added to the samples to make a final concentration of 1 mM. Reactions were stopped by addition of 500 µL acetone, samples were kept on ice until further processing (section 2.8.5) and analysis by UV-visible light spectroscopy (section 2.8.6).

Determination of BchC substrate specificity

Modified Chls and BChls used in this study were kindly provided by Prof. Dr. Hugo Scheer (LMU Munich). Pigments were dissolved in DMSO and stored at -20 °C in the dark. The respective synthesis and/or isolation is cited in Table 10. Substrates **7**, **10** and **11** were applied as epimeric mixtures with both *R* and *S* stereochemistry at C3[1], which had resulted from the formation of these molecules by borohydride reduction (H. Scheer, personal communication). All pigments were identified by their Q_y absorption bands in acetone-extracted assay samples, which were compared to the maxima of the same or similar compounds described in the literature.

Table 10: Literature values of Q_y absorption maxima and extinction coefficients applied for the identification of artificial substrates used in BchC *in vitro* activity assays. For each compound, the name is given, together with an abbreviation and a compound number, which will be used throughout the text. The literature values belong to the same or similar compounds as those pigments used in the assay. [a)]in diethylether (Struck *et al.,* 1992 for compounds **7** and **10**; Hartwich *et al.,* 1998 for compounds **8** and **9**), [b)]in acetone (Klement *et al.,* 1999), [c)]because ε of compound **7** was not available, ε at 750 nm of the similar pigment bacteriopheophytin in diethylether was used (Hartwich *et al.,* 1998), [d)]Kiesel *et al.,* 2015.

Pigment (assay)	$\lambda_{max, Qy}$ [nm]	ε [mM^{-1} cm^{-1}]
3-Hydroxyethyl-bacteriopheophorbide *a* (3^1-OH-BPheide *a*), **7**	712[a)]	67.5[c)]
Zinc-bacteriopheophorbide *a* (Zn-BPheide *a*), **8**	762[a)]	67.7[a)]
Palladium-bacteriopheophorbide *a* (Pd-BPheide *a*), **9**	753[a)]	92.0[a)]
3-Hydroxyethyl-bacteriochlorophyll *a* (3^1-OH-BChl *a*), **10**	728[a)]	66.1 ± 3.2[a)]
Zinc-3^1-13^2-di-hydroxy-pheophorbide *a* (Zn-3^1-13^2-di-OH-Pheide *a*), **11**	650[d)]	65.0[d)]
Zinc-3-acetyl-pheophorbide *a* (Zn-3-acetyl-Pheide *a*), **12**	672[b)]	65.2[b)]

Determination of BchC cofactor occupancy - Single turnover experiments

The cofactor occupancy of the purified BchC (section 2.6.2) was analyzed by omitting the externally added redox cofactor from the samples of the *in vitro* BchC activity assay. Thus, enzymatic catalysis was dependent on the amount of co-purified cofactor. BchC concentrations of 0.8, 2.0, 4.0, 6.0 and 8.0 µM were employed. As substrate, 2.9 µM Zn-3^1-13^2-di-OH-Pheide *a* was used. Samples were incubated for 3 h. Control reactions without protein or with excess cofactor (4 µM BchC and 1 mM NAD^+) were prepared.

Determination of BchC metal dependence

For the analysis of the activity of chelator-treated BchC (section 2.6.7), 3.2 µM (800 pmol) of chelator-treated BchC were used. About 10 µM 3^1-OH-BPheide *a* (**7**) or 2.6 µM Zn-3^1-13^2-di-OH-Pheide *a* (**11**) were used as substrates. Samples were incubated for 30 min. Additionally, 1.6 µM chelator-treated BchC (800 pmol) was subjected to coupled DPOR-BchF-BchC activity assays (section 2.8.3).

2.8.5 Processing of samples from activity assays

After the termination of the activity assay reaction by the addition of acetone, insoluble assay components were separated by centrifugation at 4 °C (two times 11'000 g, 15 min for *P. marinus* DPOR assays or 17'000 g, 10 min for BchC-containing assays) and the final supernatant was analyzed by UV-visible light absorption spectroscopy (section 2.8.6).

2.8.6 UV-visible light absorption spectroscopy

UV-visible light absorption spectra were recorded on a V-650 spectrophotometer (Jasco) operated with the Spectra Manager software (Jasco) to analyze acetone-extracted pigments after activity assays. As reference, acetone and the respective assay buffer (volume ratio 2:1) was used. Spectra were recorded in a range from 600 - 800 nm with a scan speed of 200 nm/min and a bandwidth of 1 nm (*P. marinus* DPOR activity assays). For all other samples, the recorded ranges were 300 - 900 nm, 350 -800 nm or 600 - 800 nm with scan speeds of 200 or 400 nm/min and a bandwidth of 1 nm. All assay samples were stored at -20 °C.

Moreover, the concentration of the isolated Pchlide and Chlide (section 2.7) was determined by UV-visible light spectroscopy. Absorption spectra of Pchlide dilutions in 80 % acetone were recorded (500 - 800 nm) and the absorption at the Q_y absorption maximum of Pchlide at 628 nm was determined. The Pchlide concentration was calculated using an extinction coefficient of ε_{626} = 30.4 $mM^{-1}cm^{-1}$ (Brouers and Michel-Wolwertz, 1983). Absorption spectra of Chlide dilutions in acetone were recorded (500 -800 nm) and the absorption at the Q_y absorption maximum of Chlide at 665 nm was determined. The Chlide concentration was calculated using an absorption coefficient of ε_{667} = 74.9 $mM^{-1}cm^{-1}$ (McFeeters *et al.,* 1971).

2.8.7 Low-temperature fluorescence spectroscopy

Apart from absorption spectroscopy, fluorescence spectroscopy was used to further analyze the samples from the coupled DPOR-BchF-BchC activity assays (section 2.8.3). This method is more sensitive than absorption spectroscopy with regard to the amount of pigment that can be detected (Kobayashi *et al.*, 2006). Thus, it was expected that also low amounts of BChl *a* precursors, which could possibly not be detected by absorption spectroscopy, could appear in a fluorescence spectrum. Moreover, the instrumental setup made it possible to record fluorescence spectra at 77 K (-196 °C). At this low temperature, the band width of excitation and emission peaks decreases, making it possible to distinguish substances with very close excitation or emission maxima (Sauer and Debreczeny, 1996). In the experimental setup, the standard sample holder of the FP-8500 spectrofluorimeter was replaced by a PMU-830 cryo-holder cooled with liquid nitrogen. The acetone-extracted samples were carefully applied to this cryo holder in NMR tubes and froze from the bottom of the tube upwards immediately upon application. It was expected that the BChl *a* precursors in the samples could be assigned to specific excitation and emission maxima so that it would be possible to specifically detect these intermediates in mixtures comprising several compounds.

Initial experiments for the characterization of the DPOR-BchF-BchC coupled activity assays by fluorescence spectroscopy had been performed before (Peters, 2013). As described above, those activity assays were improved in the present work and completed by the appropriate control reactions. Samples from the activity assays (750 µL) were transferred from -20 °C to ice. Samples were applied to the instrument in NMR sample tubes. Excitation and emission maxima of the pigments were determined using the following instrumental parameters: excitation bandwidth 2.5 nm, emission bandwidth 5 nm, response 50 msec, scan speed 500 nm/min, medium sensitivity. Using the respective option of the Spectra Manager software (Jasco), the shutter for the incident light was opened only for the measurement to minimize damage to the sample. The final spectra were recorded at excitation wavelengths of 439 nm and 470 nm.

2.8.8 HPLC analysis

The determined fluorescence properties (section 2.8.7) were used to specifically detect the BChl *a* precursors in samples from coupled DPOR-BchF-BchC activity assays (section 2.8.3) after separation *via* reversed phase HPLC. This method is based on the hydrophobic interactions of the dissolved pigments with the stationary phase of the HPLC column. The strength of this interaction depends on the hydrophobicity of the pigment and thus, pigments are retained on the column to different extents during the elution with a mobile phase.

In the present study, a method described in the literature was used with some modifications (Gough *et al.,* 2007). Acetone-extracted samples which had been stored at -20 °C were analyzed on an UltraSep ES RP18 column using a Jasco HPLC system equipped with a FP-1520 multi-wavelength fluorescence detector. Samples of 20 µL were separated at a flow rate of 0.5 mL/min, (30 °C column

temperature, max. 15 MPa) with a linear gradient ranging from 25 - 100 % (v/v) acetonitrile in H_2O with 0.005 % (v/v) triethylamine over 54 min. As standard substances, Pchlide and Chlide were used (for the preparation see section 2.7, Pchlide 1.8 µM, Chlide 0.45 µM in acetone/buffer-1 (volume ratio 2:1)). The BChl *a* precursors present in the samples were detected with their individual fluorescence settings, i.e. each sample was run four times using different detection settings each time.

All HPLC runs were kindly performed by Simone Virus.

3 Results and Discussion

In the first part of this work, the crystal structure of the MgADP•AlF_3-stabilized octameric DPOR complex is described, highlighting the dynamic switch mechanism, the docking face of the two subcomplexes and the substrate binding site of the complex. In the second part, the further investigation of the later steps of BChl *a* biosynthesis is specified, involving the enzymes BchF and BchC. Finally, the oxidoreductase BchC is characterized with regard to substrate specificity and cofactor requirements. As mentioned before, DPOR subunits will be designated L, N and B only, in order to account for the different nomenclature in Chl and BChl producing organisms.

3.1 From Pchlide to Chlide - Dark-operative protochlorophyllide *a* oxidoreductase

In the literature, the structures of the components of the multimeric DPOR enzyme from different bacteria are described (Table 1). Moreover, the structure of the enzyme nitrogenase is well-known, with which DPOR has a high degree of structural and sequence identity (Fujita *et al.,* 1993; Wätzlich *et al.,* 2009). However, it remained to be investigated, how the DPOR subunits interact with each other and accomplish the complex task of the two-electron reduction producing Chlide from Pchlide, which is mediated *via* two [4Fe-4S] clusters. To approach this question, the structure of the octameric DPOR complex was investigated.

3.1.1 Purification of the DPOR subunits N, B and L from *P. marinus* and assembly of the octameric complex

For the production of recombinant DPOR subunits, pGEX6P-1 constructs containing the genes *chlL*, *chlN* and *chlB* from *P. marinus* were chosen (Bröcker *et al.,* 2008b). The protein purification strategy (Bröcker *et al.,* 2010b) is depicted in Figure 7.

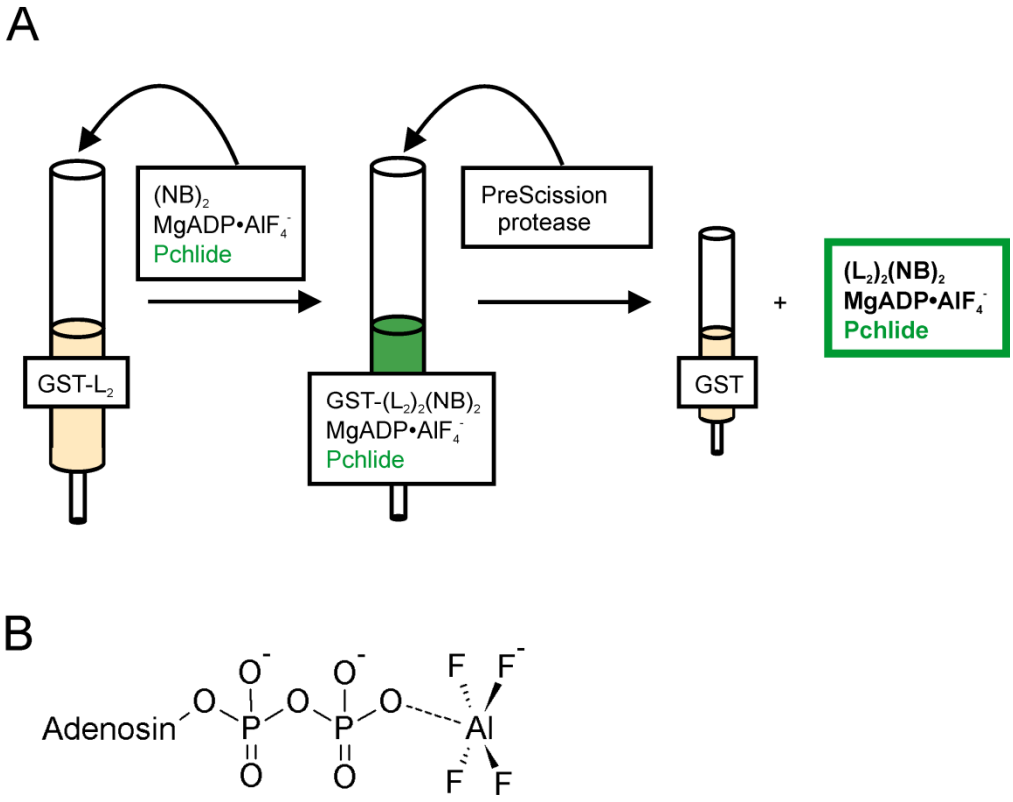

Figure 7: Purification strategy for the octameric DPOR complex (Bröcker *et al.,* 2010b). A, After the heterologous production of the DPOR subunits N and B in *E. coli* BL21-CodonPlus (DE3)-RIL (section 2.6.1), these subunits were co-purified *via* the N-terminal GST-tag of N with subsequent PreScission protease treatment (section 2.6.2, not shown). The purified subunits N and B were added to the column-bound GST-L together with the ATP analog MgADP•AlF_4^- and the substrate Pchlide. After incubation, the green colored protein complex was liberated from the column by PreScission protease treatment (section 2.6.2). **B**, Molecular structure of the ATP analog MgADP•AlF_4^-. The AlF_4^--moiety of the molecule resembles the trigonal bipyramidal transition state of the γ-phosphate group of ATP during ATP hydrolysis. MgADP•AlF_4^- was prepared *in situ* from NaADP, $AlCl_3$ and NaF in buffer-3 containing Mg^{2+} ions. The Mg^{2+} ion was omitted for clarity.

All protein subunits were heterologously produced (section 2.6.1) and purified under anoxic conditions. First, GST-N was purified *via* GST affinity chromatography and liberated by subsequent PreScission protease treatment. Subunit B was co-purified with N due to the tight interaction of the two proteins (Bröcker *et al.,* 2010b). Next, GST-L was bound and purified on a glutathione resin and the assembly of the octameric DPOR complex was performed on the column (Figure 7). The green colored DPOR complex was liberated from the column by PreScission protease treatment. The SDS-PAGE analysis of the elution steps is shown in Figure 8.

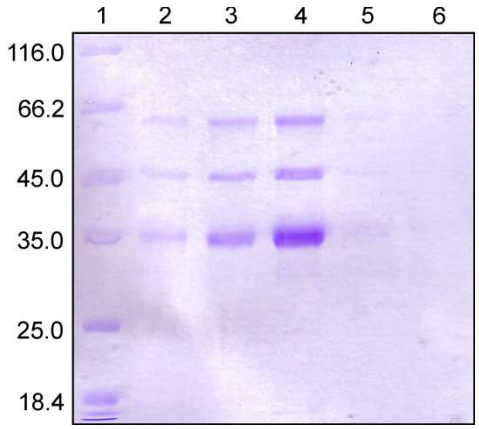

Figure 8: SDS-PAGE analysis of the elution fractions after on-column formation of the octameric DPOR complex from *P. marinus*. The octameric complex was formed by incubating the purified DPOR subunits N and B, the DPOR substrate Pchlide and the ATP analog MgADP•AlF_4^- on a glutathione agarose column with bound GST-L. The complex was liberated from the column by PreScission protease treatment. The first elution fraction was drained from the column. The following elution fractions were obtained by washing the column with buffer-3. Proteins were separated by SDS-PAGE and stained with Coomassie Brilliant Blue. Lane 1: unstained protein molecular weight marker, relative molecular masses (x 1'000) are indicated. Lane 2: first elution fraction (4 µL sample). Lane 3: first elution fraction (8 µL). Lane 4: second elution fraction (8 µL). Lane 5: third elution fraction (8 µL). Lane 6: fourth elution fraction (8 µL).

Figure 8 shows that in all elution fractions, three protein bands are present. The apparent molecular masses of the proteins (60 kDa, 45 kDa, 35 kDa) correspond to the calculated molecular masses of the three DPOR subunits B (58'729 Da), N (46'983 Da) and L (32'806 Da).

After concentrating the elution fractions to a protein concentration of 9.5 mg/mL (section 2.6.9), sitting drop crystallization experiments were performed under anoxic conditions (section 2.6.10). However, upon preparation of the first wells, the formation of protein precipitate was observed. The reason for this was probably the high protein concentration. Thus, the protein solution was diluted to a protein concentration of 7.5 mg/mL and the preparation of the sitting drop experiment was continued. The first green colored crystals were observed in a variety of reservoir conditions after 4 days. Within 1 – 4 weeks after the preparation of the sitting drop experiments, more crystals formed under several conditions. A list of all conditions containing crystals is presented in Table 17 (appendix). Figure 9 contains exemplary photographs of crystallization wells with DPOR crystals.

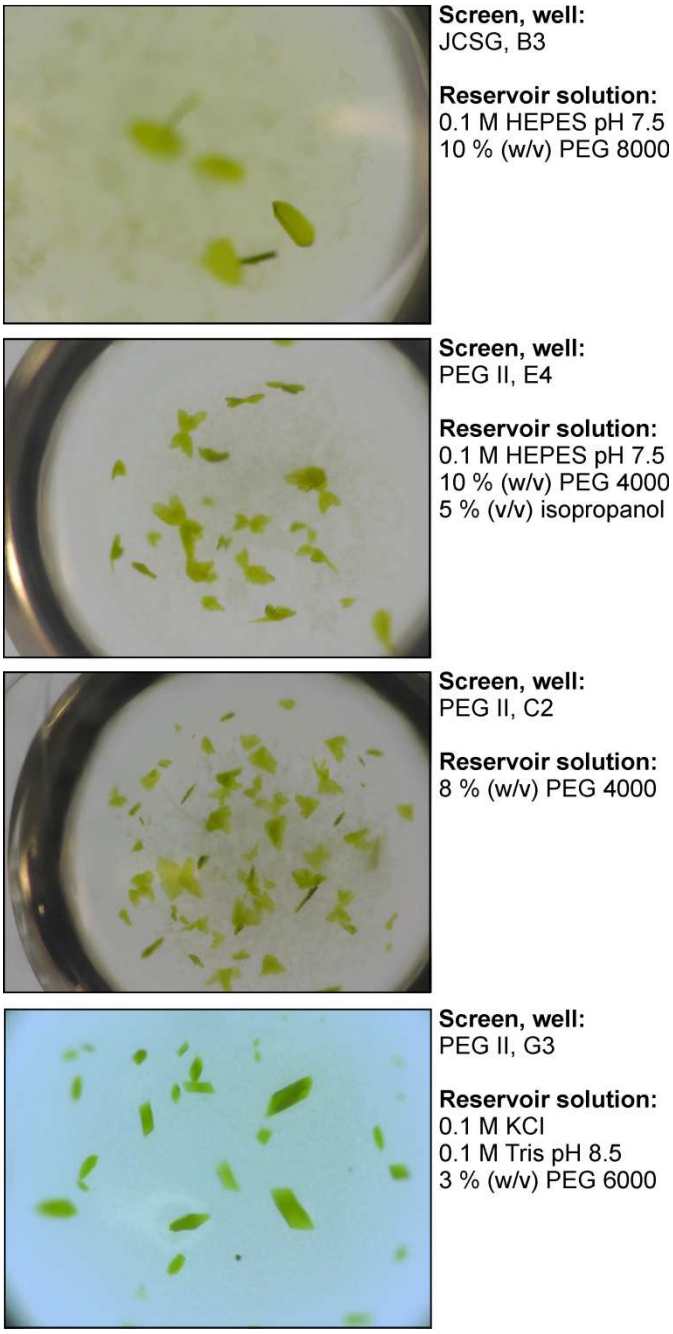

Figure 9: Exemplary photographs of crystallization wells containing green-colored DPOR crystals. All sitting drop crystallization plates were stored under anoxic conditions in the dark at 17 °C. After 4 days, the first crystals were observed (conditions JCSG B3, PEG II C2 and PEG II E4). More crystals appeared after 3 – 4 weeks after the preparation of the crystallization experiments (condition PEG II G3).

Figure 9 shows that under certain conditions, a high number of crystals was formed (for example conditions PEG II, E4 and PEG II, C2). In other conditions, only few crystals developed. The crystal suitable for data collection and

structure solving was obtained with the reservoir containing 0.1 M KCl, 0.1 M Tris (pH 8.5) and 3 % (w/v) PEG 6000 (Figure 9, bottom).

3.1.2 Data collection and structure determination

Data collection and processing up to the final structure was performed by Dr. Jörn Kraußе, Helmholtz Centre for Infection Research. A single crystal was used for the diffraction experiment. The initial dataset showed anisotropy and thus was anisotropy-corrected in order to include reflections from the higher resolution shells. Molecular replacement was used for model building based on the anisotropy-corrected dataset, using an L monomer from *R. sphaeroides* (PDB ID 3FWY) and the N and B monomers from *T. elongatus* (PDB ID 2XDQ) as search models. The obtained initial model was improved using the program phenix.mr_rosetta (DiMaio *et al.,* 2011), manually rebuilt in COOT (Emsley and Cowtan, 2004) and refined with phenix.refine (Adams *et al.,* 2010). Finally, the structure model of the substrate-bound DPOR complex from *P. marinus* was obtained and the structure was deposited in the PDB (PDB ID 2YNM). Table 11 summarizes the data collection and refinement statistics:

Table 11: Data collection and refinement statistics. The initial dataset was corrected for anisotropy, so that the anisotropy-corrected dataset was obtained. The latter was further refined until the final structure was obtained. An asterisk (*) highlights the values for the highest resolution shell, which are shown in parentheses. The hash sign (#) marks the resolution as of which the structure is reported (2.6 Å). Data of higher resolution were included in the refinement but showed completeness below 90 %. As an additional quality criterion for the final structure, a Ramachandran analysis was performed for all residues. It revealed that 97.6 % of the residues have favored backbone dihedral angles, whereas 2.2 % have allowed and 0.2 % had disallowed angles.

Parameters	**Initial**	**Anisotropy corrected**
Data collection		
Space group	C2	
Cell dimensions		
a, *b*, *c* (Å)	308.4, 74.1, 74.2	
β (°)	91.24	
Resolution (Å)	20-2.15 (2.26-2.15)*	20-2.15 (2.26-2.15)*
R_{merge}	0.064 (0.814)*	0.049 (0.256)*
$I/\sigma I$	12.9 (1.6)*	17.4 (4.5)*
Completeness (%)	98.3 (91.9)*	73.6 (16.6)*
Redundancy	3.5 (3.1)*	2.6 (0.6)*
Refinement		
Resolution (Å)		2.15 (2.6)#
No. reflections		237'398
R_{work} / R_{free}		0.2097 / 0.2416
No. atoms		11'899
Protein		11'213
Ligand/ion		143
Water		433
B-factors (Å^2)		41.4
Protein		41.8
Ligand/ion		42.2
Water		31.0
Root mean square deviations		
Bond lengths (Å)		0.004
Bond angles (°)		1.015

3.1.3 Overall structure of the octameric DPOR complex

In Figure 10, the structure of the octameric DPOR complex from *P. marinus* is shown.

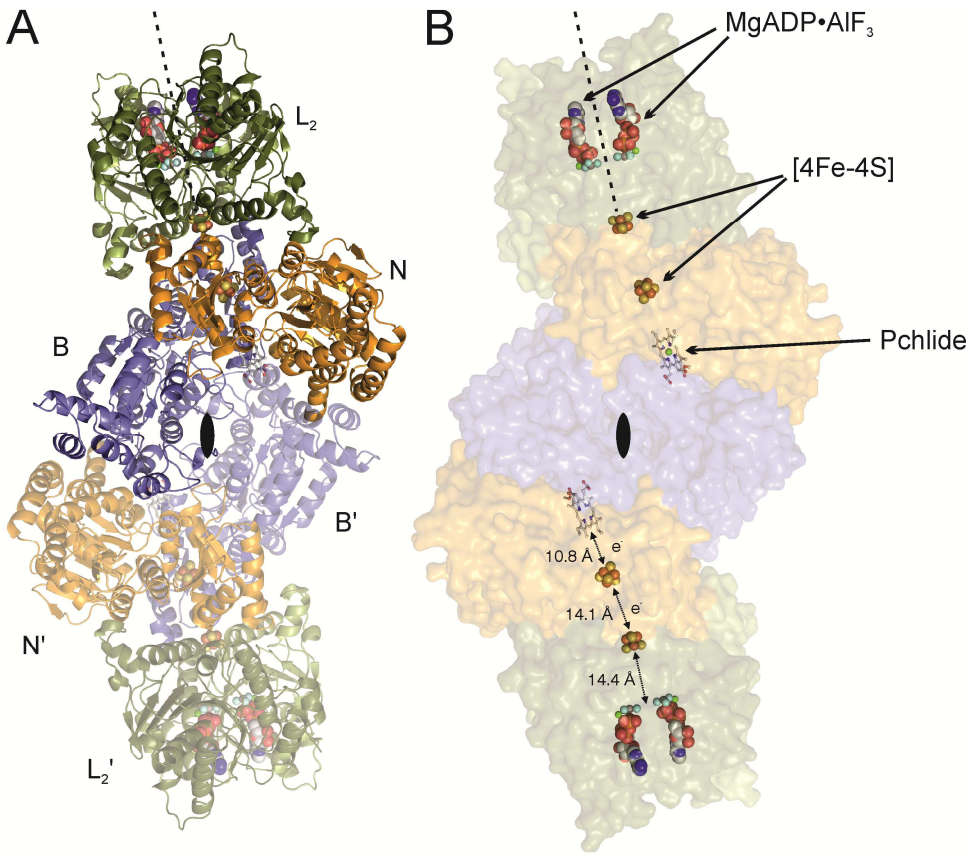

Figure 10: Structure of the octameric DPOR complex. The structure of the transient octameric DPOR complex from *P. marinus* was solved by molecular replacement and subsequent refinement specified in section 2.6.10. Structural coordinates were deposited in the PDB (PDB ID 2YNM). The octameric complex consists of subunits L (green), N (orange) and B (blue). Two L protomers form homodimers, which interact with subunits N and B. Protein-bound small molecules are displayed as ball-and-stick model (substrate Pchlide) or sphere representation ($MgADP•AlF_3$, [4Fe-4S] clusters). **A**, Cartoon display of the protein backbone. In the asymmetric unit, one L_2 homodimer and one NB heterodimer was found (dark colors). The crystallographic two-fold rotational symmetry axis (black lens) generates the symmetry-related subunits, marked L', N' and B' and displayed in light colors. **B**, Transparent surface display of the protein subunits. The crystallographic two-fold rotational symmetry axis of the whole complex is indicated (black lens). Two L protomers form a homodimer which shows a dyad axis displayed as a dashed line. Edge-to-edge distances between the small molecules are indicated. The figure was prepared with PyMOL (section 2.6.11) together with Dr. Jörn Krauße, HZI.

In the asymmetric unit of the crystal, one L_2 homodimer and one NB heterodimer was found (Figure 10 **A**, dark colored subunits). The application of a crystallographic two-fold rotational symmetry axis led to the structure of the

octameric complex. It had been suggested before by modeling (Bröcker *et al.,* 2010a) that the DPOR complex was expected to be a heterooctamer in analogy to nitrogenase (Schindelin *et al.,* 1997). Moreover, it was known from size exclusion chromatography experiments that DPOR formed an octameric complex in solution, consisting of two L_2 dimers and one $(NB)_2$ heterotetramer (Bröcker *et al.,* 2010b). The structure showed that the former possessed a local two-fold rotational symmetry axis (dotted line in Figure 10). As N and B are structural homologs, the $(NB)_2$ heterotetramer showed a local pseudo-two-fold rotational symmetry axis in line with the two-fold axis of L_2. The same symmetry elements had been described before for the octameric nitrogenase complex (Schindelin *et al.,* 1997). Each L_2 dimer bound one [4Fe-4S] cluster which was symmetrically coordinated by two cysteine residues of each L protomer. Moreover, each L protomer bound one ATP analog ($MgADP•AlF_3$). Originally, the formation of $MgADP•AlF_4^-$ had been expected. However, in a number of other structures the formation of $MgADP•AlF_3$ from ADP, $AlCl_3$ and NaF had been observed before (Bösken *et al.,* 2014; Chaudhry *et al.,* 2003; Madhusudan *et al.,* 2002; Scheffzek *et al.,* 1997; Wang *et al.,* 2002). There are hints that the precise species of the ATP analog depends on the pH and the concentration of NaF (Schlichting and Reinstein, 1999).

The core heterotetramer contained two [4Fe-4S] clusters in total. Each cluster was ligated by three cysteine residues from N and one aspartate residue of B. In the complex, the L cluster was located about 14 Å distant from the next NB-bound cluster. Both clusters were arranged in line with the substrate Pchlide, which was bound by N and B. The tetrapyrrole rings A and B pointed towards the NB-bound cluster. Upon comparison of the structure with the model of the complex gained by rigid-body docking of L_2 and $(NB)_2$ (Bröcker *et al.,* 2010a), it became clear that in the trapped complex the L-bound [4Fe-4S] cluster was shifted towards the NB-bound cluster by about 5 Å (edge-to-edge distance of 19 Å in the modeled complex compared to ~14 Å in the trapped complex).

The DPOR complex showed a high degree of structural homology to the related nitrogenase complex, which had been crystallized in a number of variants: nucleotide-free or binding ADP, AMP-PCP (Tezcan *et al.,* 2015; Tezcan *et al.,* 2005) or $ADP•AlF_4^-$ (Schindelin *et al.,* 1997; Schmid *et al.,* 2002). A structural

comparison of these nitrogenase complexes in different nucleotide states revealed that in the ADP•AlF_4^--bound complex (PDB ID 1M34), the $NifH_2$-bound [4Fe-4S] cluster was about 5 – 6.2 Å closer to the NifD/NifK-bound P cluster than in the ADP-bound complex (PDB ID 2AFI, Tezcan *et al.,* 2005). For nitrogenase, it was concluded that by this spatial arrangement, the optimal alignment of the two redox-active clusters for electron transfer was formed and that thus the electron transfer rate could be accelerated (Tezcan *et al.,* 2005). Based on the similarities of the DPOR and nitrogenase complexes, the same suggestion can be made for DPOR.

3.1.4 The dynamic switch mechanism of the DPOR L_2 homodimer

In the past, the DPOR L_2 homodimer from *P. marinus* had been characterized as a nucleotide-dependent switch protein (section 1.5.2). In the structure of the octameric DPOR complex, a complex molecule resembling the transition state of ATP hydrolysis, MgADP•AlF_3, was used to transiently stabilize the octameric complex in the high affinity state of L_2 and $(NB)_2$. It was expected that the conformation of MgADP•AlF_3-bound L_2 would resemble the previously described MgATP-bound state of the homodimer (Bröcker *et al.,* 2010b). Based on the octameric DPOR structure, the nucleotide-dependent switch was analyzed by a structure-based amino acid sequence alignment, the determination of root mean square deviation (rmsd) values and the visualization of the dynamic switch mechanism by the superposition of related structures using the program PyMOL.

Structure-based amino acid sequence alignment

The nucleotide-dependent switch mechanism had also been described for the $NifH_2$ protein of nitrogenase (Lanzilotta *et al.,* 1997; Ryle and Seefeldt, 1996; Schindelin *et al.,* 1997). A structure-based amino acid sequence alignment of MgADP•AlF_3-bound L from *P. marinus*, MgADP-bound L from *R. sphaeroides* and MgADP•AlF_4^--bound NifH from *A. vinelandii* was created (section 2.6.11, see Figure 11) to visualize differences and similarities between the proteins.

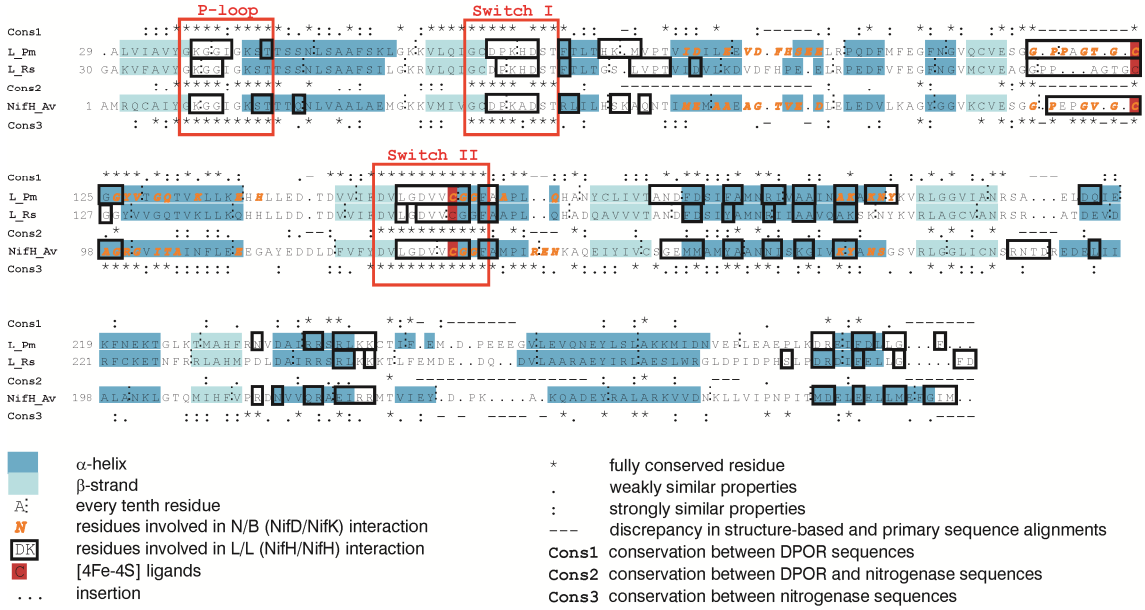

Figure 11: Structure-based amino acid sequence alignment of MgADP•AlF_3-bound L (*P. marinus,* this work), MgADP-bound L (*R. sphaeroides*, PDB ID 3FWY) and MgADP•AlF_4^--bound NifH (*A. vinelandii*, PDB ID 1M34). Helices (blue) and β-strands (light-blue) are highlighted. The conservation patterns derived from primary amino acid sequence alignments (not shown) of 14 L sequences (Cons1), 16 NifH sequences (Cons3) and all sequences (Cons2) were manually added to the structure-based amino acid sequence alignment. Dashes (—) indicate structural incongruities, which are *inter alia* caused by conformational changes. Orange font indicates residues involved in protein-protein interactions between L_2 and $(NB)_2$ or $NifH_2$ and $(NifD/NifK)_2$, respectively. Black boxes mark residues of the L_2 or $NifH_2$ dimer interface. All interface residues were identified in analyses using the PISA server (section 2.6.11). Ligands of the [4Fe-4S] clusters are highlighted by red shading. Asterisks (*) indicate fully conserved residues, colons (:) mark residues with strongly similar properties, residues with weakly similar properties are indicated by a period (.). The structure-based alignment was generated using UCSF Chimera (section 2.6.11). Primary amino acid sequence alignments were generated using ClustalW (section 2.6.11).

The structure-based amino acid sequence alignment depicted in Figure 11 reveals three core regions highly conserved among L and NifH sequences: the phosphate binding loop (P-loop) as well as the so-called switch I and switch II regions. These three motifs are conserved in a variety of nucleotide-binding proteins, such as myosins, kinesins (Sablin and Fletterick, 2001; Smith and Rayment, 1996) or guanine nucleotide binding proteins, such as the Ras-like GTPases (Li and Zhang, 2004; Vetter and Wittinghofer, 2001). The P-loop (consensus sequence GXXXXGK-T/S, Smith and Rayment, 1996; Walker *et al.,* 1982) and the switch regions I and II interact with the phosphate groups of the nucleotide, so that switch I and II can trigger a conformational rearrangement of the entire protein depending on the kind of bound nucleotide (Sablin and Fletterick, 2001; Vetter and Wittinghofer, 2001).

Determination of rmsd values

The described similarities of the L and NifH amino acid sequences suggest that their nucleotide-dependent switch mechanism might be similar. In order to detect possible similarities on a molecular level, comparisons of the complexed, MgADP•AlF_3-bound L_2 homodimer from *P. marinus* with the MgADP-bound L_2 structure from *R. sphaeroides* and various $NifH_2$ crystal structures were performed (see Table 1). The C_α atoms of the different structures were superposed with PyMOL (section 2.6.11) and the rmsd for each pair of superimposed structures was determined as a measure for the spatial deviation of two structures.

Table 12: Pairwise comparison of MgADP•AlF_3-bound L (*P. marinus*), ADP-bound L (*R. sphaeroides*) and various $NifH_2$ structures (*A. vinelandii*) based on the superpositions of C_α atoms. For each superposition of two structures, the rmsd values are given in Å. The top line in each entry gives the rmsd of the superposition of the rigid L_2 dimer with dimeric $NifH_2$. For all nitrogenase structures comprising multiple $NifH_2$ dimers in the asymmetric unit, the average of all possible combinations is given. The lower line in each entry is the rmsd of the superposition of L monomers with monomeric NifH. Highlighted numbers show the closest matches between DPOR and nitrogenase subunit structures.

	Structure (PDB ID)	DPOR	
		L_2 + ADP (3FWY)	**$(L_2)_2(NB)_2$ + ADP•AlF_3 + Pchlide** (this work)
Nitrogenase	**$NifH_2$ + ADP** (1FP6)	**1.7** **1.1**	3.0 1.7
	$NifH_2(NifD/NifK)_2$ *(no nucleotide)* (2AFH)	1.7 1.4	3.9 1.8
	$NifH_2(NifD/NifK)_2$ + ADP•AlF_4^- (1N2C)	3.7 1.1	**1.1** **1.0**
	$NifH_2(NifD/NifK)_2$ + AMPPCP *(ATP analog)* (2AFK)	3.3 1.3	1.8 1.1
	$NifH_2(NifD/NifK)_2$ + ADP•AlF_4^- (1M34)	3.6 1.1	**1.1** **1.0**
DPOR	**$(L_2)_2(NB)_2$ + ADP•AlF_3 + Pchlide** (this work)	3.4 0.8	

For the $NifH_2$ protein in its various nucleotide-bound conformations it was observed that upon the binding of MgATP, the homodimer adopts a more compact structure (Chen *et al.,* 1994). The comparison of L and NifH monomers revealed rmsd values between 0.8 and 1.8 Å (Table 12, lower lines in each entry). This indicates that there is conformational movement within the monomers depending on the bound nucleotide or nucleotide analog. To some extent, the determined rmsd values might be the result of the sequence deviations of the compared proteins, since the L proteins from *P. marinus* and *R. sphaeroides* share 69 % and *P. marinus* L and *A. vinelandii* NifH share 40 % amino acid sequence identity. However, when comparing the dimeric molecules, the rmsd values cover a broader range from 1.1 to 3.9 Å (top lines in

each entry). For instance, the ADP-bound $NifH_2$ and L_2 structures and the MgADP•AlF_3-bound L_2 structure deviate by 3.0 Å and 3.4 Å, respectively, despite the fact that the L proteins from *P. marinus* and *R. sphaeroides* share a higher sequence identity than *P. marinus* L and *A. vinelandii* NifH. On the other hand, the highest structural similarities (rmsd 1.1 Å) can be found between the MgADP•AlF_4^--bound $NifH_2$ structures and MgADP•AlF_3-bound L_2. This indicates that the two homodimers might adapt similar tertiary structures upon MgATP binding and thus might have parallels with regard to their switch mechanism. In contrast to this, CD spectroscopy experiments have shown that the CD spectra of MgADP and MgATP bound L_2 are very similar to each other and to the CD spectrum of MgADP-bound $NifH_2$, but diverge from the CD spectrum of nucleotide-free L_2 (Bröcker *et al.,* 2010b). In contrast, all three nucleotide stages of $NifH_2$ show distinct CD spectra (Ryle *et al.,* 1996a; Ryle *et al.,* 1996b; Ryle and Seefeldt, 1996). These experiments could be a hint for minor differences in the nucleotide-dependent switch mechanism of L_2 and $NifH_2$ (Bröcker *et al.,* 2010b).

Superposition of MgADP•AlF_3- and ADP-bound structures

A superposition of the MgADP•AlF_3-bound L_2 structure with the ADP-bound L_2 structure with PyMOL (section 2.6.11, see Figure 12) provided insights into the molecular mechanisms of the dynamic switch.

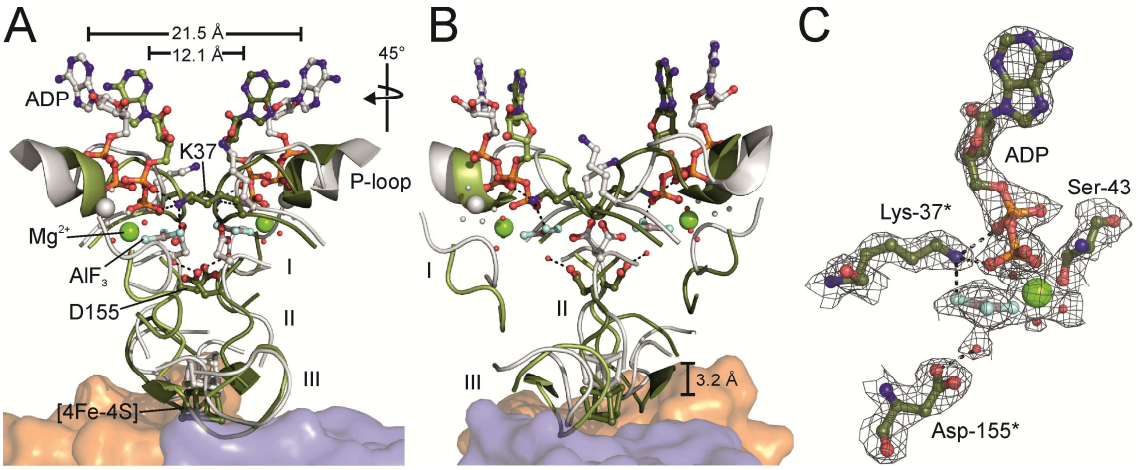

Figure 12: The dynamic switch mechanism of the DPOR L_2 homodimer. A, Superposition of ADP•AlF_3-bound, complexed L_2 from *P. marinus* (green) and ADP-bound L_2 from *R. sphaeroides* (gray, PDB ID 3FWY). Protein regions with strongly deviating C_α positions depending on the bound nucleotide are marked I (Asp-66 – Asp-70 of switch I), II (Leu-153 – Cys-158 of switch II) and III (loop region Pro-118 – Gly-126). The rest of the protein was omitted for clarity. The $(NB)_2$ core tetramer is displayed in orange and blue. The distance between the ADP molecules, measured between the N3-atoms of the two adenine bases in both structures, is indicated. Relevant water molecules are shown as red spheres. **B**, Identical superposition after a 45° clockwise rotation. **C**, Binding of ADP•AlF_3 to L_2 in the octameric DPOR complex. Residues provided by the second L monomer are indicated by asterisks. The $2F_o$-F_c electron density is contoured to 1.5σ. The superposition and the figures were prepared with PyMOL (section 2.6.11) together with Dr. Jörn Kraußе, HZI.

In both the MgADP•AlF_3 and the MgADP-bound structure, the adenosine moiety of the nucleotide is bound by the same amino acid residues (listed in Table 18, appendix), which are not involved in the structural rearrangements of the protein dimer. The conformational change of L_2 is mainly triggered by critical amino acid residues at the dimer interface, which respond to the nature of the bound nucleotides. There are two amino acid residues which undergo a particularly noticeable movement: in the MgADP-bound state, residues Asp-155 and Lys-37 are involved in contacts within one L monomer. In the MgADP•AlF_3-bound structure, however, both residues interact across the dimer interface with the nucleotide of the other protomer (Figure 12 **A** – **C**). Asp-155 seems to position and/or activate a water molecule for the subsequent ATP hydrolysis, whereas residue Lys-37 stabilizes the emerging negative charge. In the MgADP•AlF_3-bound structure, an octahedrally coordinated Mg^{2+} ion contacting the β-phosphate and the AlF_3 molecule might likewise support the hydrolysis. The same situation could be observed in the MgADP•AlF_4^--bound complexed $NifH_2$ structure (Schindelin *et al.,* 1997): Asp-129 and Lys-10 of NifH both reach

across the dimer interface to contact the MgADP•AlF_4^- molecule bound to the other protomer. It was suggested that Asp-129 activates the attacking water molecule for subsequent ATP hydrolysis, whereas Lys-10 stabilizes the leaving group. A biochemical investigation of a NifH mutant in which Asp-129 was mutated to Glu (Lanzilotta *et al.,* 1995) supported the proposed role of Asp-129.

From the dimer interface, the nucleotide state must be 'communicated' to the L_2-bound [4Fe-4S] cluster and the protein regions which are involved in interaction with $(NB)_2$ (e.g. the docking loop (Ile-84 – Glu-96) of L_2). Most likely, those protein regions with strongly deviating C_α positions between the two structures are involved in this signal transduction; they are marked in Figure 12. First, there is the switch I region (residues Gly-64 – Thr-72, *P. marinus* numbering) which is located near the γ-phosphate analog of MgADP•AlF_3. Secondly, the switch II region (Asp-151 – Phe-161) comprises the residues Asp-155 and Cys-158, the latter being one of the [4Fe-4S] cluster ligands. The importance of this region for the formation of the octameric complex has been shown in previous studies: a deletion of residue Leu-153 in the switch II region of the *P. marinus* L protein resulted in a trapped L_2 conformation with a high affinity for $(NB)_2$ (Bröcker *et al.,* 2010b). The same had been shown before for the ΔLeu-127 deletion mutant of *A. vinelandii* $NifH_2$ (Ryle and Seefeldt, 1996). Finally, also the regions Pro-118 to Gly-126 (marked with 'III' in Figure 12) and Met-79 to Glu-96 (not shown) undergo structural rearrangements depending on the bound nucleotide. These regions include the second ligand Cys-124 of the [4Fe-4S] cluster, so that this movement might help to position the cluster for electron transfer to the NB-bound cluster.

With regard to the whole L_2 dimer, the formation of the DPOR complex leads to a more compact structure of L_2: the distance between the N3 atoms of the adenine bases decreases from 21.5 Å to 12.1 Å when ADP•AlF_3 is bound instead of ADP, meaning that the nucleotide-bound L monomers rotate toward the dimer interface. Moreover, the L_2-bound [4Fe-4S] cluster is shifted by 3.2 Å towards the NB surface.

In summary, the nucleotide-dependent switch mechanisms of DPOR and nitrogenase seem to be almost identical based on the comparison of the

available three-dimensional structures. However, the abovementioned CD experiments could be a hint for minor differences between the mechanisms. Another difference was pointed out by electron paramagnetic resonance (EPR) experiments with the $(L_2\Delta Leu153)_2(NB)_2$ DPOR complex (Bröcker *et al.,* 2010b). It could be shown that the electron was not yet transferred from the [4Fe-4S] cluster of $L_2\Delta Leu153$ to the cluster of NB in the DPOR complex, whereas the corresponding $NifH_2\Delta Leu127$ [4Fe-4S] cluster transfers one electron to the P-cluster of NifD/NifK (Lanzilotta *et al.,* 1996). An explanation for this could be differences in the redox potentials of the involved metalloclusters of DPOR and nitrogenase. The redox potentials of the DPOR clusters remain to be determined.

3.1.5 The docking interface of L_2 and NB

A comparison of the docking interfaces of the DPOR and nitrogenase complexes (docking of L_2 to NB and $NifH_2$ to NifD/NifK, respectively) gave insights into the interaction mechanism of these homologous enzymes and the specificity of the subunits interaction. The docking interfaces of the octameric DPOR complex and the MgADP•AlF_4^--stabilized nitrogenase complex from *A. vinelandii* (Schmid *et al.,* 2002) were analyzed using the PISA server (section 2.6.11). This tool identifies residues located at the interface of two protein subunits and detects hydrogen bonds and salt bridges between individual residues. A detailed list of all residues involved in the interaction of the DPOR and nitrogenase subunits of the aluminum fluoride stabilized complexes is given in tables 19 - 22 (appendix). Moreover, the interacting residues were highlighted in the structure-based amino acid sequence alignments of DPOR subunits N and B displayed in Figure 27 and Figure 28 (appendix). Figure 13 illustrates the comparison of the docking interfaces.

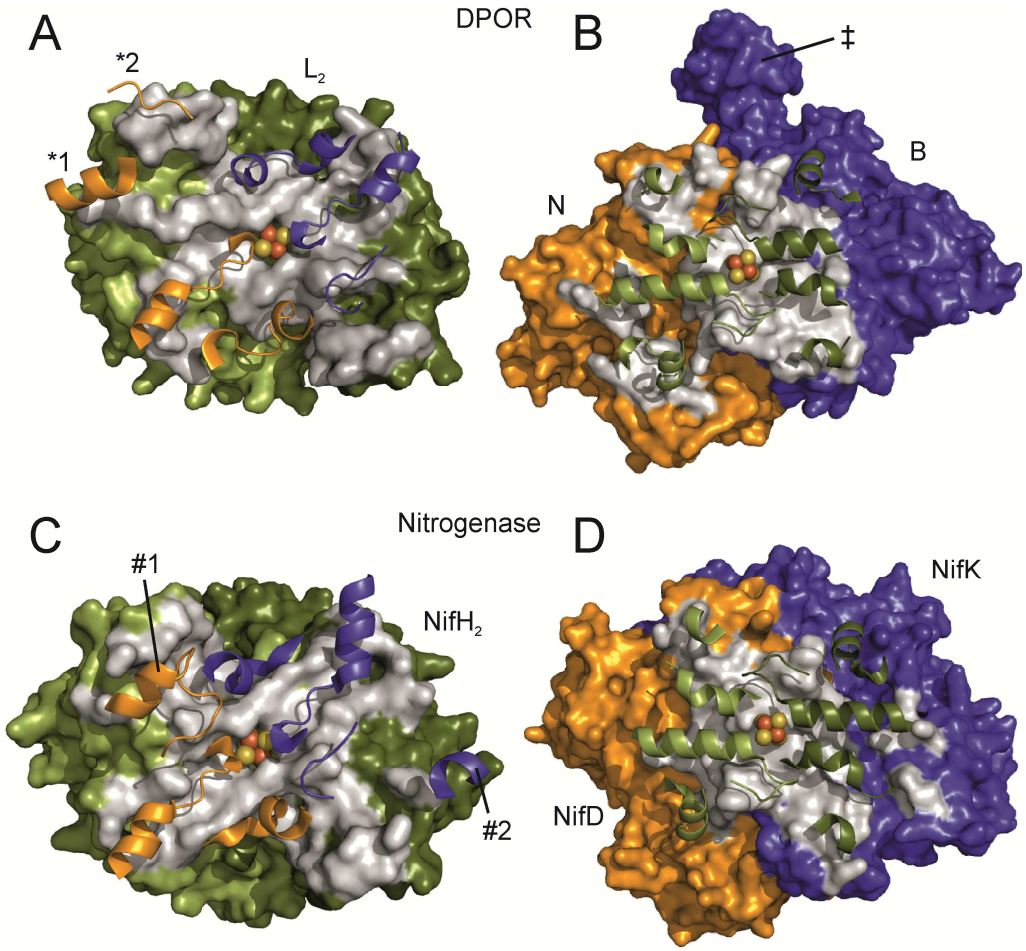

Figure 13: Subcomplex interaction surfaces in the octameric complexes of DPOR and nitrogenase (PDB ID 1M34). Van der Waals surfaces of L_2, $NifH_2$, NB and NifD/NifK are shown. For clarity, only half of each core tetramer is depicted as one functional unit. The key secondary structure elements of the respective docking partner as analyzed with the PISA server are displayed as cartoon. Surface areas of residues involved in protein-protein interactions are shown in gray. **A**, Surface of L_2 viewed along the pseudo-two-fold rotational symmetry axis from (NB). **B**, Surface of (NB) viewed along the two-fold rotational symmetry axis from L_2. **C**, $NifH_2$ surface (chains E and F) viewed in the same orientation as in panel A. **D**, (NifD/NifK) surface (chains A and B) viewed in the same orientation as in panel B. Colors are: subunit L chain A (NifH chain F), dark green; subunit L chain B (NifH chain E), light green; subunit N (NifD), orange; subunit B (NifK), blue. The [4Fe-4S] clusters located on L_2 and $NifH_2$ are shown as spheres. Secondary structural elements involved in the docking of DPOR (*1 and *2 of subunit N) or nitrogenase (#1 of NifD and #2 of NifK), as well as the C-terminal extension of DPOR subunit B (‡), are labeled. Figures were prepared with PyMOL (section 2.6.11)

The structure-based amino acid sequence alignment (Figure 11) revealed that residues of L_2 and $NifH_2$ which contact the surface of subunits N (or NifD, respectively) and B (or NifK, respectively) occupy similar positions within DPOR and nitrogenase. This is reflected by the C_α positions in the three-dimensional structures (Figure 13 **A** and **C**, gray surface area and **B** and **D**, green cartoon representation). Many of these residues are conserved among L or NifH

sequences. However, the chemical character of the amino acid residues is not conserved between the two different enzymes. For example, the L sequence contains more charged residues in the docking regions and the charged surface residues are differently distributed over the L_2 and $NifH_2$ surface. This correlates with the results from a previous study, in which $NifH_2$ from *A. vinelandii* was not able to transfer electrons to $(NB)_2$ from *P. marinus* or *T. elongatus* in *in vitro* activity assays (Wätzlich *et al.,* 2009). In another study it was also shown that L_2 from *R. sphaeroides* was unable to transfer electrons to the $(NifD/NifK)_2$ protein from *A. vinelandii* (Sarma *et al.,* 2008). From the two mentioned studies it was deduced that the altered charge distribution leads to the required specificity for the interaction of the two subcomplexes. In organisms possessing both enzymes, this is relevant to prevent cross-interactions between DPOR and nitrogenase subcomplexes (Sarma *et al.,* 2008). The docking sites observed in the octameric DPOR complex fully support these conclusions.

Upon comparison of residues in N and B contacting L_2 with the respective nitrogenase subunits, fewer similarities were observed: there are only a few central secondary structure elements present in both $(NB)_2$ and $(NifD/NifK)_2$ that are involved in the binding of L_2 and $NifH_2$ in the respective protein complex (Figure 13 **A** and **C**, blue and orange cartoon representation). Apart from these analogous structural elements, there are additional secondary structure elements specific for $(NB)_2$ that contribute to the complex formation with L_2. These are for example an additional helix (Thr-218 – Asp-226, *1) and a loop sequence (Tyr-319 – Glu-323, *2) in subunit N (Figure 13 **A**). Secondary structure elements specific for nitrogenase can also be found (Figure 13 **C**): a loop followed by a helix (Arg-182 – His-196 in NifD, #1) and a helical segment in NifK (Glu-299 – Lys-303, #2) are involved in $NifH_2$ docking. These nitrogenase-specific elements are not found at the interface of the DPOR complex.

Based on amino acid sequence alignments, the DPOR subunit N had always been related to the nitrogenase subunit NifD, and B to NifK due to highest sequence similarities. Upon comparison of the octameric complexes, however, it became obvious that the additional helix in DPOR subunit N (*1 in Figure 13 **A**) is related to the additional docking residues of a helix of nitrogenase subunit NifK (#2 in Figure 13 **C**) when the pseudo-two-fold rotational symmetry of the

complex is applied. Secondly, from the list of docking residues displayed in Table 19 (appendix) it appears that chain F of $NifH_2$ and chain B of L_2 both have more contacts to NifK and N than to NifD or subunit B. In consequence, when the heterotetrameric $NifH_2$(NifD/NifK) complex was structurally aligned to the heterotetrameric L_2NB complex in PyMOL, subunit N was superposed to NifK and subunit B to NifD (not shown). Thus, the docking interface suggests that subunit N rather corresponds to NifK and B to NifD with regard to the spatial position relative to the L_2 or $NifH_2$ dimer. These results support earlier suggestions according to which the subunits of both complexes could have diverged from a more symmetric ancestor (Bröcker *et al.,* 2010a).

3.1.6 The substrate binding pocket

In a previous study, the crystal structure of the heterotetrameric $(NB)_2$ complex from *R. capsulatus* in its Pchlide-bound state had been solved (Muraki *et al.,* 2010). A comparison of the substrate binding in this structure with the octameric DPOR complex might reveal the influence of complex formation on substrate binding.

In the octameric *P. marinus* DPOR structure and the Pchlide-bound *R. capsulatus* $(NB)_2$ complex, the ring system of Pchlide is buried in a cavity formed mainly by hydrophobic amino acid residues provided by both subunits N and B. Therefore, it is likely that distinctive conformational changes are necessary to channel the substrate into this pocket. In both substrate-bound DPOR structures, a partially unwound helix of subunit B from *P. marinus* (residues Pro-421 - Gly-425) or *R. capsulatus* (residues Pro-405 - Gly-409, *R. capsulatus* numbering), respectively, “closes” the substrate binding cavity of the symmetry-related N’B’ heterodimer (Muraki *et al.,* 2010, not shown for the present study). In the Pchlide-free *R. capsulatus* $(NB)_2$ structure the entire sequence (Phe-392 - Asp-421) shows an α-helical conformation. In the *P. marinus* DPOR structure, a C-terminal domain of subunit B (His-480 - Phe-528, Figure 13 **B**, ‡) could be resolved which had been disordered in the protein structures determined before (Bröcker *et al.,* 2010a; Muraki *et al.,* 2010). This C-terminal domain additionally seems to close the substrate-binding cavity

at the NB interface, which might assist to prevent Pchlide-induced photodynamic damage of the cell by keeping the molecule in a protein-bound state. Figure 14 illustrates the detailed binding of the substrate Pchlide in the octameric DPOR complex.

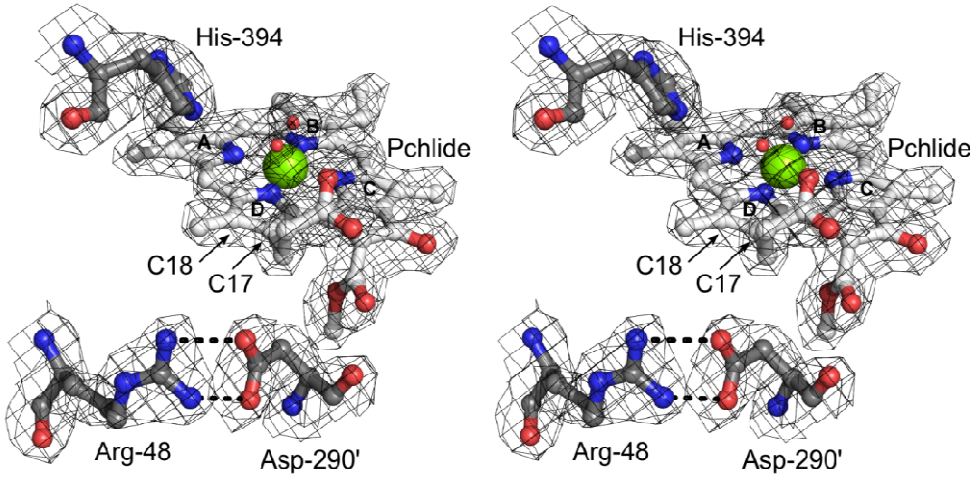

Figure 14: Stereo view of Pchlide binding in the MgADP•AlF_3-stabilized DPOR complex. Three polar amino acid residues are in close proximity to the substrate Pchlide: residues His-394 and Arg-48 are located on one B subunit; whereas Asp-290' is provided by the other B subunit. Pchlide and the amino acid residues are displayed in ball-and-stick mode. The tetrapyrrole rings A – D of the substrate are labeled. Two water molecules in close proximity to Pchlide are displayed as red spheres and the central magnesium of Pchlide as a green sphere. The $2F_o$-F_c electron density is contoured to 1.0σ. The figure was prepared together with Dr. Jörn Kraußе, HZI.

In the structure of the octameric DPOR complex, three polar amino acid residues are located around the substrate Pchlide: residues His-394 and Arg-48 are located on one B subunit whereas Asp-290' is provided by the other B subunit. Two water molecules (displayed as red spheres) are in notable positions with regard to the Pchlide ring system: one of them is an axial ligand to the central magnesium (green sphere) whereas the other one is positioned above the tetrapyrrole ring D. From these structural arrangements it was suggested that Asp290' could be directly responsible for the protonation of Pchlide at C17, as it is located about 5 Å beneath the ring D. When this residue was replaced by alanine, the resulting mutant protein revealed only 2 % residual activity when compared to the wild type enzyme (Table 13). This is in agreement with an earlier study, in which the same mutation (Asp274Ala) was

investigated for the *R. capsulatus* enzyme (Muraki *et al.,* 2010). The structure of the octameric complex revealed that Asp-290' is positioned for protonation by salt bridge formation with the guanidinium group of Arg-48 of the symmetry mate (Figure 14). Mutation of Arg-48 to alanine results in 10 % residual activity compared to the wild type enzyme, indicating the importance of this residue for product formation.

Table 13: Mutational analysis of amino acid residues potentially involved in Pchlide protonation. All three residues are located on subunit B. The purified enzymes were tested for their activity (section 2.8.1) and compared to the wild type enzyme activity.

Mutation	Residual activity in % of wild type activity
Arg48Ala	10
Asp290Ala	2
His394Ala	35

Based on the octameric DPOR structure, the Pchlide C18 protonation could be assisted by residue His-394. Upon mutation of His-394 to alanine, residual activity of 35 % was obtained (Table 13). It was suggested that His-394 positions a water molecule at a distance of 3.2 Å from C18 above the ring (red sphere, Figure 14) which then may act as the proton donor for C18. This suggestion partially contradicts the conclusions from the non-complexed Pchlide-bound *R. capsulatus* structure (Muraki *et al.,* 2010). From this structure it was proposed that the C17 propionate side chain of Pchlide can directly function as the proton donor for the protonation at C18. This suggestion was supported by the observation that the C17-C18 double bond of the competitive inhibitor Chl *c*, which possesses an acrylate instead of a propionate side chain at C17, was not reduced by DPOR. A comparison of the Pchlide binding site of the complexed (*P. marinus*) and non-complexed (*R. capsulatus*) DPOR structures is depicted in Figure 15:

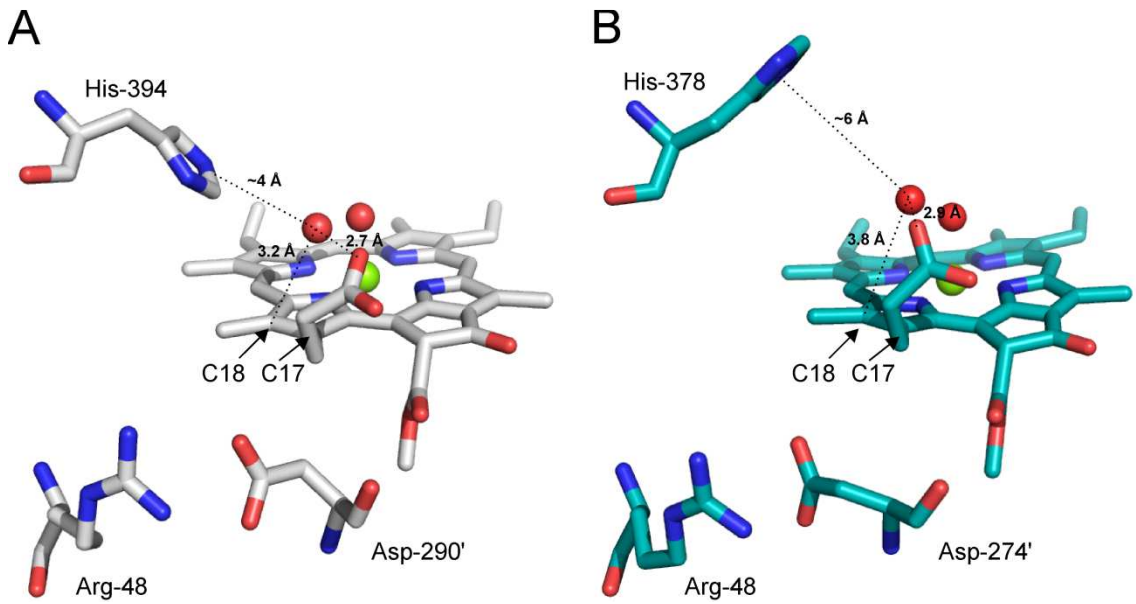

Figure 15: Comparison of Pchlide binding in the complexed and the non-complexed DPOR structure. A, Octameric DPOR complex from *P. marinus*. **B**, Heterotetrameric $(NB)_2$ complex from *R. capsulatus* (PDB ID 3AEK). The three polar amino acid residues in close proximity to the substrate Pchlide are shown. The histidine and arginine residues are located on one B subunit; whereas the aspartate residue is provided by the other B subunit (‘). Pchlide and the amino acid residues are displayed as sticks. The two water molecules above the Pchlide ring system are displayed as red spheres and the central magnesium of Pchlide as a green sphere. The distances between the C17 propionate side chain of Pchlide, the water molecule above ring D and the histidine residue possibly involved in substrate protonation are indicated. The figure was prepared using PyMOL (section 2.6.11).

Figure 15 illustrates that in the complexed (*P. marinus*) and the non-complexed (*R. capsulatus*) DPOR structure, the propionate side chain of Pchlide has a similar distance to the C18 atom of ring D (4.3 Å and 4.2 Å, respectively) and to the water molecule positioned above the ring (2.7 Å and 2.9 Å, respectively). However, the side chain of His-378 adopts a different conformation in the *R. capsulatus* structure (Figure 15 **B**), leading to a distance of ~6 Å to the water molecule located above the ring. This might be the reason why His-378 was not considered as being involved in the protonation mechanism by Muraki *et al.,* 2010. In another recent investigation by Nomata *et al.,* 2014, the authors made use of the Asp274Ala DPOR mutant to block the protonation of C17. Furthermore, Chl *c* was used as a substrate to inhibit the protonation of C18. From EPR and absorption spectroscopy experiments of the Asp274Ala mutant with the natural substrate Pchlide, the formation of an anion intermediate with a reduced C18 atom was proposed (due to the inhibition of the protonation by Asp-274). A combination of the Asp274Ala mutant and Chl *c* suggested the

existence of a substrate anion radical as an intermediate, due to the complete inhibition of substrate protonation. In the same study, His-378 was suggested to represent the proton donor for the propionate side chain of Pchlide, which then transfers a proton to C18. A residual activity of 19 % was detected when His-378 was mutated to alanine, which is comparable to the residual activity of 35 % detected in this study.

The precise role of the histidine residue remains ambiguous. Results from biochemical studies involving the substrate analog Chl *c* point towards the propionate side chain as the direct donor for the C18 protonation (Muraki *et al.,* 2010; Nomata *et al.,* 2014). However, the structure of the octameric complex shows that His-394 is much closer to the substrate than in the non-complexed structure (Figure 15), which could indicate that this residue has a more direct role in C18 protonation. In summary, a C18 protonation mechanism *via* a water molecule distinctly placed 3.2 Å above C18 is suggested. The water molecule is positioned by the interaction with residue His-394 and the C17 propionate side chain of Pchlide.

The Pchlide-bound octameric DPOR structure showed that the substrate molecule is accurately placed in the substrate binding cavity by the protein environment in order to undergo two-electron reduction and protonation. Interestingly, it was shown that DPOR is also able to accomplish the two-electron reduction of the smaller substrates azide (N_3^-) and hydrazine (N_2H_4), thus forming NH_3 (Moser *et al.,* 2013). These substrates are also reduced by nitrogenase and by a nitrogenase variant lacking the FeMoco (“apo nitrogenase”; Moser *et al.,* 2013). However, DPOR was not able to reduce more complex nitrogenase substrates with triple bonds, such as N_2, acetylene (C_2H_2) and CO, which was attributed to the presence of different metal cofactors in the DPOR NB and nitrogenase NifD/NifK subunits (Moser *et al.,* 2013).

3.2 The oxidation of the 3-vinyl substituent to a 3-acetyl moiety – BchF and BchC

Following the DPOR-catalyzed reduction of Pchlide to Chlide, three additional enzymatic steps lead to the formation of BChlide (Figure 4). In the second part of this study, the elucidation of the late steps of BChlide biosynthesis using the recombinantly produced enzymes DPOR, BchF and BchC from *C. tepidum* is described.

3.2.1 Solubilization of His_6-BchF from the *E. coli* membrane fraction

Theoretical analyses using the TMpred program (Hofmann and Stoffel, 1993) revealed four putative membrane spanning helices for different orthologous BchF sequences (Figure 16). For the *C. tepidum* protein, the transmembrane segments comprise (I) residues Ile-23 to Tyr-42, (II) residues Phe-56 to Leu-77, (III) residues Phe-94 to Ile-113 and (IV) residues His-118 to Ile-140.

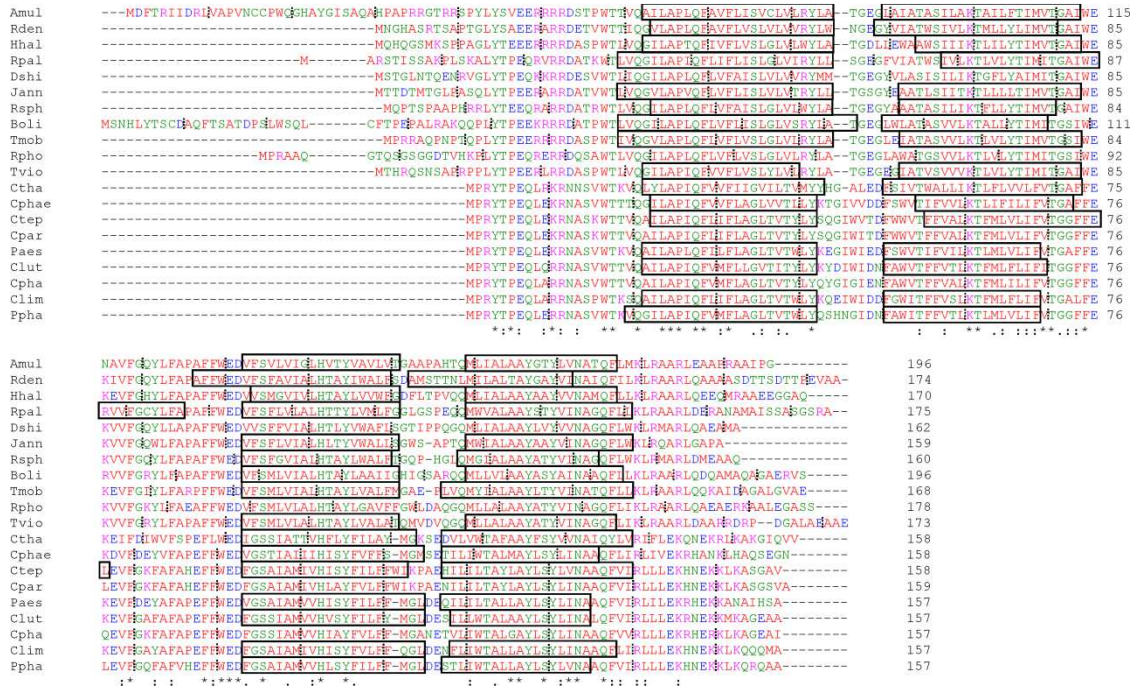

Figure 16: Amino acid sequence alignment of BchF sequences from different organisms. Twenty BchF sequences were used for the alignment. Purple bacteria and green sulfur bacteria were included. Purple bacteria: Amul (*Acidiphilum multivorum*), Boli (*Bradyrhizobium oligotrophicum*), Dshi (*D. shibae*), Jann (*Jannaschia sp.*), Rden (*R. denitrificans*), Rpal (*Rhodopseudomonas palustris*), Rpho (*Rhodospirillum photometricum*), Rsph (*R. sphaeroides*), Hhal (*Halorhodospira halophila*), Tmob (*Thioflavicoccus mobilis*), Tvio (*Thiocystis violascens*). Green sulfur bacteria: Ctha (*Chloroherpeton thalassium*), Cphae (*Chlorobium phaeobacteroides*), Ctep (*C. tepidum*), Cpar (*Chlorobaculum parvum*), Paes (*Prosthecochloris aestuarii*), Clut (*Chlorobium luteolum*), Cpha (*Chlorobium phaeovibrioides*), Clim (*Chlorobium limicola*), Ppha (*Pelodictyon phaeoclathratiforme*). Black boxes show the location of predicted transmembrane helices according to the program TMpred (section 2.6.11). The orientation of the helices is not unambiguously clear in most cases, so that the conserved N-terminal residues might be located on the inside or outside of the inner bacterial membrane. For some sequences, the position of the helices could not be clearly located and is therefore not indicated. The alignment was generated with Clustal Omega (section 2.6.11). Asterisks (*) indicate fully conserved residues, colons (:) mark residues with strongly similar properties, residues with weakly similar properties are indicated by a period (.). In each sequence, every tenth residue is followed by a vertical line.

Initial trials had suggested that recombinant fusion proteins of *C. tepidum* BchF with an N-terminal GST or thioredoxin/His_6/S-tag were integral to the bacterial membrane after heterologous production in an *E. coli* host (J. Moser and S. Virus, personal communication). In those experiments, the total *E. coli* membrane fraction was isolated and purified by sucrose gradient centrifugation and membrane proteins were solubilized using Triton™ X-100.

In this study, the small His_6-tag was chosen to eliminate a possible influence of the large N-terminal fusion tags on BchF preparation or function. After

heterologous expression (section 2.6.1), membrane proteins were prepared by differential centrifugation and solubilized (section 2.6.2). The SDS-PAGE analysis of this experiment is presented in Figure 17.

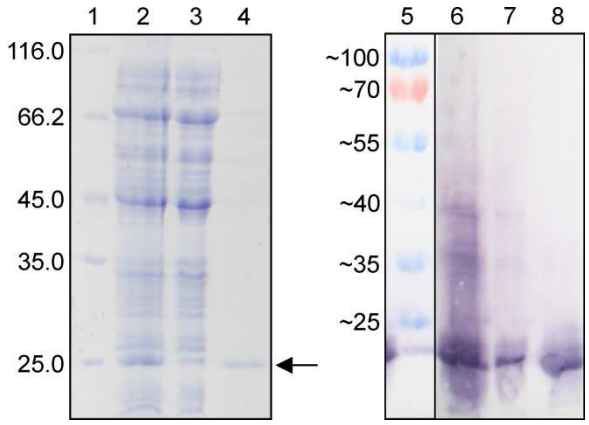

Figure 17: Isolation of heterologously produced *C. tepidum* BchF. His_6-BchF was produced from plasmid pACYCDuet-1_bchF in *E. coli* BL21 (DE3) as described in section 2.6.1. Membrane proteins were prepared by differential centrifugation and subsequent solubilization: cells from 0.5 L *E. coli* culture producing His_6-BchF were disrupted by French Press treatment, yielding a crude cellular extract. After low-speed centrifugation, the total membrane fraction was sedimented by ultracentrifugation. After short washing steps, membrane proteins were solubilized by Triton™ X-100. The supernatant from the subsequent ultracentrifugation contained the solubilized membrane proteins. Samples for SDS-PAGE analysis were supplemented with loading dye and treated at 40 °C for 30 min. Proteins were separated and stained with Coomassie Brilliant Blue (lanes 1 - 4) or analyzed by western blotting detecting the N-terminal His_6-tag (lanes 5 - 8). Lane 1: unstained protein molecular weight marker, molecular masses (x 1'000) are indicated. Lanes 2 and 6: crude cellular extract (5 µL sample). Lanes 3 and 7: supernatant after first ultracentrifugation (5 µL). Lanes 4 and 8: supernatant after Triton™ X-100 solubilization and subsequent high speed ultracentrifugation (5 µL). The arrow indicates the solubilized His_6-BchF protein with an apparent molecular mass of about 25 kDa. Lane 5: prestained protein molecular weight marker, approximate molecular masses (x 1'000) are indicated.

A dominant protein band with an apparent molecular mass of about 25 kDa was detected in the crude cellular extract after cell disruption (Figure 17, lane 2). After sedimentation of remaining unbroken cells and potential inclusion bodies by low speed centrifugation, the total membrane fraction was sedimented by ultracentrifugation. After this ultracentrifugation step, the dominant protein band was less intense in the supernatant (lane 3). This indicated that most of the protein had been sedimented together with the *E. coli* membrane fraction. After solubilization using Triton™ X-100 and repeated ultracentrifugation, a single protein band was detectable in the supernatant by Coomassie Brilliant Blue

staining (lane 4, arrow). This protein was considered as solubilized (Lin and Guidotti, 2009). When the same samples were analyzed by western blotting against the N-terminal His_6-tag of BchF (Figure 17, lanes 6 - 8), a protein with an approximate apparent molecular mass of 20 kDa was detected in all samples. The mobility of His_6-BchF in the SDS-PAGE (apparent molecular mass of about 25 kDa using the unstained protein molecular weight marker) differed from the calculated molecular mass of 20'008 Da, as observed for other transmembrane proteins (Rath *et al.,* 2009).

N-terminal amino acid sequencing of His_6-BchF

The identity of the solubilized protein was verified by N-terminal amino acid sequencing. Fourteen N-terminal amino acids were identified (GSSHHHHHHSQDPM), which corresponded to the N-terminus specific for the pACYCDuet-1 vector (first MCS). Two more amino acids were identified in low amounts (KL), which do not correspond to the first N-terminal amino acids of BchF from *C. tepidum*. However, this was attributed to the decreasing sensitivity of the sequencing method with the increasing number of identified amino acids.

Altogether, these experiments indicate that heterologously expressed *C. tepidum* BchF carrying an N-terminal His_6-tag is located in the membrane of the *E. coli* host. However, the western blot analysis showed that BchF was also present in the subcellular fraction after the first ultracentrifugation step, which was thought to contain only soluble and not membrane-bound proteins. This might be explained by the incomplete sedimentation of the cellular membranes, resulting in a contamination of the soluble protein fraction.

3.2.2 Protein purification of *C. tepidum* BchC

In order to characterize *C. tepidum* BchC biochemically, the protein was heterologously produced (section 2.6.1) and purified (section 2.6.2). A typical SDS-PAGE analysis of the affinity purification of *C. tepidum* BchC is shown in Figure 18.

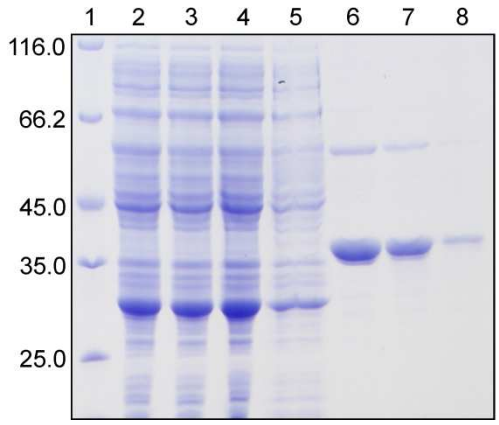

Figure 18: Affinity purification of heterologously produced *C. tepidum* BchC. GST-BchC was expressed from plasmid pGEX6P-1_bchC in *E. coli* BL21 (DE3) as described in section 2.6.1. For affinity purification, cells from 1 L *E. coli* culture expressing GST-BchC were disrupted by French Press treatment. A cell-free extract was prepared by ultracentrifugation and was subsequently applied to 1 mL of Protino® Glutathione Agarose 4B. The first flowthrough was collected and applied to the column a second time. After a washing step, 60 units PreScission protease were added to the column. After incubation, the liberated BchC was drained from the column. For analysis, proteins were separated by SDS-PAGE and stained with Coomassie Brilliant Blue. Lane 1: unstained protein molecular weight marker, molecular masses (x 1'000) are indicated. Lane 2: cell-free extract (2 µL sample). Lane 3: first flowthrough (2 µL). Lane 4: second flowthrough (2 µL). Lane 5: washing fraction (10 µL). Lanes 6 – 8: elution fractions (5 µL) containing untagged BchC with an apparent molecular mass of about 37 kDa.

The GST-BchC fusion protein with a calculated molecular mass of 63'481 Da was present in the soluble protein fraction after cell disruption and ultracentrifugation (Figure 18, lane 2). After immobilization on Protino® Glutathione Agarose 4B (flowthrough 1 and 2 shown in lanes 3 and 4) and a washing step (lane 5), a protein with an apparent molecular mass of about 37'000 was liberated from the column by PreScission protease treatment (lanes 6 – 8). It corresponds well with the calculated molecular mass of 37'068 Da of BchC. The only contamination was a protein with an apparent molecular mass of about 60 kDa. An overall of 3 mg of an almost homogeneous protein was obtained from 1 L cell culture. The purified protein was stable for several weeks when stored at 4°C.

N-terminal amino acid sequencing of BchC

The identity of the purified protein was verified by N-terminal amino acid sequencing. Twelve N-terminal amino acids were identified (GPLGSMEAKKSK), which corresponded to the spacer sequence specific for the pGEX6P-1 vector (GPLGS) and the seven N-terminal amino acids of BchC from *C. tepidum*. The contaminating protein with an apparent molecular mass of about 60 kDa was also analyzed by N-terminal amino acid sequencing. Twelve N-terminal amino acids were identified (KFGNDARVKMLR). A BLAST search identified this sequence as the fragment Lys-7 - Arg-18 of the 60 kDa chaperonin, or GroEL, from *E. coli*.

3.2.3 Artificial substrates of BchC

In order to elucidate BchC substrate specificity, BchC activity was tested *in vitro* in the presence of artificial substrates. The use of modified pigment molecules is an established method to characterize important determinants of substrate recognition (Bröcker *et al.,* 2008b; Griffiths, 1980; Helfrich *et al.,* 1996; Klement *et al.,* 1999; Rüdiger *et al.,* 2005). All artificial substrates were kindly provided by Prof. Dr. Hugo Scheer (LMU Munich). In the present study, Chls and BChls with modified side chains of the tetrapyrrole rings A and E were used. Furthermore, there was variation in the oxidation state of the B ring (chlorin/bacteriochlorin) and the nature and the presence of the central metal ion as well as a hydrophobic side chain. The molecular structures of the artificial substrates are depicted in Figure 19.

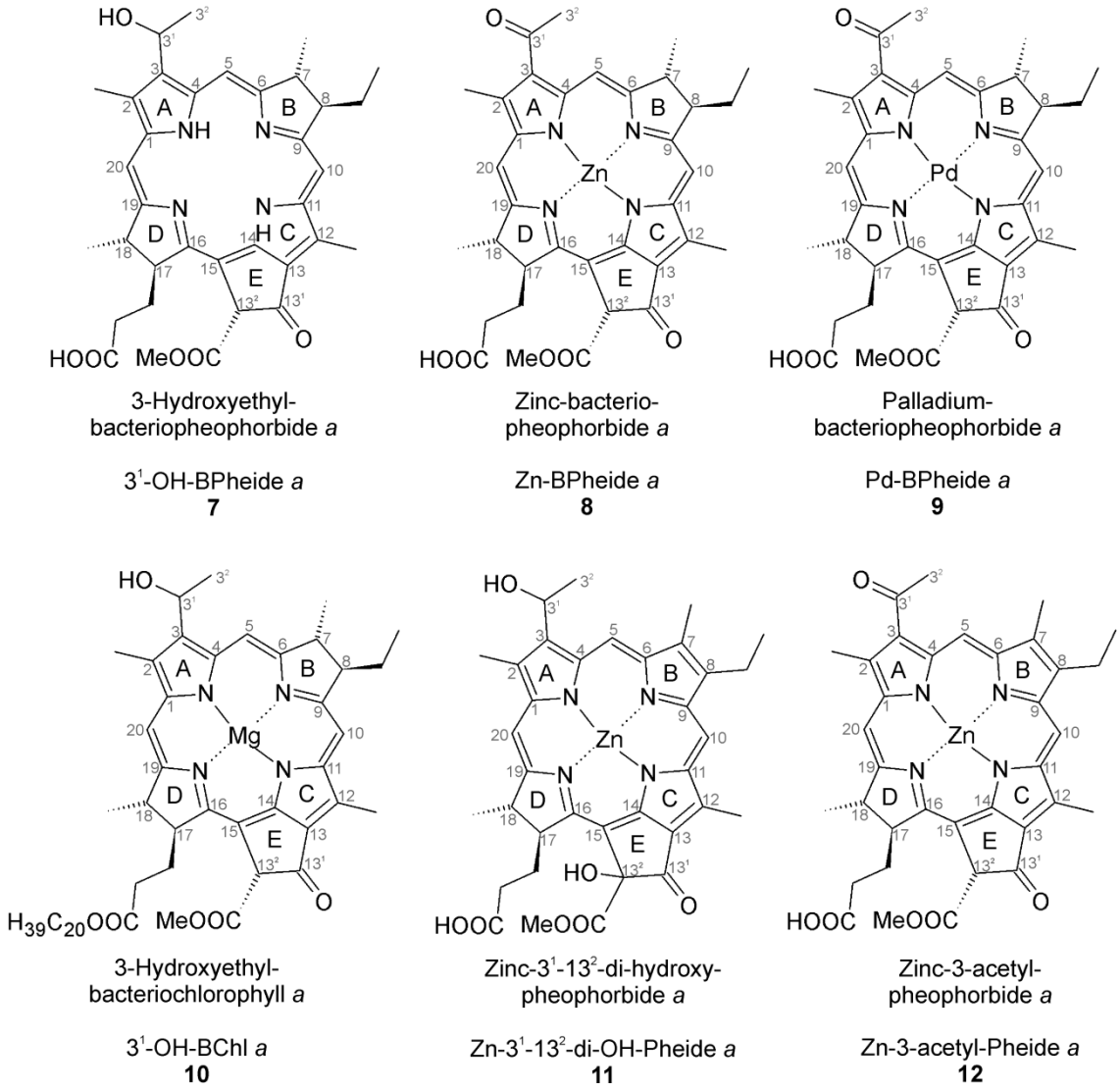

Figure 19: Molecular structures of the artificial BchC substrates used in this study. For each compound, the name is given, together with an abbreviation and a compound number, which will be used throughout the text. The 3-[(1-hydroxy)-ethyl] substituent is often referred to as 3-hydroxyethyl or 3^1-OH in the present literature. The tetrapyrrole rings are labeled A - E. Substrates **7**, **10** and **11** were applied as epimeric mixtures with both *R* and *S* stereochemistry at $C3^1$.

Assay samples contained purified BchC, the respective substrate and NAD^+ as the redox cofactor and were performed as described in section 2.8.4. In the case of substrates carrying a 3-acetyl group (compounds **8**, **9** and **12**), NADH was used as a cofactor and the reverse BchC reaction was investigated. Substrates **7**, **10** and **11** were applied as epimeric mixtures with both *R* and *S* stereochemistry at $C3^1$, which had resulted from the formation of these molecules by borohydride reduction (H. Scheer, personal communication). All pigments were identified by their Q_y absorption bands in acetone-extracted

assay samples. The measured absorption maxima were compared to the maxima of the same or similar compounds described in the literature (see Table 14). Representative absorption spectra are displayed in Figure 20.

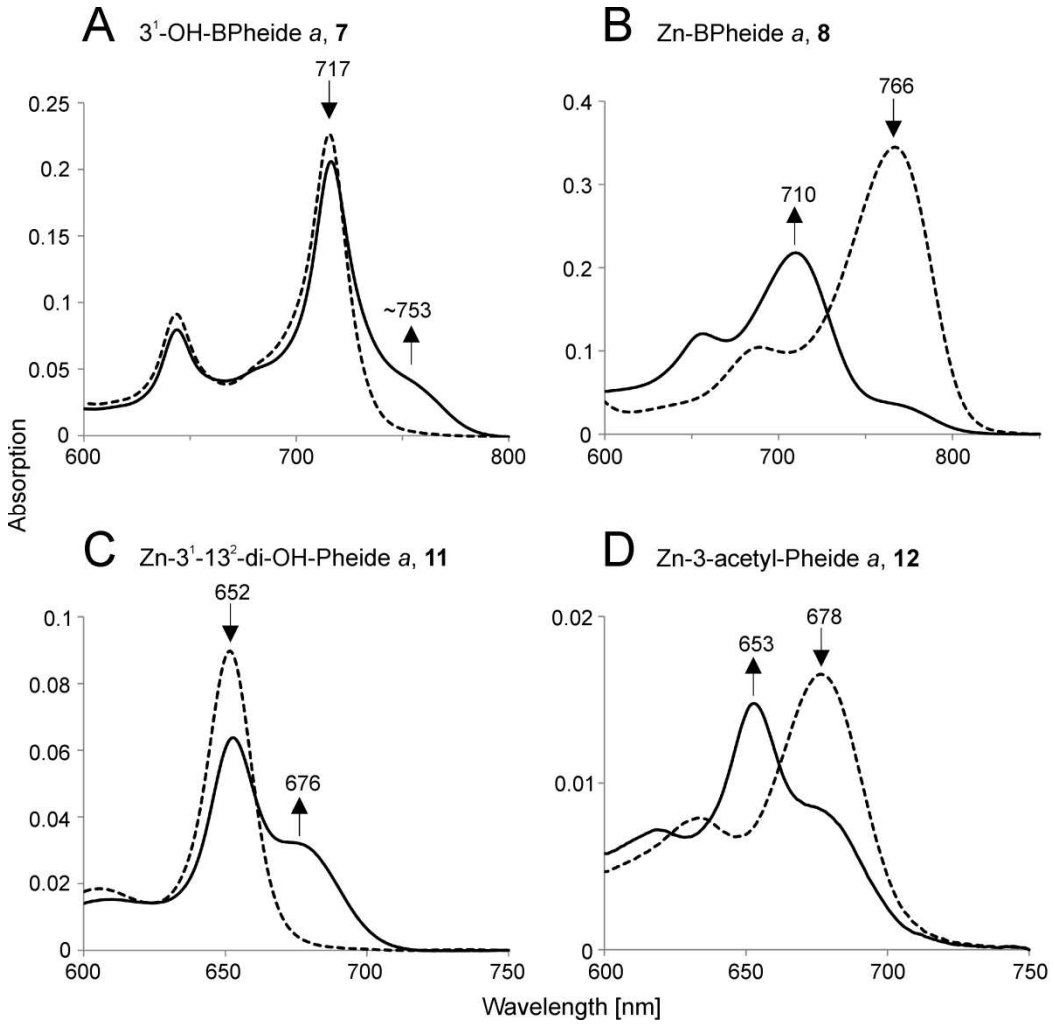

Figure 20: UV-visible light absorption spectra of acetone-extracted samples from *in vitro* BchC activity assays. Assay samples contained purified BchC and the respective substrate in different amounts as well as either 1 mM NAD^+ or NADH in a total of 250 µL buffer-1 (section 2.8.4). Samples were incubated (3 h or 30 min, 34 °C, 600 rpm, darkness) and reactions were terminated by the addition of acetone. Samples were centrifuged twice (17'000 g, 10 min, 4 °C) and absorption spectra were recorded using acetone/50 mM Tris-HCl pH 8.0 (volume ratio 2:1) as reference. Experiments containing BchC (solid lines) and control experiments without BchC (dotted lines) are shown. **A**, ~10 µM 3^1-OH-BPheide *a* (**7**), NAD^+ and 3.2 µM BchC, **B**, 15.3 µM Zn-BPheide *a* (**8**), NADH and 4.8 µM BchC, **C**, 4.2 µM Zn-3^1-13^2-di-OH-Pheide *a* (**11**), NAD^+ and 6.2 µM BchC, **D**, 750 nM Zn-3-acetyl-Pheide *a* (**12**), NADH and 4.0 µM BchC. The characteristic Q_y wavelengths of the reaction products were compared to literature values as listed in Table 14.

In Table 14, the characteristic Q_y maxima of the substrates and products are compared to literature values of the same or comparable compounds.

Table 14: Spectroscopic details of artificial substrates (left) used in BchC *in vitro* activity assays, and the resulting BchC reaction products (right). Assay samples contained purified BchC, the respective substrate and either 1 mM NAD^+ (compounds **7**, **10** and **11**) or NADH (substrates **8**, **9** and **12**) as the redox cofactor in a total of 250 µl buffer-1 (section 2.8.4). Samples were incubated (3 h or 30 min, 34 °C, 600 rpm, darkness) and reactions were terminated by the addition of acetone. Samples were centrifuged twice (17'000 g, 10 min, 4 °C) and absorption spectra were recorded using acetone/50 mM Tris-HCl pH 8.0 (volume ratio 2:1) as reference. Significant substrate utilization for compounds **7**, **8**, **11** and **12** was determined. For compounds **9** and **10**, no significant conversion by BchC was detected (-). [a)]this study, measured in acetone/50 mM Tris-HCl pH 8.0 (volume ratio 2:1), [b)]in diethylether (Struck *et al.,* 1992, for compounds **7** and **10**; Hartwich *et al.,* 1998, for compounds **8**, **9** and **13**), [c)]in acetone (Klement *et al.,* 1999), n.a.: not available.

BchC Substrate	Pigment	$\lambda_{max, Qy}$ [nm][a)]	$\lambda_{max, Qy}$ [nm] (literature)	Product formed by BchC catalysis (Abbreviation)	$\lambda_{max, Qy}$ [nm][a)]	$\lambda_{max, Qy}$ [nm] (literature)
+	3^1-OH-BPheide *a*, **7**	717	712[b)]	Bacteriopheophorbide *a* (BPheide *a*, **13**)	~753	750[b)]
+	Zn-BPheide *a*, **8**	767	762[b)]	Zinc-3-hydroxyethyl-bacteriopheophorbide *a* (Zn-3^1-OH-BPheide *a*, **14**)	710	n.a.
-	Pd-BPheide *a*, **9**	758	753[b)]	-	-	-
-	3^1-OH-BChl *a*, **10**	716	728[b)]	-	-	-
+	Zn-3^1-13^2-di-OH-Pheide *a*, **11**	652	653[a)]	Zinc-3-acetyl-13^2-hydroxy-pheophorbide *a* (Zn-3-acetyl-13^2-OH-Pheide *a*, **15**)	676	672[c)]
+	Zn-3-acetyl-Pheide *a*, **12**	676	672[c)]	Zinc-3-hydroxyethyl-pheophorbide *a* (Zn-3^1-OH-Pheide *a*, **16**)	653	652[a)]

Bacteriochlorin derivatives

In the current literature, the bacteriochlorin 3^1-OH-BChlide (**4**) is indicated as the natural substrate of BchC. The artificial substrate 3^1-OH-BPheide *a* (**7**) is a demetallated analog of 3^1-OH-BChlide (**4**). When the analog **7** was used in the *in vitro* BchC activity assay, its NAD^+-dependent oxidation resulted in a bathochromic absorption shift of 36 nm and a new Q_y band at 753 nm (Figure 20 **A**). This was indicative of the formation of BPheide *a* (**13**), suggesting that

the presence of the central magnesium ion is not a prerequisite for BchC substrate recognition.

Thus, compounds with different central metal ions were also considered as artificial substrates of BchC: Zn-BPheide *a* (**8**) carries a 3-acetyl group instead of a 3-hydroxyethyl moiety at ring A and was therefore subjected to the reverse BchC reaction in the presence of NADH. A hypsochromic absorption shift of 56 nm was observed due to the reduction of the 3-acetyl moiety, i.e. the formation of Zn-3^1-OH-BPheide *a* (**14**, Figure 20 **B**). When Pd-BPheide *a* (**9**) was used as a substrate, only a low amount of product formation could be observed after 3 h of incubation (not shown). Obviously, the presence of the Pd^{2+} central metal ion impedes the BchC catalyzed (back) reaction. As the last bacteriochlorin compound, 3^1-OH-BChl *a* (**10**) was used in the *in vitro* BchC activity assay in the presence of NAD^+. Since no change in the absorption spectrum was observed (not shown), it was concluded that the presence of a bulky hydrophobic ester side chain on ring D abolishes enzymatic substrate oxidation, possibly due to steric effects.

Following the described results, additional experiments were conducted in our group towards a quantitative investigation of BchC substrate utilization (Lange *et al.,* 2015). The specific activity of BchC was determined using the substrates **7**, **8**, and **9**. Specific activities of 1.1 nmol min^{-1} mg^{-1} for 3^1-OH-BPheide *a* (**7**) and 64.9 nmol min^{-1} mg^{-1} for Zn-BPheide *a* (**8**) were determined. For Pd-BPheide *a* (**9**), no specific activity above the detection limit of the assay (0.4 nmol min^{-1} mg^{-1}) could be determined.

Chlorin derivatives

The conjugated π system of bacteriochlorins (compounds **7** - **10**, Figure 19) is mainly responsible for the absorption properties of BChl *a* and its derivatives. Chlorin molecules, however, possess an oxidized tetrapyrrole B ring which leads to absorption maxima of the Q_y bands at approximately 100 nm shorter wavelengths (compounds **11** and **12**, Figure 19). Although no chlorin

intermediates have been described as a substrate of BchC, compounds **11** and **12** were tested as *in vitro* BchC substrates.

When Zn-3^1-13^2-di-OH-Pheide *a* (**11**) was used as a substrate with NAD^+ as the redox cofactor, a bathochromic absorption shift of 24 nm was observed (Figure 20 **C**) due to the oxidation of the hydroxyl group at C3^1. Apparently, neither the chlorin ring structure nor the central zinc ion or the additional hydroxyl group at C13^2 (ring E) impeded BchC catalysis. This finding was supported by the result of the experiments employing the chlorin Zn-3-acetyl-Pheide *a* (**12**) as a substrate (Figure 20 **D**). In this reverse BchC assay, Zn-3-acetyl-Pheide *a* (**12**) was reduced to Zn-3^1-OH-Pheide *a* (**16**) with a Q_y band at 653 nm. This absorption maximum was almost identical to the Q_y absorption maximum of Zn-3^1-13^2-di-OH-Pheide *a* (**11**) at 652 nm.

The following quantification of the BchC substrate utilization (Lange *et al.,* 2015) revealed a specific activity of 21.4 nmol min^{-1} mg^{-1} for Zn-3^1-13^2-di-OH-Pheid *a* (**11**) and 172.5 nmol min^{-1} mg^{-1} for Zn-3-acetyl-Pheid *a* (**12**).

Summary of BchC substrate specificity

Overall, the experiments using artificial BchC substrates showed that magnesium is not crucial as the central metal ion for BchC catalysis. The central magnesium ion can be absent (compound **7**) or replaced by zinc (compounds **8**, **11** and **12**). It has been shown for other enzymes of the (bacterio)chlorophyll biosynthetic pathway that they can process substrates in which the central magnesium ion has been replaced by zinc, for example DPOR (Bröcker *et al.,* 2008b), COR (Kiesel *et al.,* 2015), LPOR (Griffiths, 1980; Helfrich *et al.,* 1996; Rüdiger *et al.,* 2005) and chlorophyll synthetase (Helfrich and Rüdiger, 1992; Helfrich *et al.,* 1994). Moreover, a hydroxyl group at C13^2 was tolerated by BchC (compound **11**), which might indicate that ring E is not involved in substrate recognition. On the other hand, a bulky side chain attached to ring D abolished BchC activity (compound **10**). The results point out that BchC is able to convert not only bacteriochlorin substrates, but also chlorin derivatives. In fact, higher specific activities were determined for the chlorin

compounds compared to the bacteriochlorin compounds (Lange *et al.,* 2015). The oxidation state of the B ring was not crucial for BchC catalysis, although the reduction of ring B changes the spatial orientation of the C7 and C8 substituents. This might mean that the B ring is also not involved in substrate recognition. Altogether, these results indicate that mainly rings A and D might be involved in BchC substrate recognition.

Substrates **7**, **10** and **11** were applied as epimeric mixtures with both *R* and *S* stereochemistry at C3^1. It was assumed that BchC would only be able to use one specific diastereomer as a substrate and operates in a stereospecific manner. However, the investigation of the stereochemistry of BchC catalysis was out of focus of this study.

With regard to the natural substrate of BchC, the results led to the suggestion that the chlorin 3^1-OH-Chlide (**5**) might also be a natural substrate of BchC, although it has never been observed as an accumulated substance in mutants lacking BchC.

3.2.4 Reconstitution of the DPOR-BchF-BchC pathway

Coupled activity assays comprising the BChl *a* biosynthetic enzymes DPOR and COR are well-established (Kiesel *et al.,* 2015; Yamamoto *et al.,* 2014). In order to extend this reconstituted pathway, initial coupled activity assays involving the enzymes DPOR, BchF and BchC from *C. tepidum* had been performed (Peters, 2013). These pathway reconstitution experiments made use of an *E. coli* strain for the polycistronic overproduction of DPOR subunits N, B and L (Bröcker *et al.,* 2008a). In addition, a crude cellular *E. coli* extract containing co-expressed S-tagged BchC (BchC-S) and His_6-BchF was used. However, these initial experiments lacked the appropriate control experiments. Thus, appropriate control plasmids were constructed containing either the *bchC* (Peters, 2013) or the *bchF* gene (section 2.2).

The assay system was based on the conversion of Pchlide to Chlide by *C. tepidum* DPOR (section 2.8.2). In the following step, BchF and BchC were added, together with NAD^+ as the redox cofactor and - in some cases -

additional Pchlide and zinc acetate (section 2.8.3) and samples were further incubated. Reactions were terminated by the addition of acetone and after further processing (section 2.8.5) they were analyzed spectroscopically.

UV-visible light absorption spectroscopy

Figure 21 shows exemplary UV-visible light absorption spectra of the assay samples after acetone extraction.

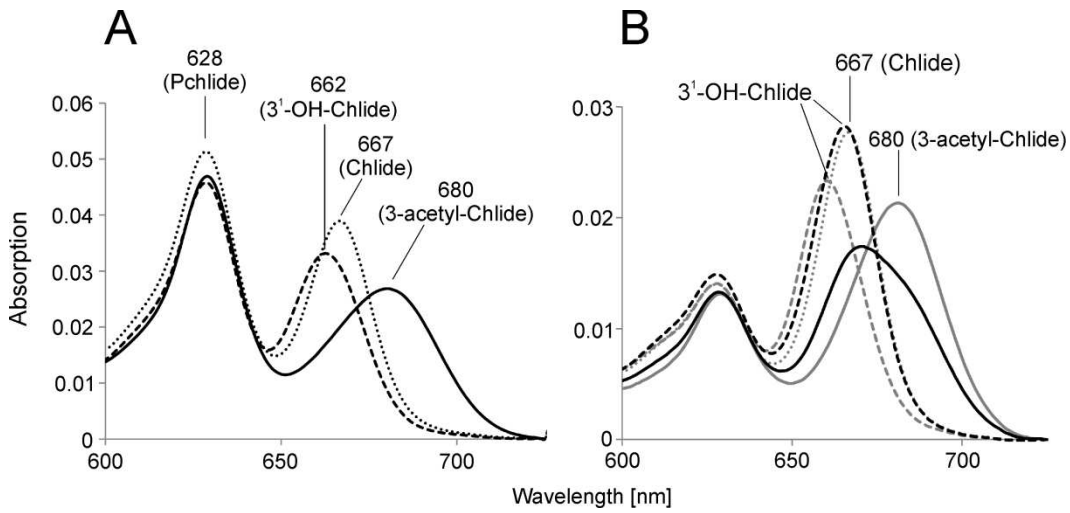

Figure 21: UV-visible light absorption spectra of acetone-extracted samples from a coupled DPOR-BchF-BchC activity assay. Assay samples were set up according to section 2.8.3 and were based on the transformation of Pchlide by DPOR (34 °C, 1 h, 600 rpm, darkness, anoxic conditions). Subsequently, either BchF (crude cellular extract of *E. coli* cells producing His_6-BchF, or solubilized His_6-BchF), BchC (crude cellular extract of *E. coli* cells producing BchC-S, or purified BchC) or both BchF and BchC (crude cellular extract of *E. coli* cells producing both His_6-BchF and BchC-S) as well as other assay components were added and incubation was continued (34°C, 30 min, 600 rpm, darkness). Reactions were stopped by the addition of acetone. Samples were centrifuged twice (17'000 g, 10 min, 4 °C) and absorption spectra were recorded using acetone/50 mM Tris-HCl pH 8.0 (volume ratio 2:1) as reference. Characteristic Q_y wavelengths of the reaction products were compared to literature values as listed in Table 15. **A**, Samples contained DPOR and BchC (crude cellular extract, dotted line), DPOR and BchF (crude cellular extract, dashed line) or DPOR, BchF and BchC (crude cellular extract, continuous line). **B**, Samples contained DPOR (dotted line), DPOR and BchF (crude cellular extract, gray dashed line), DPOR, BchF and BchC (crude cellular extract His_6-BchF and purified BchC, gray continuous line), DPOR and solubilized His_6-BchF (black dashed line) or DPOR, solubilized His_6-BchF and purified BchC (black continuous line).

The control reaction containing DPOR and BchC (Figure 21 **A**, dotted line) showed the Q_y absorption band of the DPOR product Chlide at 667 nm. BchC

was not able to convert Chlide due to a lack of a suitable functional group at C3 and the same result was obtained when only the DPOR enzyme was applied to the assay. Remaining DPOR substrate Pchlide was detected (red-most absorption maximum at 628 nm). In the sample containing DPOR and BchF, the red-most absorption peak was shifted to 662 nm (Figure 21 **A**, dashed line). This indicated that a product other than the DPOR product Chlide had been formed, most likely by BchF catalysis. According to literature values for the Q_y absorption maximum of similar pigments, this product probably is 3^1-OH-Chlide (for references of Q_y absorption maxima, see Table 15). When DPOR, BchF and BchC were subjected to the assay, a new red-most absorption peak at 680 nm was detected (Figure 21 **A**, continuous line). Most likely, BchC was able to convert the BchF product 3^1-OH Chlide to 3-acetyl-chlorophyllide *a* (3-acetyl-Chlide, for references of the Q_y absorption peak see Table 15). The absorption maximum at 680 nm was also detectable when DPOR, BchF and the purified BchC protein were used (Figure 21 **B**, gray continuous line). The utilization of solubilized His_6-BchF in the activity assay lead to a small blueshift of the Q_y absorption maximum compared to the Chlide absorption (Figure 21 **B**, black dashed line), possibly by the formation of 3^1-OH Chlide. By the addition of purified BchC, a “shoulder” at about 680 nm was formed (Figure 21 **B**, black continuous line). This is likely due to the formation of small amounts of 3-acetyl-Chlide. It is possible that either solubilized His_6-BchF and/or BchC did not display full activity in the presence of Triton™ X-100. Interestingly, full BchF activity could also be detected when the subcellular fraction containing only the soluble proteins was used in the coupled DPOR-BchF activity assay (Figure 17, lanes 3 and 7). This is consistent with the detection of His_6-BchF in this sample and might be due to incomplete sedimentation of the membrane fraction.

In summary, four different BChl *a* precursors could be detected by absorption spectroscopy. The Q_y absorption maxima of Chlide and 3^1-OH-Chlide only differed by about 5 nm under the employed experimental conditions.

Fluorescence spectroscopy

Apart from absorption spectroscopy, fluorescence spectroscopy was used to further analyze the samples from the coupled DPOR-BchF-BchC activity assays (section 2.8.3). This method is more sensitive than absorption spectroscopy with regard to the amount of pigment that can be detected (Kobayashi *et al.*, 2006). Moreover, the instrumental setup made it possible to record fluorescence spectra at 77 K (-196 °C). At this low temperature, the band width of excitation and emission peaks decreases, making it possible to distinguish substances with close excitation or emission maxima (Sauer and Debreczeny, 1996).

Initial experiments for the characterization of the DPOR-BchF-BchC coupled activity assays by fluorescence spectroscopy had already been performed in our group (Peters, 2013). These experiments had revealed that the BchC product 3-acetyl-Chlide showed specific excitation and emission maxima which made it possible to distinguish 3-acetyl-Chlide from Pchlide and Chlide. As described above, the initial activity assays were improved in this work and completed by the appropriate control reactions. Finally, specific excitation and emission maxima for all four BChl *a* precursors could be determined:

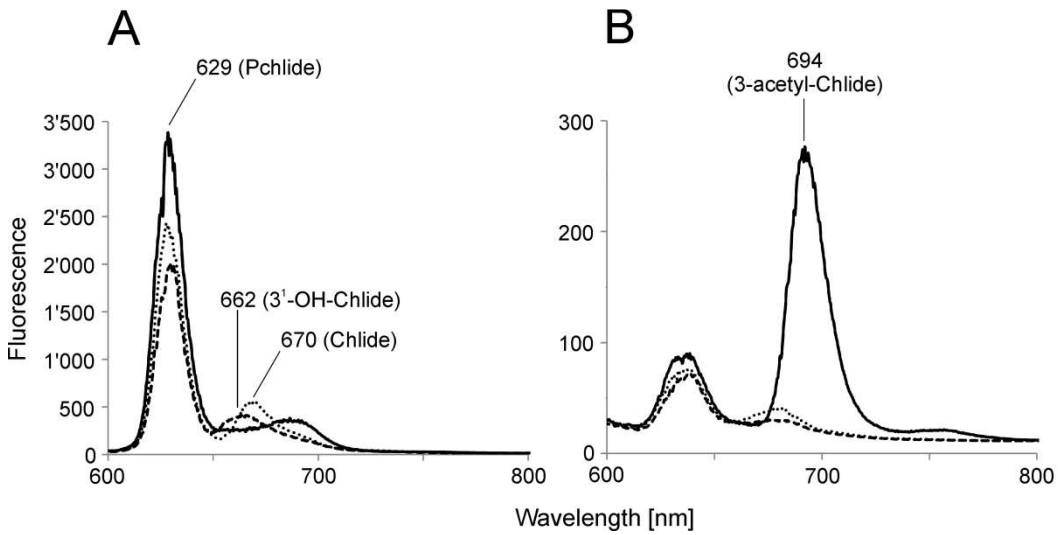

Figure 22: Fluorescence spectra of acetone-extracted samples from a coupled DPOR-BchF-BchC activity assay recorded at 77 K. Samples are the same as shown in Figure 21 **A** and contained DPOR and BchC (crude cellular extract, dotted line), DPOR and BchF (crude cellular extract, dashed line) or DPOR, BchF and BchC (crude cellular extract, continuous line). Fluorescence maxima of the individual compounds are indicated. **A**, Excitation wavelength = 439 nm, **B**, Excitation wavelength = 470 nm.

Figure 22 shows the fluorescence emission spectra of the coupled assay samples after acetone extraction (excitation wavelength λ_{Ex} = 439 nm in panel **A**, or 470 nm in panel **B**). The control reaction containing DPOR and BchC (dotted lines) showed the fluorescence emission of the DPOR product Chlide at 670 nm (λ_{Ex} = 439 nm). The remaining DPOR substrate Pchlide showed emission at 629 nm. In a sample containing DPOR and BchF (dashed lines), a broad emission band at about 662 nm (λ_{Ex} = 439 nm) was observed. This supported the conclusion from the absorption spectroscopy analysis (see Figure 21) that a product other than Chlide had been formed by BchF catalysis. When DPOR, BchF and BchC were present in the assay mixture, the newly formed intermediate 3-acetyl-Chlide, which also had been detected by absorption spectroscopy, showed no specific fluorescence (λ_{Ex} = 439 nm). However, when the samples were excited at 470 nm, this compound showed a distinct fluorescence at 694 nm. This emission maximum was also detectable when the purified BchC protein was used, in addition to DPOR cell-free extract and BchF crude cellular extract (not shown). Thus, the newly detected compound 3-acetyl-Chlide could be distinguished from its precursors Pchlide, Chlide and 3^1-OH-Chlide by its fluorescence properties. Table 15 summarizes the spectroscopic characteristics of the four investigated BChl *a* precursors.

Table 15: Spectroscopic characterization of the BChl *a* precursors detected as the DPOR-BchF-BchC reconstituted pathway intermediates. Pigments from the coupled DPOR-BchF-BchC activity assay were characterized by absorption spectroscopy (see also Figure 21) and low temperature fluorescence spectroscopy (77 K, in acetone/50 mM Tris-HCl pH 8.0, volume ratio 2:1). Specific absorption, excitation and emission maxima could be determined for all four intermediates under the given conditions. The determined fluorescence parameters allow for the specific detection of 3-acetyl-Chlide (**17**) in mixtures containing Pchlide, Chlide and/or 3^1-OH-Chlide (**5**). [a)]this study, measured in acetone/50 mM Tris-HCl pH 8.0 (volume ratio 2:1), [b)]in 80 % acetone (Brouers and Michel-Wolwertz, 1983), [c)]in 50 % acetone (McFeeters *et al.,* 1971), [d)]in diethyl ether (Jones, 1964; Richards and Lascelles, 1969), [e)]in diethyl ether (Lascelles, 1966), [f)]in diethyl ether (Richards and Lascelles, 1969), [g)]in acetone (Smith and Calvin, 1966)

Pigment	$\lambda_{max,\ Qy}$ [nm][a)]	$\lambda_{max,\ Qy}$ [nm] (literature)	$\lambda_{max,\ Em}$ [nm][a)] (λ_{Ex} = 439 nm)	$\lambda_{max,\ Em}$ [nm] [a)] (λ_{Ex} = 470 nm)
Pchlide, **1**	628	626[b)]	629	637
Chlide, **12**	667	667[c)]	670	no emission
3^1-OH-Chlide, **5**	662	659[d)] 660[e)]	662 (broad)	no emission
3-acetyl-Chlide, **17**	680	682[f)] 681[g)]	no emission	694

HPLC analysis

Samples from coupled DPOR-BchF-BchC activity assays (section 2.8.3) were further analyzed by reversed phase HPLC with subsequent multi-wavelength fluorescence detection. The previously determined fluorescence parameters (Table 15) were applied for the specific detection of each BChl *a* precursor, i.e. identical samples were run four times using different detection settings each time.

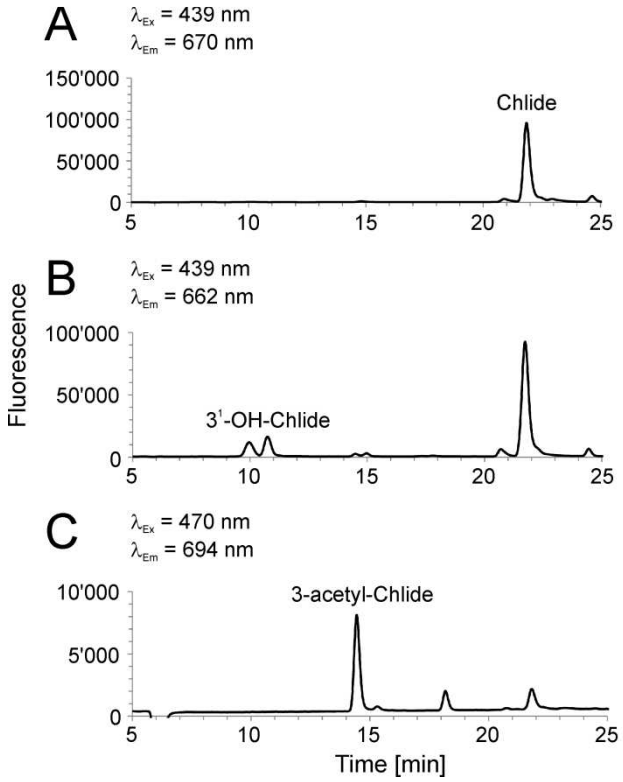

Figure 23: HPLC analysis of acetone-extracted samples from coupled DPOR-BchF-BchC activity assays. Acetone-extracted samples from the coupled DPOR-BchF-BchC activity assays were analyzed on a Jasco HPLC system equipped with a FP-1520 multi-wavelength fluorescence detector using an UltraSep ES RP18 column. A method described by Gough *et al.*, 2007, was used with some modifications. Samples of 20 µL were separated at a flow rate of 0.5 mL/min at 30°C using a linear gradient of 25 – 100 % (v/v) acetonitrile in H_2O containing 0.005 % (v/v) triethylamine over 54 min. The four BChl *a* precursors present in the samples were detected with their individual fluorescence settings as listed in Table 15 and indicated in panels A - C. In panel **A**, a control experiment comprising only the DPOR reaction is shown. The fluorescence detection settings specific for the DPOR product Chlide were used. Panel **B** shows the analysis of the coupled DPOR-BchF assay upon detection of the BchF product 3^1-OH-Chlide. In panel **C**, the coupled DPOR-BchF-BchC assay is shown. The fluorescence detection settings specific for product 3-acetyl-Chlide were used.

The analysis of the sample comprising only the DPOR reaction showed that a compound with the spectroscopic characteristics of Chlide was formed (λ_{Ex} = 439 nm, λ_{Em} = 670 nm) which eluted at 21.8 min (Figure 23 **A**). In the sample containing DPOR and BchF, a product could be detected eluting as a double peak at 10.0 and 10.8 min. This product most likely is 3^1-OH-Chlide (**5**) (λ_{Ex} = 439 nm, λ_{Em} = 662 nm, Figure 23 **B**). Panel **C** in Figure 23 shows that 3-acetyl-Chlide (**17**) was formed in the presence of BchC (λ_{Ex} = 470 nm, λ_{Em} = 694 nm) and eluted at 14.4 min. It is unclear why the assumed 3^1-OH-Chlide (**5**) eluted as a double peak in the HPLC analysis. As this molecule possesses a chiral center at $C3^1$, it was considered that the two peaks could

have emerged from the *R* and *S* epimers. However, this would contradict the assumption that BchF has to provide only one of the two diastereomers for BchC, which most likely operates in a stereospecific manner. However, a recent report confirmed the assumption of a dual stereochemistry of BchF (Harada *et al.,* 2015): it was shown in *in vitro* assays that *C. tepidum* BchF catalyzes the formation of both 3^1-OH-Chlide epimers (*R* or *S* configuration at $C3^1$). Moreover, the authors constructed a *C. tepidum bchF* as well as a *bchV* deletion mutant (see section 1.6). The investigation of the accumulated pigments revealed that BchF is also involved in the biosynthesis of BChl *c* pigments and that in the absence of BchV, BchF has the preference to produce epimers with *R* configuration at $C3^1$ (Harada *et al.,* 2015).

Summary of BchC substrate utilization in vitro *and* in vivo

The results from the *in vitro* BchC assays in the presence of artificial substrates (section 3.2.3) and the coupled DPOR-BchF-BchC assays (section 3.2.4) might have implications on the pathway variants for the biosynthesis of BChl *a*. In Figure 24, an extension of the scheme shown in the introduction (Figure 4) is presented:

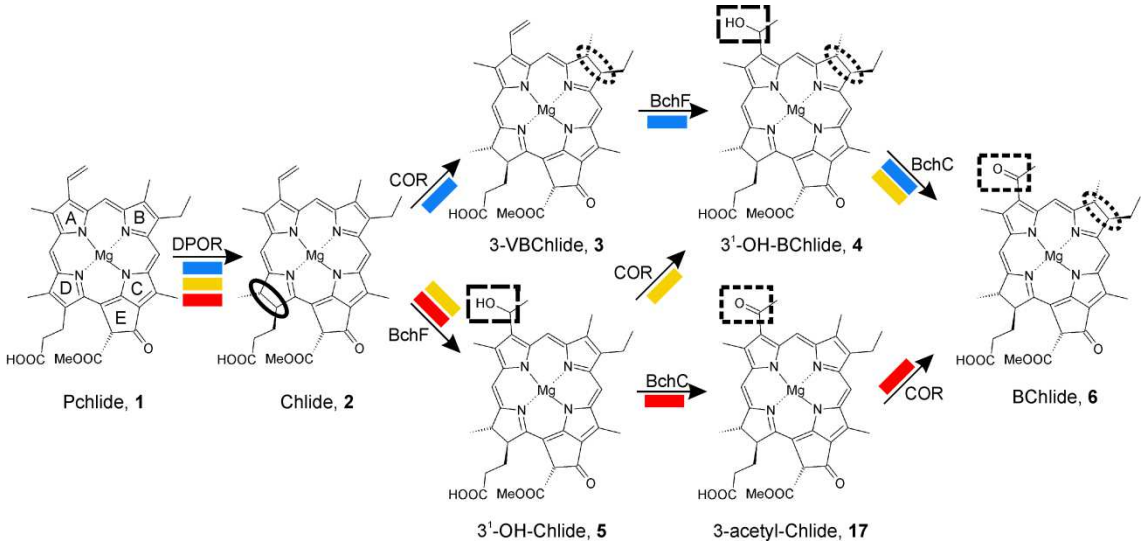

Figure 24: The branched pathway of Bchl *a* biosynthesis from Pchlide to BChlide. The molecular structures of the intermediates are shown and the involved enzymes are named. Previously described enzymatic steps (blue and yellow markings) and the newly suggested enzyme order variant (red markings) are included. The modifications which are introduced by the different enzymes are indicated by boxes and ovals (DPOR: solid oval, COR: dotted oval, BchF: dashed box, BchC: dotted box). For each compound, the abbreviation and compound number is given.

In the past, the upper and the middle pathway variants of the reaction scheme in Figure 24 (labeled with blue and yellow markings) had been elucidated based on the spectroscopic analyses of accumulated precursors from different *Rhodobacter* mutant strains (for references see Table 16). By those analyses, the DPOR product Chlide (**2**) had been identified as the central hub of the biosynthetic pathway leading to BChlide (**6**) and eventually to BChl *a*. In the meantime, not only the *in vivo* accumulation experiments, but also more recent *in vitro* studies characterizing the biosynthetic enzymes of the pathway have given additional evidence for the reaction sequences DPOR-COR-BchF-BchC (blue) and DPOR-BchF-COR-BchC (yellow). Table 16 lists exemplary studies from the literature which support both reaction sequences. Recently, the characterization of the COR enzyme supported the reaction sequence DPOR-COR-BchF-BchC. COR enzymes from *R. capsulatus* and *R. denitrificans* efficiently converted Chlide (**2**) as a direct substrate (Kiesel *et al.,* 2015; Nomata *et al.,* 2006b). In *C. tepidum*, however, comparable mutational studies concerning the BChl *a* biosynthetic pathway are not (yet) existent, but the same

enzyme order variants for BChlide biosynthesis as for the *Rhodobacter* species have been suggested (Frigaard *et al.*, 2006; Liu and Bryant, 2012). The present study revealed the BchF-dependent synthesis of 3^1-OH-Chlide, supporting the reaction sequence *via* DPOR-BchF in *C. tepidum*. The finding that COR from *R. denitrificans* is able to use a substrate with a hydroxyl group at $C3^1$ (Zn-3^1-13^2-di-OH-Pheide *a*, compound **5**) supports the reaction sequence DPOR-BchF-COR-BchC (Kiesel *et al.,* 2015). These findings might indicate that the biosynthesis of BChl *a* proceeds *via* similar steps in *C. tepidum* and *R. denitrificans* with respect to those two reaction sequences.

In the present study, the investigation of *C. tepidum* BchC substrate specificity using artificial substrates revealed that BchC can convert bacteriochlorin (compounds **7** and **8**) and chlorin substrates (compounds **11** and **12**). Moreover, the chlorin 3^1-OH-Chlide (**5**) was identified as BchC substrate in the coupled activity assays and it was concluded that 3^1-OH-Chlide might also be a natural substrate of BchC, although it has never been observed as an accumulated substance in mutants lacking BchC. This would mean that BChl *a* biosynthesis in *C. tepidum* might include an additional branching point which is based on the BchC catalyzed conversion of 3^1-OH-Chlide to 3-acetyl-Chlide. The new biosynthetic route, DPOR-BchF-BchC-COR, is implemented in Figure 24 (red markings). In an earlier *C. tepidum* mutant study (Liu and Bryant, 2011), 3-acetyl-pheophorbide *a* (3-acetyl-Chlide without the central magnesium atom) has been detected, indicating that the new enzyme order variant DPOR-BchF-BchC-COR deduced from the presented *in vitro* study might indeed play a role *in vivo* in *C. tepidum*. Moreover, a recent finding that COR from the purple bacterium *R. denitrificans* can also process an artificial substrate carrying a 3-acetyl group at C3, instead of a 3-hydroxyethyl or a 3-vinyl group (Kiesel *et al.,* 2015) gives a hint that the new reaction sequence might also be relevant for BChl *a* synthesis in purple bacteria.

Table 16: The branched pathway of BChl *a* biosynthesis from Pchlide to BChlide. Experimental evidence for the individual reaction steps displayed in Figure 24 is summarized by listing exemplary studies. *In vivo* mutant accumulation studies and *in vitro* activity experiments with substrate analogs were considered.

Pigment	Substrate for …	Substrate accumulation in mutant studies	*In vitro* substrate utilization experiments
Pchlide, **1**	DPOR	Burke *et al.,* 1993; Yang and Bauer, 1990	Fujita, 2000; Nomata *et al.,* 2005
Chlide, **2**	COR / BchF	Bollivar *et al.,* 1994a; Burke *et al.,* 1993	Kiesel *et al.,* 2015; Nomata *et al.,* 2006b this work
3^1-OH Chlide, **5**	COR / BchC	Bollivar *et al.,* 1994a; Coomber *et al.,* 1990; Hunter and Coomber, 1988; Wellington and Beatty, 1989; Young *et al.,* 1989	Kiesel *et al.,* 2015 this work: pigments **11**, **12**
3-acetyl-Chlide, **17**	COR	no mutant described	Kiesel *et al.,* 2015
3-VBChlide, **3**	BchF	Bollivar *et al.,* 1994a; Burke *et al.,* 1993	-
3^1-OH-BChlide, **4**	BchC	Coomber *et al.,* 1990; Hunter and Coomber, 1988; Wellington and Beatty, 1989	this work: pigments **7**, **8**
BChlide, **6**	BchG	Addlesee *et al.,* 2000; Bollivar *et al.,* 1994b	Addlesee *et al.,* 2000; Oster *et al.,* 1997

3.2.5 Protein characterization of BchC

Bioinformatics analysis

Bioinformatics analyses related *C. tepidum* BchC to the MDR superfamily (Hedlund *et al.,* 2010; Riveros-Rosas *et al.,* 2003). Using the tool InterProScan (section 2.6.11), the N-terminal part of BchC from *C. tepidum* was predicted as a GroES-like domain, whereas the C-terminal part comprises an $NAD(P)^+$ binding site, both of which are typical features of the MDR superfamily (Hedlund *et al.,* 2010). MDRs use either NAD(H) or NADP(H) as redox cofactor, and many MDRs bind one or two zinc ions (Hedlund *et al.,* 2010). These are either directly involved in the dehydrogenase/reductase catalytic activity or exhibit an important structural function (Auld and Bergman, 2008). Thus, MDRs can also

be classified as zinc-containing or non-zinc-containing proteins (Hedlund *et al.,* 2010).

On the one hand, NCBI BLAST analyses (Altschul *et al.,* 1990) of the *C. tepidum* BchC sequence against the sequences deposited in the protein data bank or the non-redundant UniProtKB/SwissProt sequences showed, that among the sequence hits with low E-values and high sequence identity were mainly members of different zinc-containing MDR families. Examples were the well-characterized enzymes sorbitol dehydrogenase (21 % sequence identity, PDB ID 1E3J) and threonine dehydrogenase (30 % sequence identity, PDB ID 3GFB). These orthologous MDRs perform zinc- and NAD(H)/NADP(H)-dependent catalysis which indicated that BchC could also be a zinc-dependent enzyme.

However, manual inspection of a *C. tepidum* BchC amino acid sequence alignment with sequences of structurally characterized zinc-dependent and zinc-independent MDRs (Figure 25) did not reveal a coherent ligand pattern as expected for a zinc-dependent oxidoreductase. The alignment reveals that the conserved ligands of the catalytic zinc ion (labeled in yellow or pink, respectively, in Figure 25) in the zinc-dependent MDRs are not conserved in BchC. In a similar position to the zinc-coordinating cysteine residue, BchC contains the conserved residues Ser-39, Ser-42 and Glu-46. Instead of the zinc-coordinating histidine, the conserved residue Tyr-67 is present in the BchC sequence. The first conserved, zinc-coordinating glutamate residue is also conserved among BchC sequences. Instead of the second zinc-binding glutamate residue, His-141 is conserved in BchC.

Based on these analyses, it was questioned whether BchC was a zinc-dependent member of the MDR superfamily with unusual zinc ligands, or a zinc-independent enzyme. ICP-MS and chelator-treatment of the purified BchC protein in combination with activity assays were performed for analysis. Moreover, BchC was subjected to site-directed mutagenesis in a first approach and the cofactor specificity of BchC was elucidated.

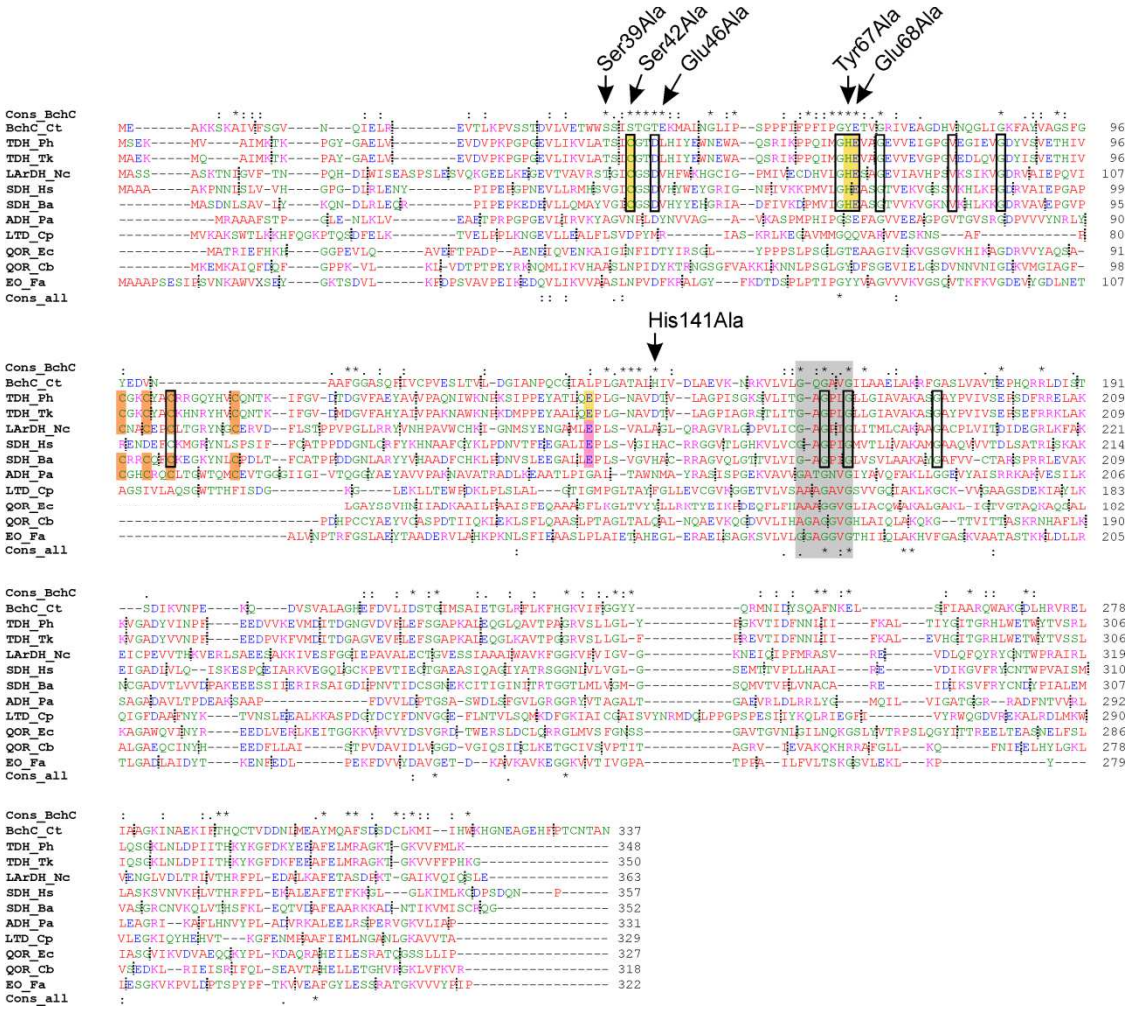

Figure 25: Amino acid sequence alignment of *C. tepidum* BchC with zinc-containing and zinc-independent MDRs. Cons_BchC shows the conservation pattern for an alignment of 19 BchC sequences (see Figure 29, appendix) and has been manually added to the amino acid sequence alignment of orthologous MDRs. Zinc-containing MDRs are: TDH_Ph (L-threonine dehydrogenase *Pyrococcus horikoshii*), TDH_Tk (L-threonine dehydrogenase *Thermococcus kodakarensis*), LarDH_Nc (L-arabinitol 4-dehydrogenase *Neurospora crassa*), SDH_Hs (sorbitol dehydrogenase *Homo sapiens*), SDH_Ba (sorbitol dehydrogenase *Bemisia argentifolii*). Zinc-independent MDRs: LTD_Cp (leukotriene B_4 12-hydroxydehydrogenase/15-oxo-prostaglandin 13-reductase (LTB_4 12-HD/PGR) *Cavia porcellus*), QOR_Ec (quinone oxidoreductase *E. coli*), QOR_Cb (quinone oxidoreductase *Coxiella burnetii*), EO_Fa (enone oxidoreductase *Fragaria vesca*). The alcohol dehydrogenase from *Pyrobaculum aerophilum* (ADH_Pa) possesses a structural, but no catalytic zinc ion. Catalytic zinc-binding residues are highlighted in yellow. Residues coordinating a water molecule ligating the catalytic zinc ion are marked in pink. Ligands for a structural zinc ion are highlighted in orange. Black boxes indicate conserved residues among MDRs with a catalytic zinc ion (information derived from an alignment of 11 zinc-containing MDR sequences, see Figure 30, appendix). Highlighted in gray is the nucleotide binding motif. Arrows indicate *C. tepidum* BchC residues which were mutagenized in the present study. Cons_all shows the sequence conservation of the overall alignment. Asterisks (*) indicate fully conserved residues, colons (:) mark residues with strongly similar properties, residues with weakly similar properties are indicated by a period (.). The alignment was created with Clustal Omega (section 2.6.11).

Activity assays of BchC mutant proteins

Highly conserved BchC residues were identified from an extended sequence alignment of BchC sequences (compare conservation pattern of the BchC alignment implemented in the alignment shown in Figure 25). A potential role of residues Ser-39, Ser-42, Glu-46, Tyr-67, Glu-68 and His-141 as alternative zinc ligands was hypothesized. Accordingly, these residues were each replaced by alanine residues and the respective mutant proteins were purified according to the wild-type enzyme (section 2.6.2). Enzymatic activity was analyzed in coupled *in vitro* activity assays (section 2.8.3).

For mutant proteins BchC Ser39Ala and Ser42Ala, residual activities of about 7 and 40 % were observed when compared to the wild type enzyme (3 h incubation). For Glu46Ala, Tyr67Ala, Glu68Ala and His141Ala no enzyme activity could be detected, i.e. no absorption of the BchC product at 680 nm was visible (not shown). These results are indicative for a key catalytic role of residues Glu-46, Tyr-67, Glu-68 and His-141 in BchC catalysis. In order to rule out protein instability as the source of the lacking activity, supplementary fluorescence thermal shift assays were conducted in our group for all mutant proteins, confirming their integrity (Lange *et al.,* 2015). However, from these experiments no evidence concerning potential zinc ligands of BchC or about the metal dependence in general could be gained. From mutant studies of zinc-dependent MDR enzymes it is known that a conversion of the zinc ligands to alanine abolishes the enzymatic activity of these enzymes. Examples for this are the mutations Cys37Ala, His59Ala and Asp150Ala in the alcohol dehydrogenase from *Thermoanaerobacter brockii* (Bogin *et al.,* 1997), the Glu70Ala mutation in cinnamyl alcohol dehydrogenase from *Arabidopsis thaliana* (Youn *et al.,* 2006a) or the Glu155Ala mutation in sorbitol dehydrogenase from *Rattus norvegicus* (Karlsson and Höög, 1993).

Chelator treatment of BchC

In order to analyze a potential metal dependence of BchC, the chelating substances EDTA and EGTA were used to remove the potential zinc ion from

the active site of BchC. The protocol was derived from earlier studies with zinc-dependent MDRs in which their metal dependence was elucidated (Bashir *et al.,* 2009; Machielsen and van der Oost, 2006; Magonet *et al.,* 1992). Samples of purified BchC were incubated in the presence of EDTA or EGTA, the chelating agent was removed by buffer exchange (section 2.6.7) and BchC was applied to activity experiments (section 2.8.3). In order to rule out potential interfering effects by the cell-free DPOR extract or the crude cellular BchF extract, the chelator-treated BchC was also applied to activity assays in the presence of the artificial substrates 3^1-OH-BPheide *a* (**7**) or Zn-3^1-13^2-di-OH-Pheide *a* (**11**).

In all samples of the coupled activity assays containing BchC, the Q_y maximum of 3-acetyl-Chlide at 680 nm could be observed. When compound **7** was used as a substrate, a Q_y maximum of about 753 nm was detected in the presence of BchC. Using substrate **11**, the product of BchC catalysis showed a Q_y absorption at 676 nm. These results indicate that all assays containing chelator-treated BchC showed full BchC activity. However, this outcome did not reflect the comparable findings for well-characterized zinc-dependent MDR enzymes: chelation of the zinc ions of yeast alcohol dehydrogenase (Magonet *et al.,* 1992) and L-threonine dehydrogenases from *Pyrococcus furiosus* and *Thermococcus kodakaraensis* with EDTA (Bashir *et al.,* 2009; Machielsen and van der Oost, 2006) resulted in enzymatic inactivation. Based on these results, a zinc-independent BchC catalysis was considered.

Inductively coupled plasma mass spectrometry

ICP-MS has been applied to some zinc-dependent MDRs to detect catalytic and/or structural zinc ions (Tiwari *et al.,* 2012; Ying and Ma, 2011). For evidence about the metal status of BchC, the zinc content of the purified BchC enzyme was analyzed by ICP-MS. As a negative control, the C-terminal domain of alanyl-phosphatidylglycerol synthase (A-$PGS_{543-881}$) was purified in analogy to BchC. A zinc content of 0.110 µg/mL was determined for BchC (protein concentration 24 µM) and 0.023 µg/mL for A-PGS (protein concentration 16 µM). Thus, a zinc content of 7 % for BchC and 2 % for the control protein A-

PGS could be calculated. As A-PGS had been shown to be zinc-independent (Hebecker *et al.,* 2011), it was concluded that BchC does not contain a zinc ion. This is supported by the results from the artificial substrate BchC activity assays (section 3.2.3), showing that purified BchC was active without the addition of external zinc ions. Contaminating proteins might be responsible for the measured zinc content of 7 % for the BchC preparation. Also, the chelator treatment experiments (section 3.2.5) are indicative for a zinc-independent BchC catalysis, contradicting the initial BLAST analysis which suggested that BchC was most similar to the zinc-dependent members of the MDR superfamily. Nevertheless, the concluded zinc-independent catalysis of BchC reflects the absence of the highly conserved ligands of a catalytic zinc ion as shown in Figure 25 for the zinc-dependent MDR sequences (cysteine, histidine and glutamate).

Cofactor specificity of BchC and single turnover experiments

Among MDRs, NAD(H) or NADP(H) are the redox cofactors necessary for catalysis (Hedlund *et al.,* 2010). In anabolic pathways, usually NADP(H) is used as a redox cofactor. To test whether $NADP^+$ was also a suitable redox cofactor for BchC, a coupled DPOR-BchF-BchC activity assay (section 2.8.3) was performed in the presence of $NADP^+$ instead of NAD^+.

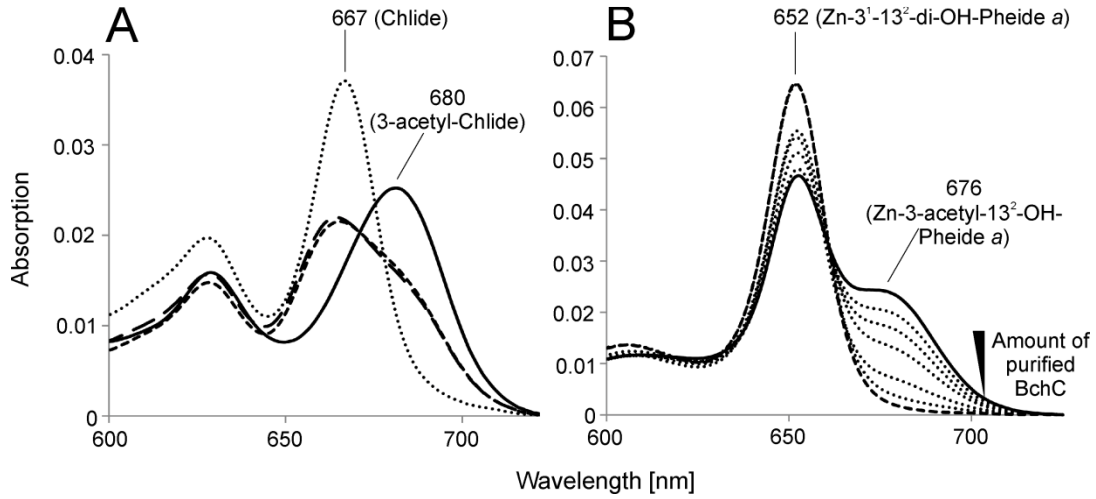

Figure 26: Cofactor specificity and occupancy of BchC. A, UV-visible light absorption spectra of acetone-extracted samples from a coupled DPOR-BchF-BchC activity assay in the presence of different redox cofactors. Assay samples were set up according to section 2.8.3 and were based on the transformation of Pchlide by DPOR (34 °C, 1 h, 600 rpm, darkness, anoxic conditions). Subsequently, BchF (crude cellular extract of *E. coli* cells producing His_6-BchF), purified BchC and the other assay components were added and incubation continued (34 °C, 30 min, 600 rpm, darkness). Reactions were stopped by the addition of acetone. Samples were centrifuged twice (17'000 g, 10 min, 4 °C) and absorption spectra were recorded against acetone/50 mM Tris-HCl pH 8.0 (volume ratio 2:1) as reference. Samples contained only DPOR (dotted line) or DPOR, BchF and BchC without additional cofactor (long dashes), 500 µM $NADP^+$ (short dashes) or 500 µM NAD^+ (continuous line). **B**, UV-visible light absorption spectra of acetone-extracted samples from the *in vitro* BchC single turnover activity assay. Different amounts of purified BchC (0.8, 2.0, 4.0, 6.0 and 8.0 µM) were incubated (34 °C, 3 h, 600 rpm, darkness) with 2.9 µM of the artificial substrate Zn-3^1-13^2-di-OH-Pheide *a* (**11**) in the absence of additional cofactor (dotted lines) in a total of 250 µL buffer-1. Reactions were terminated by the addition of acetone. Samples were centrifuged twice (17'000 g, 10 min, 4 °C) and absorption spectra were recorded against acetone/50 mM Tris-HCl pH 8.0 (volume ratio 2:1) as reference. Increasing amounts of BchC are indicated by an arrowhead. Control experiments without BchC (dashed line) or containing 4 µM BchC, 2.9 µM substrate **11** and 1 mM NAD^+ (continuous line) are shown.

In analogy to the coupled activity assays (section 3.2.4), Figure 26 shows that the BchC product 3-acetyl-Chlide was formed in the presence of NAD^+ (**A**, solid line). When NAD^+ was replaced by $NADP^+$ however, a low degree of product formation was observed (Figure 26 **A**, short dashes). A control experiment without externally added nucleotide cofactor showed an almost identical absorption spectrum (Figure 26 **A**, long dashes), so that the two spectra overlap. These results indicated that NAD^+ was the preferred cofactor of BchC and that $NADP^+$ was not used. However, the question remained why residual activity was detected when $NADP^+$ or no additional cofactor was present in the samples. Either, the crude cellular extract involved in the experiments supplied

a certain amount of NAD^+ for BchC catalysis, or BchC was purified in a binary complex with its cofactor.

Thus, single turnover experiments were conducted. Purified BchC was incubated with the artificial substrate Zn-3^1-13^2-di-OH-Pheide *a* without external addition of NAD^+. Increasing BchC concentrations were used (0.8, 2.0, 4.0, 6.0 and 8.0 µM), while the substrate concentration remained constant (2.9 µM). With this experimental setup, BchC would only be able to catalyze a single turnover, due to the lack of externally added cofactor. If NAD^+ was bound to BchC and not lost during purification, catalysis could take place. The experiments revealed that with increasing BchC concentration, gradually increasing product concentrations were observed (Figure 26 **B**, dotted lines), as judged from the increasing absorption at 676 nm. A control experiment with 1 mM NAD^+ excess (continuous line) showed a higher product concentration. A control assay without BchC did not indicate BchC product formation (dashed line). It was concluded that the overproduced *C. tepidum* BchC was purified partially in complex with its specific cofactor NAD^+. In an experiment conducted later in our group it was shown that 1 mM $NADP^+$ excess did not stimulate BchC activity (Lange *et al.,* 2015).

From the *C. tepidum* BchC experiments in the present study it was concluded that this enzyme is a zinc-independent oxidoreductase which specifically uses NAD^+ as a redox cofactor. These findings support a recent bioinformatics investigation: Hedlund *et al.*, 2010, developed a Hidden Markov Model (HMM) for each of the different protein families within the MDR superfamily by iterative refinement. In total, 86 HMMs were developed and the BchC sequences were assigned to a separate MDR family (MDR057). The authors describe a common correlation between the zinc content and the cofactor specificity of MDR enzymes: enzymes which bind two Zn^{2+} ions usually use NAD^+ as a cofactor and show dehydrogenase function whereas enzymes without Zn^{2+} ions use mainly NADPH and exhibit reductase function. However, the BchC enzymes, besides three other MDR families, were proposed to differ from this pattern: BchC enzymes were predicted as NAD^+-dependent enzymes despite lacking a catalytic or structural Zn^{2+} ion. This is now experimentally confirmed by the data of the present study. A few other enzymes have been characterized that differ

from the common pattern: the zinc-independent enone oxidoreductase from *Fragaria x ananassa* catalyzes the formation of the flavor compound 4-hydroxy-2,5-dimethyl-3(2*H*)-furanone by the reduction of a polar C=C double bond (PDB ID 4IDA, Schiefner *et al.,* 2013). The enzyme is able to use both NADPH and NADH for the reduction (with a preference for NADPH), thus representing another zinc-independent MDR able to use NADH. Another example, the zinc-independent LTB_4 12-HD/PGR (PDB ID 1V3T) from *Cavia porcellus* is a bifunctional enzyme. One of its functions is the $NADP^+$-dependent oxidation of a secondary hydroxyl function of its substrate leukotriene B_4 (Hori *et al.,* 2004; Yamamoto *et al.,* 2001). Based on the present literature, it was not possible to deduce a common reaction mechanism for the different zinc-independent MDRs characterized. However, mechanisms have been proposed for several individual enzymes and suggest the formation of an enolate anion intermediate. The latter is supposed to be stabilized by the active site residue Tyr-260 in the alkenal double bond reductase from *A. thaliana* (Youn *et al.,* 2006b) and Tyr-245 in LTB_4 12-HD/PGR from *C. porcellus*, respectively (Hori *et al.,* 2004, see also Figure 25). In the enoyl reductase LovC from *Aspergillus terreus* (Ames *et al.,* 2012) and the enone oxidoreductase from *F. x ananassa* (Schiefner *et al.,* 2013), the stabilizing residues are suggested to be Lys-54 and Lys-59, respectively. Thus, a potential involvement of the corresponding BchC residues Tyr-244 or Lys-47 could be supposed, although the lysine residue is replaced by an arginine residue in some species. In the present study, critical involvement of residues Glu-46, Tyr-67, Glu-68 and His-141 in BchC catalysis was shown. However, the comparison of BchC with members of different MDR families (Figure 25) does not reveal the conservation of these key catalytic BchC residues among the other MDR enzymes. This might indicate that BchC has a differing pattern for substrate ligation/activation, but no detailed role of these residues in the catalytic mechanism can be deduced yet.

4 Summary

During the complex pathway of (bacterio)chlorophyll biosynthesis, the characteristic chlorin ring system is formed by the stereospecific two-electron reduction of the tetrapyrrole D ring. The enzyme DPOR, comprised of subunits L, N and B, catalyzes this reduction in an ATP-dependent manner, using [4Fe-4S] clusters for electron transfer. In the first part of the present work, the substrate-bound octameric DPOR complex from *P. marinus* was crystallized and its three-dimensional structure was determined by X-ray crystallography (PDB ID 2YNM). At the final resolution of 2.6 Å, details of the protein-bound substrate Pchlide, the ATP analog MgADP•AlF_3 as well as the oxygen-sensitive [4Fe-4S] clusters were resolved in the obtained model. The octameric complex, comprised of two L_2 and one $(NB)_2$ subcomplex, revealed a high degree of structural homology to the related nitrogenase complex and showed a linear arrangement of the L_2- and NB-bound redox-active [4Fe-4S] clusters with the substrate Pchlide. Detailed comparison of MgADP•AlF_3-bound L_2 with structures of the nitrogenase $NifH_2$ dimer indicated a closely related nucleotide-dependent switch mechanisms of DPOR and nitrogenase. Comparative analyses of MgADP- and MgADP•AlF_3-bound L_2 structures revealed a nucleotide-dependent conformational change of L_2, mainly triggered by critical amino acid residues at the dimer interface responding to the nature of the bound nucleotides. The dynamic switch of L_2 leads to a repositioning of the L_2-bound [4Fe-4S] cluster and might be a measure to control electron transfer from the L_2 to the NB cluster. Furthermore, the model of the octameric complex showed that the docking interfaces of the DPOR subcomplexes L_2 and NB and the respective nitrogenase subcomplexes $NifH_2$ and NifD/NifK differ with regard to the nature of the involved amino acids and secondary structure elements. Moreover, subunit N rather seems to correspond to NifK and B to NifD with regard to the spatial position relative to L_2 or $NifH_2$. In the DPOR complex, three polar amino acid residues (His-394, Arg-48 and Asp-290 of B) and two water molecules are located around the substrate Pchlide. Based on this structural arrangement and due to mutational studies, a C18 protonation mechanism *via* a water molecule is suggested. This water molecule is positioned by His-394 and the C17 propionate side chain of Pchlide.

The second part of this work described the characterization of the recombinantly produced enzymes BchF and BchC from *C. tepidum*. Bioinformatics and localization analyses indicated that BchF is a transmembrane protein, whereas BchC was purified from the soluble cell fraction *via* its GST fusion tag and subsequent protease cleavage. A BchC activity assay using artificial, chemically modified substrates was established. BchC catalyzed the NAD(H)-dependent conversion of bacteriochlorin and chlorin derivatives with 3^1-OH and 3-acetyl substituents at ring A, indicating that mainly rings A and D might be involved in substrate recognition. Moreover, a coupled activity assay comprising DPOR, BchF and BchC was established, revealing the presence of the BchF product 3^1-OH-Chlide and the BchC product 3-acetyl-Chlide. The detection of the two pigments indicated a new reaction sequence for BChl *a* biosynthesis. Furthermore, BchC was shown to be a zinc-independent oxidoreductase with the catalytically crucial residues Glu-46, Tyr-67, Glu-68 and His-141.

5 Outlook

In order to reveal further differences and/or similarities between DPOR and nitrogenase catalysis, DPOR could be further investigated with regard to the following aspects:

- Determination of the redox potentials of the DPOR [4Fe-4S] clusters
- Crystallization of the DPOR complex or L_2 with different nucleotide states (e.g. ADP-bound)

For the further characterization of BchF and BchC, the following investigations are suggested:

- Determination of the X-ray crystal structure of BchC
- Use of additional modified BchC substrates for a more detailed picture of BchC substrate specificity and stereochemistry (e.g. “pyro” compounds lacking the methoxycarbonyl substituent at C13^2). How does BchC discriminate the potential *in vivo* substrates 3^1-OH-Chlide and BChlide *d*?
- Determination of the BchC catalytic mechanism (e.g. the role of Tyr-244 and Lys-47)
- Determination of the BchF stereochemistry in the coupled activity assay. Can *C. tepidum* BchV replace BchF in the coupled activity assay?
- Establishing of a BchF assay system. Is 3-VBChlide a substrate for *C. tepidum* BchF?

6 References

Adams PD, Afonine PV, Bunkoczi G, Chen VB, Davis IW, Echols N, Headd JJ, Hung L, Kapral GJ, Grosse-Kunstleve RW, McCoy AJ, Moriarty NW, Oeffner R, Read RJ, Richardson DC, Richardson JS, Terwilliger TC, Zwart PH. 2010. PHENIX: a comprehensive Python-based system for macromolecular structure solution. Acta Crystallogr. D Biol. Crystallogr. **66**(Pt 2)**:**213–221.

Addlesee HA, Fiedor L, Hunter CN. 2000. Physical mapping of *bchG*, *orf427*, and *orf177* in the photosynthesis gene cluster of *Rhodobacter sphaeroides*: functional assignment of the bacteriochlorophyll synthetase gene. J. Bacteriol. **182**(11)**:**3175–3182.

Altschul SF, Gish W, Miller W, Myers EW, Lipman DJ. 1990. Basic local alignment search tool. J. Mol. Biol. **215**(3)**:**403–410.

Ames BD, Nguyen C, Bruegger J, Smith P, Xu W, Ma S, Wong E, Wong S, Xie X, Li JW, Vederas JC, Tang Y, Tsai S. 2012. Crystal structure and biochemical studies of the trans-acting polyketide enoyl reductase LovC from lovastatin biosynthesis. Proc. Natl. Acad. Sci. U.S.A. **109**(28)**:**11144–11149.

Arendt W, Groenewold MK, Hebecker S, Dickschat JS, Moser J. 2013. Identification and characterization of a periplasmic aminoacyl-phosphatidylglycerol hydrolase responsible for *Pseudomonas aeruginosa* lipid homeostasis. J. Biol. Chem. **288**(34)**:**24717–24730.

Auld DS, Bergman T. 2008. Medium- and short-chain dehydrogenase/reductase gene and protein families. The role of zinc for alcohol dehydrogenase structure and function. Cell. Mol. Life Sci. **65**(24)**:**3961–3970.

Baker ME. 1994. Protochlorophyllide reductase is homologous to human carbonyl reductase and pig 20 beta-hydroxysteroid dehydrogenase. Biochem. J. **300**(2)**:**605–607.

Barber J. 2002. Photosystem II: a multisubunit membrane protein that oxidises water. Curr. Opin. Struct. Biol. **12**(4)**:**523–530.

Bashir Q, Rashid N, Jamil F, Imanaka T, Akhtar M. 2009. Highly thermostable L-threonine dehydrogenase from the hyperthermophilic archaeon *Thermococcus kodakaraensis.* J. Biochem. **146**(1)**:**95–102.

Battersby AR. 2000. Tetrapyrroles: the pigments of life. Nat. Prod. Rep. **17**(6)**:**507–526.

Blake MS, Johnston KH, Russell-Jones GJ, Gotschlich EC. 1984. A rapid, sensitive method for detection of alkaline phosphatase-conjugated anti-antibody on Western blots. Anal. Biochem. **136**(1)**:**175–179.

Blankenship RE. 2014. Molecular mechanisms of photosynthesis, 2nd ed. John Wiley & Sons, Inc., Chichester, West Sussex.

Bogin O, Peretz M, Burstein Y. 1997. *Thermoanaerobacter brockii* alcohol dehydrogenase: characterization of the active site metal and its ligand amino acids. Protein. Sci. **6**(2)**:**450–458.

Bollivar D, Braumann I, Berendt K, Gough SP, Hansson M. 2014. The Ycf54 protein is part of the membrane component of Mg-protoporphyrin IX

monomethyl ester cyclase from barley (*Hordeum vulgare* L.). FEBS J. **281**(10)**:**2377–2386.

Bollivar DW, Suzuki JY, Beatty JT, Dobrowolski JM, Bauer CE. 1994a. Directed mutational analysis of bacteriochlorophyll *a* biosynthesis in *Rhodobacter capsulatus.* J. Mol. Biol. **237**(5)**:**622–640.

Bollivar DW, Wang S, Allen JP, Bauer CE. 1994b. Molecular genetic analysis of terminal steps in bacteriochlorophyll a biosynthesis: characterization of a *Rhodobacter capsulatus* strain that synthesizes geranylgeraniol-esterified bacteriochlorophyll *a.* Biochemistry **33**(43)**:**12763–12768.

Bösken CA, Farnung L, Hintermair C, Merzel Schachter M, Vogel-Bachmayr K, Blazek D, Anand K, Fisher RP, Eick D, Geyer M. 2014. The structure and substrate specificity of human Cdk12/Cyclin K. Nat. Commun. **5:**3505.

Bradford MM. 1976. A rapid and sensitive method for the quantitation of microgram quantities of protein utilizing the principle of protein-dye binding. Anal. Biochem. **72:**248–254.

Bröcker MJ, Jahn D, Moser J. 2012. Key enzymes of chlorophyll biosynthesis, p 1–43. *In* Kadish KM, Smith KM, Guilard R (ed), Chlorophylls and related systems. Handbook of porphyrin science, vol 20. World Scientific, Singapore.

Bröcker MJ, Schomburg S, Heinz DW, Jahn D, Schubert W, Moser J. 2010a. Crystal structure of the nitrogenase-like dark operative protochlorophyllide oxidoreductase catalytic complex $(ChlN/ChlB)_2$. J. Biol. Chem. **285**(35)**:**27336–27345.

Bröcker MJ, Virus S, Ganskow S, Heathcote P, Heinz DW, Schubert W, Jahn D, Moser J. 2008a. ATP-driven reduction by dark-operative protochlorophyllide oxidoreductase from *Chlorobium tepidum* mechanistically resembles nitrogenase catalysis. J. Biol. Chem. **283**(16)**:**10559–10567.

Bröcker MJ, Wätzlich D, Saggu M, Lendzian F, Moser J, Jahn D. 2010b. Biosynthesis of (bacterio)chlorophylls: ATP-dependent transient subunit interaction and electron transfer of dark operative protochlorophyllide oxidoreductase. J. Biol. Chem. **285**(11)**:**8268–8277.

Bröcker MJ, Wätzlich D, Uliczka F, Virus S, Saggu M, Lendzian F, Scheer H, Rüdiger W, Moser J, Jahn D. 2008b. Substrate recognition of nitrogenase-like dark operative protochlorophyllide oxidoreductase from *Prochlorococcus marinus.* J. Biol. Chem. **283**(44)**:**29873–29881.

Brouers M, Michel-Wolwertz MR. 1983. Estimation of protochlorophyll(ide) contents in plant extracts; re-evaluation of the molar absorption coefficient of protochlorophyll(ide). Photosyn. Res. **4**(3)**:**265–270.

Bryant DA, Frigaard N. 2006. Prokaryotic photosynthesis and phototrophy illuminated. Trends Microbiol. **14**(11)**:**488–496.

Burke DH, Alberti M, Hearst JE. 1993. *bchFNBH* bacteriochlorophyll synthesis genes of *Rhodobacter capsulatus* and identification of the third subunit of light-independent protochlorophyllide reductase in bacteria and plants. J. Bacteriol. **175**(8)**:**2414–2422.

Canniffe DP, Chidgey JW, Hunter CN. 2014. Elucidation of the preferred routes of C8-vinyl reduction in chlorophyll and bacteriochlorophyll biosynthesis. Biochem. J. **462**(3)**:**433–440.

Chaudhry C, Farr GW, Todd MJ, Rye HS, Brunger AT, Adams PD, Horwich AL, Sigler PB. 2003. Role of the gamma-phosphate of ATP in triggering protein folding by GroEL-GroES: function, structure and energetics. EMBO J. **22**(19)**:**4877–4887.

Chen L, Gavini N, Tsuruta H, Eliezer D, Burgess BK, Doniach S, Hodgson KO. 1994. MgATP-induced conformational changes in the iron protein from *Azotobacter vinelandii*, as studied by small-angle x-ray scattering. J. Biol. Chem. **269**(5)**:**3290–3294.

Chen M. 2014. Chlorophyll modifications and their spectral extension in oxygenic photosynthesis. Annu. Rev. Biochem. **83:**317–340.

Chen M, Schliep M, Willows RD, Cai Z, Neilan BA, Scheer H. 2010. A red-shifted chlorophyll. Science **329**(5997)**:**1318–1319.

Chen X, Wang X, Feng J, Chen Y, Fang Y, Zhao S, Zhao A, Zhang M, Liu L. 2014. Structural insights into the catalytic mechanism of *Synechocystis* magnesium protoporphyrin IX O-methyltransferase (ChlM). J. Biol. Chem. **289**(37)**:**25690–25698.

Chew AGM, Bryant DA. 2007. Chlorophyll biosynthesis in bacteria: the origins of structural and functional diversity. Annu. Rev. Microbiol. **61:**113–129.

Collaborative Computational Project, Number 4. 1994. The CCP4 suite: programs for protein crystallography. Acta Crystallogr. D Biol. Crystallogr. **50**(Pt 5)**:**760–763.

Coomber SA, Chaudhri M, Connor A, Britton G, Hunter CN. 1990. Localized transposon Tn5 mutagenesis of the photosynthetic gene cluster of *Rhodobacter sphaeroides.* Mol. Microbiol. **4**(6)**:**977–989.

Croce R, van Amerongen H. 2013. Light-harvesting in photosystem I. Photosyn. Res. **116**(2-3)**:**153–166.

Dailey HA. 2002. Terminal steps of haem biosynthesis. Biochem. Soc. Trans **30**(4)**:**590–595.

DiMaio F, Terwilliger TC, Read RJ, Wlodawer A, Oberdorfer G, Wagner U, Valkov E, Alon A, Fass D, Axelrod HL, Das D, Vorobiev SM, Iwaï H, Pokkuluri PR, Baker D. 2011. Improved molecular replacement by density- and energy-guided protein structure optimization. Nature **473**(7348)**:**540–543.

Eisen JA, Nelson KE, Paulsen IT, Heidelberg JF, Wu M, Dodson RJ, Deboy R, Gwinn ML, Nelson WC, Haft DH, Hickey EK, Peterson JD, Durkin AS, Kolonay JL, Yang F, Holt I, Umayam LA, Mason T, Brenner M, Shea TP, Parksey D, Nierman WC, Feldblyum TV, Hansen CL, Craven MB, Radune D, Vamathevan J, Khouri H, White O, Gruber TM, Ketchum KA, Venter JC, Tettelin H, Bryant DA, Fraser CM. 2002. The complete genome sequence of *Chlorobium tepidum* TLS, a photosynthetic, anaerobic, green-sulfur bacterium. Proc. Natl. Acad. Sci. U.S.A. **99**(14)**:**9509–9514.

Eklund H, Ramaswamy S. 2008. Medium- and short-chain dehydrogenase/reductase gene and protein families. Three-dimensional structures of MDR alcohol dehydrogenases. Cell. Mol. Life Sci. **65**(24)**:**3907–3917.

Emsley P, Cowtan K. 2004. Coot: model-building tools for molecular graphics. Acta Crystallogr. D Biol. Crystallogr. **60**(Pt 12 Pt 1)**:**2126–2132.

Fages F, Griebenow N, Griebenow K, Holzwarth AR, Schaffner K. 1990. Characterization of light-harvesting pigments of *Chloroflexus aurantiacus*. Two new chlorophylls: oleyl (octadec-9-enyl) and cetyl (hexadecanyl) bacteriochlorophyllides-c. J. Chem. Soc., Perkin Trans. 1(10)**:**2791.

Frankenberg N, Lagarias JC. 2003. Biosynthesis and biological functions of bilins, p 211–235. *In* Kadish KM, Smith KM, Guilard R (ed), Chlorophylls and bilins. Biosynthesis, synthesis, and degradation. The Porphyrin handbook, vol 13. Academic Press, San Diego, California.

Frigaard N, Chew AGM, Maresca JA, Bryant DA. 2006. Bacteriochlorophyll Biosynthesis in Green Bacteria, p 201–221. *In* Grimm B, Porra RJ, Rüdiger W, Scheer H (ed), Chlorophylls and bacteriochlorophylls. Biochemistry, biophysics, functions and applications. Advances in photosynthesis and respiration, vol 25. Springer, Dordrecht, Netherlands.

Fujita Y. 1996. Protochlorophyllide reduction: a key step in the greening of plants. Plant Cell Physiol. **37**(4)**:**411–421.

Fujita Y, Bauer CE. 2000. Reconstitution of light-independent protochlorophyllide reductase from purified BchL and BchN-BchB subunits. *In vitro c*onfirmation of nitrogenase-like features of a bacteriochlorophyll biosynthesis enzyme. J. Biol. Chem. **275**(31)**:**23583–23588.

Fujita Y, Matsumoto H, Takahashi Y, Matsubara H. 1993. Identification of a *nifDK*-like gene (ORF467) involved in the biosynthesis of chlorophyll in the cyanobacterium *Plectonema boryanum.* Plant Cell Physiol. **34**(2)**:**305–314.

Ganapathy S, Oostergetel GT, Reus M, Tsukatani Y, Chew AGM, Buda F, Bryant DA, Holzwarth AR, de Groot HJM. 2012. Structural variability in wild-type and bchQ bchR mutant chlorosomes of the green sulfur bacterium *Chlorobaculum tepidum.* Biochemistry **51**(22)**:**4488–4498.

Ganapathy S, Oostergetel GT, Wawrzyniak PK, Reus M, Chew AGM, Buda F, Boekema EJ, Bryant DA, Holzwarth AR, de Groot HJM. 2009. Alternating syn-anti bacteriochlorophylls form concentric helical nanotubes in chlorosomes. Proc. Natl. Acad. Sci. U.S.A. **106**(21)**:**8525–8530.

Garcia Costas AM, Tsukatani Y, Rijpstra WIC, Schouten S, Welander PV, Summons RE, Bryant DA. 2012. Identification of the bacteriochlorophylls, carotenoids, quinones, lipids, and hopanoids of "*Candidatus* Chloracidobacterium thermophilum". J. Bacteriol. **194**(5)**:**1158–1168.

Gough SP, Rzeznicka K, Peterson Wulff R, da Cruz Francisco J, Hansson A, Jensen PE, Hansson M. 2007. A new method for isolating physiologically active Mg-protoporphyrin monomethyl ester, the substrate of the cyclase enzyme of the chlorophyll biosynthetic pathway. Plant Physiol. Biochem. **45**(12)**:**932–936.

Goujon M, McWilliam H, Li W, Valentin F, Squizzato S, Paern J, Lopez R. 2010. A new bioinformatics analysis tools framework at EMBL-EBI. Nucleic Acids Res. **38**(Web Server issue)**:**W695-9.

Griffiths WT. 1980. Substrate-specificity studies on protochlorophyllide reductase in barley (*Hordeum vulgare*) etioplast membranes. Biochem. J. **186**(1)**:**267–278.

Harada J, Mizoguchi T, Tsukatani Y, Yokono M, Tanaka A, Tamiaki H. 2014. Chlorophyllide *a* oxidoreductase works as one of the divinyl reductases specifically involved in bacteriochlorophyll *a* biosynthesis. J. Biol. Chem. **289**(18)**:**12716–12726.

Harada J, Teramura M, Mizoguchi T, Tsukatani Y, Yamamoto K, Tamiaki H. 2015. Stereochemical conversion of C3-vinyl group to 1-hydroxyethyl group in bacteriochlorophyll *c* by the hydratases BchF and BchV: adaptation of green sulfur bacteria to limited-light environments. Mol. Microbiol. **98**(6):1184–1198.

Hartwich G, Fiedor L, Simonin I, Cmiel E, Schäfer W, Noy D, Scherz A, Scheer H. 1998. Metal-substituted bacteriochlorophylls. 1. Preparation and influence of metal and coordination on spectra. J. Am. Chem. Soc. **120**(15)**:**3675–3683.

Hebecker S, Arendt W, Heinemann IU, Tiefenau, Jana H J, Nimtz M, Rohde M, Soll D, Moser J. 2011. Alanyl-phosphatidylglycerol synthase: mechanism of substrate recognition during tRNA-dependent lipid modification in *Pseudomonas aeruginosa.* Mol. Microbiol. **80**(4)**:**935–950.

Hedlund J, Jörnvall H, Persson B. 2010. Subdivision of the MDR superfamily of medium-chain dehydrogenases/reductases through iterative hidden Markov model refinement. BMC Bioinformatics **11:**534.

Helfrich M, Rüdiger W. 1992. Various metallopheophorbides as substrates for chlorophyll synthetase. Z. Naturforsch. Sect. C J. Biosci. **47**(47)**:**231–238.

Helfrich M, Schoch S, Lempert U, Cmiel E, Rüdiger W. 1994. Chlorophyll synthetase cannot synthesize chlorophyll a'. Eur. J. Biochem. **219**(1-2)**:**267–275.

Helfrich M, Schoch S, Schäfer W, Ryberg M, Rüdiger W. 1996. Absolute configuration of protochlorophyllide *a* and substrate specificity of NADPH−protochlorophyllide oxidoreductase. J. Am. Chem. Soc. **118**(11)**:**2606–2611.

Heyes DJ, Kruk J, Hunter CN. 2006. Spectroscopic and kinetic characterization of the light-dependent enzyme protochlorophyllide oxidoreductase (POR) using monovinyl and divinyl substrates. Biochem. J. **394**(Pt 1)**:**243–248.

Heyes DJ, Ruban AV, Wilks HM, Hunter CN. 2002. Enzymology below 200 K: the kinetics and thermodynamics of the photochemistry catalyzed by protochlorophyllide oxidoreductase. Proc. Natl. Acad. Sci. U.S.A. **99**(17)**:**11145–11150.

Hofmann K, Stoffel W. 1993. TMBASE – a database of membrane spanning protein segments. Biol. Chem. Hoppe-Seyler **374:**166.

Hollingshead S, Kopecná J, Jackson PJ, Canniffe DP, Davison PA, Dickman MJ, Sobotka R, Hunter CN. 2012. Conserved chloroplast open-reading frame ycf54 is required for activity of the magnesium protoporphyrin monomethylester oxidative cyclase in *Synechocystis* PCC 6803. J. Biol. Chem. **287**(33)**:**27823–27833.

Hori T, Yokomizo T, Ago H, Sugahara M, Ueno G, Yamamoto M, Kumasaka T, Shimizu T, Miyano M. 2004. Structural Basis of Leukotriene B4 12-Hydroxydehydrogenase/15-Oxo-prostaglandin 13-Reductase Catalytic Mechanism and a Possible Src Homology 3 Domain Binding Loop. J. Biol. Chem. **279**(21)**:**22615–22623.

Hunter CN, Coomber SA. 1988. Cloning and oxygen-regulated expression of the bacteriochlorophyll biosynthesis genes *bch E*, *B*, *A* and *C* of *Rhodobacter sphaeroides.* J. Gen. Microbiol. **134**(6)**:**1491–1497.

Jahn D, Hungerer C, Troup B. 1996. Ungewöhnliche Wege und umweltregulierte Gene der bakteriellen Hämbiosynthese. Naturwissenschaften **83**(9)**:**389–400.

Jang SB, Seefeldt LC, Peters JW. 2000. Insights into Nucleotide Signal Transduction in Nitrogenase: Structure of an Iron Protein with MgADP Bound. Biochemistry **39**(48)**:**14745–14752.

Jensen PE, Gibson LC, Hunter CN. 1999. ATPase activity associated with the magnesium-protoporphyrin IX chelatase enzyme of Synechocystis PCC6803: evidence for ATP hydrolysis during Mg2+ insertion, and the MgATP-dependent interaction of the ChlI and ChlD subunits. Biochem. J. **339**(1)**:**127.

Jones OT. 1964. Studies on the structure of a pigment related to chlorophyll *a* produced by *Rhodopseudomonas spheroides.* Biochem. J. **91**(3)**:**572–576.

Kabsch W. 2010. Integration, scaling, space-group assignment and post-refinement. Acta Crystallogr. D Biol. Crystallogr. **66**(Pt 2)**:**133–144.

Karlsson C, Höög JO. 1993. Zinc coordination in mammalian sorbitol dehydrogenase. Replacement of putative zinc ligands by site-directed mutagenesis. Eur. J. Biochem. **216**(1)**:**103–107.

Kaschner M, Loeschcke A, Krause J, Minh BQ, Heck A, Endres S, Svensson V, Wirtz A, Haeseler A von, Jaeger K, Drepper T, Krauss U. 2014. Discovery of the first light-dependent protochlorophyllide oxidoreductase in anoxygenic phototrophic bacteria. Mol. Microbiol. **93**(5)**:**1066–1078.

Kavanagh KL, Jörnvall H, Persson B, Oppermann U. 2008. Medium- and short-chain dehydrogenase/reductase gene and protein families. The SDR superfamily: functional and structural diversity within a family of metabolic and regulatory enzymes. Cell. Mol. Life Sci. **65**(24)**:**3895–3906.

Kiesel S, Wätzlich D, Lange C, Reijerse E, Bröcker MJ, Rüdiger W, Lubitz W, Scheer H, Moser J, Jahn D. 2015. Iron-sulfur cluster-dependent catalysis of chlorophyllide *a* oxidoreductase from *Roseobacter denitrificans.* J. Biol. Chem. **290**(2)**:**1141–1154.

Kim E, Kim J, Lee I, Rhee HJ, Lee JK. 2008. Superoxide generation by chlorophyllide *a* reductase of *Rhodobacter sphaeroides.* J. Biol. Chem. **283**(7)**:**3718–3730.

Klein S, Lorenzo C, Hoffmann S, Walther JM, Storbeck S, Piekarski T, Tindall BJ, Wray V, Nimtz M, Moser J. 2009. Adaptation of *Pseudomonas aeruginosa* to various conditions includes tRNA-dependent formation of alanyl-phosphatidylglycerol. Mol. Microbiol. **71**(3)**:**551–565.

Klement H, Helfrich M, Oster U, Schoch S, Rüdiger W. 1999. Pigment-free NADPH:protochlorophyllide oxidoreductase from *Avena sativa* L. Purification and substrate specificity. Eur. J. Biochem. **265**(3)**:**862–874.

Kobayashi M, Akiyama M, Kano H, Kise H. 2006. Spectroscopy and structure determination, p 79–94. *In* Grimm B, Porra RJ, Rüdiger W, Scheer H (ed), Chlorophylls and bacteriochlorophylls. Biochemistry, biophysics, functions and applications. Advances in photosynthesis and respiration, vol 25. Springer, Dordrecht, Netherlands.

Kondo T, Nomata J, Fujita Y, Itoh S. 2011. EPR study of 1Asp-3Cys ligated 4Fe-4S iron-sulfur cluster in NB-protein (BchN-BchB) of a dark-operative protochlorophyllide reductase complex. FEBS Lett. **585**(1)**:**214–218.

Krissinel E, Henrick K. 2007. Inference of macromolecular assemblies from crystalline state. J. Mol. Biol. **372**(3)**:**774–797.

Laemmli UK. 1970. Cleavage of Structural Proteins during the Assembly of the Head of Bacteriophage T4. Nature **227**(5259)**:**680–685.

Lange C, Kiesel S, Peters S, Virus S, Scheer H, Jahn D, Moser J. 2015. Broadened substrate specificity of 3-hydroxyethyl bacteriochlorophyllide *a* dehydrogenase (BchC) indicates a new route for the biosynthesis of bacteriochlorophyll *a.* J. Biol. Chem. **290**(32)**:**19697–19709.

Lanzilotta WN, Fisher K, Seefeldt LC. 1996. Evidence for electron transfer from the nitrogenase iron protein to the molybdenum-iron protein without MgATP hydrolysis: characterization of a tight protein-protein complex. Biochemistry **35**(22)**:**7188–7196.

Lanzilotta WN, Fisher K, Seefeldt LC. 1997. Evidence for electron transfer-dependent formation of a nitrogenase iron protein-molybdenum-iron protein tight complex. The role of aspartate 39. J. Biol. Chem. **272**(7)**:**4157–4165.

Lanzilotta WN, Ryle MJ, Seefeldt LC. 1995. Nucleotide hydrolysis and protein conformational changes in *Azotobacter vinelandii* nitrogenase iron protein: defining the function of aspartate 129. Biochemistry **34**(34)**:**10713–10723.

Larkin MA, Blackshields G, Brown NP, Chenna R, McGettigan PA, McWilliam H, Valentin F, Wallace IM, Wilm A, Lopez R, Thompson JD, Gibson TJ, Higgins DG. 2007. Clustal W and Clustal X version 2.0. Bioinformatics **23**(21)**:**2947–2948.

Lascelles J. 1966. The accumulation of bacteriochlorophyll precursors by mutant and wild-type strains of *Rhodopseudomonas spheroides.* Biochem. J. **100**(1)**:**175–183.

Leskovac V, Trivic S, Pericin D. 2002. The three zinc-containing alcohol dehydrogenases from baker's yeast, *Saccharomyces cerevisiae.* FEMS Yeast Res. **2**(4)**:**481–494.

Li G, Zhang XC. 2004. GTP hydrolysis mechanism of Ras-like GTPases. J. Mol. Biol. **340**(5)**:**921–932.

Lin S, Guidotti G. 2009. Purification of Membrane Proteins, p 619–629. *In* Burgess RR, Deutscher MP (ed), Guide to Protein Purification, 2nd Edition. Methods in Enzymology, vol 463. Elsevier Inc.

Liu Z, Bryant DA. 2011. Identification of a gene essential for the first committed step in the biosynthesis of bacteriochlorophyll *c.* J. Biol. Chem. **286**(25)**:**22393–22402.

Liu Z, Bryant DA. 2012. Bacteriochlorophyll biosynthesis and assembly in green chlorophototrophic bacteria: Theme and variations, p 107–140. *In* Kadish KM, Smith KM, Guilard R (ed), Chlorophylls and related systems. Handbook of porphyrin science, vol 20. World Scientific, Singapore.

Machielsen R, van der Oost J. 2006. Production and characterization of a thermostable L-threonine dehydrogenase from the hyperthermophilic archaeon *Pyrococcus furiosus.* FEBS J. **273**(12)**:**2722–2729.

Madhusudan, Akamine P, Xuong N, Taylor SS. 2002. Crystal structure of a transition state mimic of the catalytic subunit of cAMP-dependent protein kinase. Nat. Struct. Biol. **9**(4)**:**273–277.

Magonet E, Hayen P, Delforge D, Delaive E, Remacle J. 1992. Importance of the structural zinc atom for the stability of yeast alcohol dehydrogenase. Biochem. J. **287**(Pt 2)**:**361–365.

Masuda T. 2008. Recent overview of the Mg branch of the tetrapyrrole biosynthesis leading to chlorophylls. Photosyn. Res. **96**(2)**:**121–143.

Masuda T, Fujita Y. 2008. Regulation and evolution of chlorophyll metabolism. Photochem. Photobiol. Sci. **7**(10)**:**1131–1149.

McFeeters RF, Chichester CO, Whitaker JR. 1971. Purification and properties of chlorophyllase from *Ailanthus altissima* (Tree-of-Heaven). Plant Physiol. **47**(5)**:**609–618.

McWilliam H, Li W, Uludag M, Squizzato S, Park YM, Buso N, Cowley AP, Lopez R. 2013. Analysis tool web services from the EMBL-EBI. Nucleic Acids Res. **41**(Web Server issue)**:**W597-600.

Meng EC, Pettersen EF, Couch GS, Huang CC, Ferrin TE. 2006. Tools for integrated sequence-structure analysis with UCSF Chimera. BMC Bioinformatics **7:**339.

Moser J, Bröcker MJ. 2011. Methods for nitrogenase-like dark operative protochlorophyllide oxidoreductase, p 129–143. *In* Ribbe MW (ed), Nitrogen fixation. Methods and protocols. Methods in molecular biology, vol 766. Humana; Springer, New York.

Moser J, Lange C, Krausze J, Rebelein J, Schubert W, Ribbe MW, Heinz DW, Jahn D. 2013. Structure of ADP-aluminium fluoride-stabilized protochlorophyllide oxidoreductase complex. Proc. Natl. Acad. Sci. U.S.A. **110**(6)**:**2094–2098.

Moss GP. 1988. Nomenclature of tetrapyrroles. Recommendations 1986. Eur. J. Biochem. **178**(2)**:**277–328.

Müller AH, Gough SP, Bollivar DW, Meldal M, Willows RD, Hansson M. 2011. Methods for the preparation of chlorophyllide *a*: An intermediate of the chlorophyll biosynthetic pathway. Anal. Biochem. **419**(2)**:**271–276.

Muraki N, Nomata J, Ebata K, Mizoguchi T, Shiba T, Tamiaki H, Kurisu G, Fujita Y. 2010. X-ray crystal structure of the light-independent protochlorophyllide reductase. Nature **465**(7294)**:**110–114.

Nomata J, Kitashima M, Inoue K, Fujita Y. 2006a. Nitrogenase Fe protein-like Fe-S cluster is conserved in L-protein (BchL) of dark-operative protochlorophyllide reductase from *Rhodobacter capsulatus.* FEBS Lett. **580**(26)**:**6151–6154.

Nomata J, Kondo T, Itoh S, Fujita Y. 2013. Nicotinamide is a specific inhibitor of dark-operative protochlorophyllide oxidoreductase, a nitrogenase-like enzyme, from *Rhodobacter capsulatus.* FEBS Lett. **587**(18)**:**3142–3147.

Nomata J, Kondo T, Mizoguchi T, Tamiaki H, Itoh S, Fujita Y. 2014. Dark-operative protochlorophyllide oxidoreductase generates substrate radicals by an iron-sulphur cluster in bacteriochlorophyll biosynthesis. Sci. Rep. **4:**5455.

Nomata J, Mizoguchi T, Tamiaki H, Fujita Y. 2006b. A second nitrogenase-like enzyme for bacteriochlorophyll biosynthesis: reconstitution of chlorophyllide *a* reductase with purified X-protein (BchX) and YZ-protein (BchY-BchZ) from *Rhodobacter capsulatus.* J. Biol. Chem. **281**(21)**:**15021–15028.

Nomata J, Ogawa T, Kitashima M, Inoue K, Fujita Y. 2008. NB-protein (BchN-BchB) of dark-operative protochlorophyllide reductase is the catalytic component containing oxygen-tolerant Fe-S clusters. FEBS Lett. **582**(9)**:**1346–1350.

Nomata J, Swem LR, Bauer CE, Fujita Y. 2005. Overexpression and characterization of dark-operative protochlorophyllide reductase from *Rhodobacter capsulatus.* Biochim. Biophys. Acta **1708**(2)**:**229–237.

Oster U, Bauer CE, Rüdiger W. 1997. Characterization of chlorophyll *a* and bacteriochlorophyll *a* synthases by heterologous expression in *Escherichia coli.* J. Biol. Chem. **272**(15)**:**9671–9676.

Overmann J, Garcia-Pichel F. 2006. The Phototrophic Way of Life, p 32–85. *In* Dworkin M, Falkow S, Rosenberg E, Schleifer K, Stackebrandt E (ed), Ecophysiology and Biochemistry. The Prokaryotes, vol 2. Springer New York, New York.

Partensky F, Hess WR, Vaulot D. 1999. Prochlorococcus, a marine photosynthetic prokaryote of global significance. Microbiol. Mol. Biol. Rev. **63**(1)**:**106–127.

Persson B, Hedlund J, Jörnvall H. 2008. Medium- and short-chain dehydrogenase/reductase gene and protein families. The MDR superfamily. Cell. Mol. Life Sci. **65**(24)**:**3879–3894.

Peters S. 2013. Late enzymes of bacteriochlorophyll *a* biosynthesis. Diplomarbeit. Technische Universität Braunschweig, Braunschweig.

Pettersen EF, Goddard TD, Huang CC, Couch GS, Greenblatt DM, Meng EC, Ferrin TE. 2004. UCSF Chimera--a visualization system for exploratory research and analysis. J. Comput. Chem. **25**(13)**:**1605–1612.

Porra RJ, Schäfer W, Gad'on N, Katheder I, Drews G, Scheer H. 1996. Origin of the two carbonyl oxygens of bacteriochlorophyll *a*. Demonstration of two different pathways for the formation of ring E in *Rhodobacter sphaeroides* and *Roseobacter denitrificans*, and a common hydratase mechanism for 3-acetyl group formation. Eur. J. Biochem. **239**(1)**:**85–92.

Porra RJ, Urzinger M, Winkler J, Bubenzer C, Scheer H. 1998. Biosynthesis of the 3-acetyl and 13(1)-oxo groups of bacteriochlorophyll *a* in the facultative aerobic bacterium, *Rhodovulum sulfidophilum*. The presence of both oxygenase and hydratase pathways for isocyclic ring formation. Eur. J. Biochem. **257**(1)**:**185–191.

Pulavarti S, He Y, Feldmann EA, Eletsky A, Acton TB, Xiao R, Everett JK, Montelione GT, Kennedy MA, Szyperski T. 2013. Solution NMR structures provide first structural coverage of the large protein domain family PF08369 and complementary structural coverage of dark operative protochlorophyllide oxidoreductase complexes. J. Struct. Funct. Genomics **14**(3)**:**119–126.

Rath A, Glibowicka M, Nadeau VG, Chen G, Deber CM. 2009. Detergent binding explains anomalous SDS-PAGE migration of membrane proteins. Proc. Natl. Acad. Sci. U.S.A. **106**(6)**:**1760–1765.

Reinbothe C, El Bakkouri M, Buhr F, Muraki N, Nomata J, Kurisu G, Fujita Y, Reinbothe S. 2010. Chlorophyll biosynthesis: spotlight on protochlorophyllide reduction. Trends Plant. Sci. **15**(11)**:**614–624.

Rhodes G. 2006. Crystallography made crystal clear. A guide for users of macromolecular models, 3rd ed. Academic Press; Elsevier Inc.

Richards W, Lascelles J. 1969. The biosynthesis of bacteriochlorophyll. The characterization of latter stage intermediates from mutants of *Rhodopseudomonas spheroides.* Biochemistry **8**(8)**:**3473–3482.

Riveros-Rosas H, Julian-Sanchez A, Villalobos-Molina R, Pardo JP, Pina E. 2003. Diversity, taxonomy and evolution of medium-chain dehydrogenase/reductase superfamily. Eur. J. Biochem. **270**(16)**:**3309–3334.

Rüdiger W, Böhm S, Helfrich M, Schulz S, Schoch S. 2005. Enzymes of the last steps of chlorophyll biosynthesis: modification of the substrate structure helps to understand the topology of the active centers. Biochemistry **44**(32)**:**10864–10872.

Rupp B. 2010. Biomolecular crystallography. Principles, practice, and application to structural biology. Garland Science, New York.

Ryle MJ, Lanzilotta WN, Seefeldt LC. 1996a. Elucidating the mechanism of nucleotide-dependent changes in the redox potential of the 4Fe-4S cluster in nitrogenase iron protein: the role of phenylalanine 135. Biochemistry **35**(29)**:**9424–9434.

Ryle MJ, Lanzilotta WN, Seefeldt LC, Scarrow RC, Jensen GM. 1996b. Circular dichroism and x-ray spectroscopies of *Azotobacter vinelandii* nitrogenase iron protein. MgATP and MgADP induced protein conformational changes affecting the 4Fe-4S cluster and characterization of a 2Fe-2S form. J. Biol. Chem. **271**(3)**:**1551–1557.

Ryle MJ, Seefeldt LC. 1996. Elucidation of a MgATP signal transduction pathway in the nitrogenase iron protein: formation of a conformation resembling the MgATP-bound state by protein engineering. Biochemistry **35**(15)**:**4766–4775.

Sablin EP, Fletterick RJ. 2001. Nucleotide switches in molecular motors: structural analysis of kinesins and myosins. Curr. Opin. Struct. Biol. **11**(6)**:**716–724.

Sambrook J, Russell DW. 2001. Molecular cloning. A laboratory manual, 3rd ed. Cold Spring Harbor Laboratory Press, Cold Spring Harbor, New York.

Sanger F, Nicklen S, Coulson AR. 1977. DNA sequencing with chain-terminating inhibitors. Proc. Natl. Acad. Sci. U.S.A. **74**(12)**:**5463–5467.

Sarma R, Barney BM, Hamilton TL, Jones A, Seefeldt LC, Peters JW. 2008. Crystal structure of the L protein of *Rhodobacter sphaeroides* light-independent protochlorophyllide reductase with MgADP bound: a homologue of the nitrogenase Fe protein. Biochemistry **47**(49)**:**13004–13015.

Sauer K, Debreczeny M. 1996. Fluorescence, p 41–61. *In* Amesz J, Hoff AJ (ed), Biophysical Techniques in Photosynthesis. Advances in photosynthesis, vol 3. Kluwer Academic Publishers, Dordrecht, Netherlands.

Scheer H. 2006. An overview of chlorophylls and bacteriochlorophylls: Biochemistry, biophysics, functions and applications, p 1–26. *In* Grimm B, Porra RJ, Rüdiger W, Scheer H (ed), Chlorophylls and bacteriochlorophylls. Biochemistry, biophysics, functions and applications. Advances in photosynthesis and respiration, vol 25. Springer, Dordrecht, Netherlands.

Scheffzek K, Ahmadian MR, Kabsch W, Wiesmuller L, Lautwein A, Schmitz F, Wittinghofer A. 1997. The Ras-RasGAP complex: structural basis for GTPase activation and its loss in oncogenic Ras mutants. Science **277**(5324)**:**333–338.

Schiefner A, Sinz Q, Neumaier I, Schwab W, Skerra A. 2013. Structural basis for the enzymatic formation of the key strawberry flavor compound 4-hydroxy-2,5-dimethyl-3(2H)-furanone. J. Biol. Chem. **288**(23)**:**16815–16826.

Schindelin H, Kisker C, Schlessman JL, Howard JB, Rees DC. 1997. Structure of ADP•AlF_4^--stabilized nitrogenase complex and its implications for signal transduction. Nature **387**(6631)**:**370–376.

Schlichting I, Reinstein J. 1999. pH influences fluoride coordination number of the AlF_x phosphoryl transfer transition state analog. Nat. Struct. Biol. **6**(8)**:**721–723.

Schmid B, Einsle O, Chiu H, Willing A, Yoshida M, Howard JB, Rees DC. 2002. Biochemical and structural characterization of the cross-linked complex of nitrogenase: comparison to the ADP-AlF_4^--stabilized structure. Biochemistry **41**(52)**:**15557–15565.

Schrödinger LL. 2010. The PyMOL Molecular Graphics System, Version 1.3.

Scrutton NS, Groot ML, Heyes DJ. 2012. Excited state dynamics and catalytic mechanism of the light-driven enzyme protochlorophyllide oxidoreductase. Phys. Chem. Chem. Phys. **14**(25)**:**8818–8824.

Seefeldt LC, Hoffman BM, Dean DR. 2009. Mechanism of Mo-dependent nitrogenase. Annu. Rev. Biochem. **78:**701–722.

Senge MO, Smith KM. 1995. Biosynthesis and structures of the bacteriochlorophylls, p 137–151. *In* Blankenship RE, Madigan MT, Bauer CE (ed), Anoxygenic photosynthetic bacteria. Advances in photosynthesis, vol 2. Kluwer Academic Publishers, Dordrecht, Netherlands.

Senge MO, Wiehe A, Ryppa C. 2006. Synthesis, reactivity and structure of chlorophylls, p 27–37. *In* Grimm B, Porra RJ, Rüdiger W, Scheer H (ed), Chlorophylls and bacteriochlorophylls. Biochemistry, biophysics, functions and applications. Advances in photosynthesis and respiration, vol 25. Springer, Dordrecht, Netherlands.

Sievers F, Wilm A, Dineen D, Gibson TJ, Karplus K, Li W, Lopez R, McWilliam H, Remmert M, Söding J, Thompson JD, Higgins DG. 2011. Fast, scalable generation of high-quality protein multiple sequence alignments using Clustal Omega. Mol. Syst. Biol. **7:**539.

Smith CA, Rayment I. 1996. Active site comparisons highlight structural similarities between myosin and other P-loop proteins. Biophys. J. **70**(4)**:**1590–1602.

Smith J, Calvin M. 1966. Studies on the chemical and photochemical oxidation of bacteriochlorophyll. J. Am. Chem. Soc. **88**(19)**:**4500–4506.

Smith KM, Craig G, Kehres LA, Pfennig N. 1983. Reversed-phase high-performance liquid chromatography and structural assignments of the bacteriochlorophylls-c. J. Chromatogr. A **281:**209–223.

Spatzal T. 2015. The center of biological nitrogen fixation: FeMo-cofactor. Z. anorg. allg. Chem. **641**(1)**:**10–17.

Strong M, Sawaya MR, Wang S, Phillips M, Cascio D, Eisenberg D. 2006. Toward the structural genomics of complexes: crystal structure of a PE/PPE protein complex from *Mycobacterium tuberculosis.* Proc. Natl. Acad. Sci. U.S.A. **103**(21)**:**8060–8065.

Struck A, Cmiel E, Katheder I, Schäfer W, Scheer H. 1992. Bacteriochlorophylls modified at position C-3: long-range intramolecular interaction with position C-13$^{2.}$ Biochim. Biophys. Acta **1101**(3)**:**321–328.

Studier FW, Moffatt BA. 1986. Use of bacteriophage T7 RNA polymerase to direct selective high-level expression of cloned genes. J. Mol. Biol. **189**(1)**:**113–130.

Taylor DP, Cohen SN, Clark WG, Marrs B. 1983. Alignment of genetic and restriction maps of the photosynthesis region of the *Rhodopseudomonas capsulata* chromosome by a conjugation-mediated marker rescue technique. J. Bacteriol. **154**(2)**:**580–590.

Tezcan FA, Kaiser JT, Howard JB, Rees DC. 2015. Structural evidence for asymmetrical nucleotide interactions in nitrogenase. J. Am. Chem. Soc. **137**(1)**:**146–149.

Tezcan FA, Kaiser JT, Mustafi D, Walton MY, Howard JB, Rees DC. 2005. Nitrogenase complexes: multiple docking sites for a nucleotide switch protein. Science **309**(5739)**:**1377–1380.

Tiwari MK, Singh RK, Singh R, Jeya M, Zhao H, Lee J. 2012. Role of conserved glycine in zinc-dependent medium chain dehydrogenase/reductase superfamily. J. Biol. Chem. **287**(23)**:**19429–19439.

Towbin H, Staehelin T, Gordon J. 1979. Electrophoretic transfer of proteins from polyacrylamide gels to nitrocellulose sheets: procedure and some applications. Proc. Natl. Acad. Sci. U.S.A. **76**(9)**:**4350–4354.

Tsukatani Y, Romberger SP, Golbeck JH, Bryant DA. 2012. Isolation and characterization of homodimeric type-I reaction center complex from *Candidatus* Chloracidobacterium thermophilum, an aerobic chlorophototroph. J. Biol. Chem. **287**(8)**:**5720–5732.

Tsukatani Y, Yamamoto H, Harada J, Yoshitomi T, Nomata J, Kasahara M, Mizoguchi T, Fujita Y, Tamiaki H. 2013a. An unexpectedly branched biosynthetic pathway for bacteriochlorophyll b capable of absorbing near-infrared light. Sci. Rep. **3:**1217.

Tsukatani Y, Yamamoto H, Mizoguchi T, Fujita Y, Tamiaki H. 2013b. Completion of biosynthetic pathways for bacteriochlorophyll *g* in *Heliobacterium modesticaldum*: The C8-ethylidene group formation. Biochim. Biophys. Acta **1827**(10)**:**1200–1204.

Uliczka F. 2007. Überproduktion und Charakterisierung der lichtunabhängigen Protochlorophyllid Oxidoreduktase aus *Thermosynechococcus elongatus* und *Prochlorococcus marinus*. Diplomarbeit. Technische Universität Braunschweig, Braunschweig.

Vetter IR, Wittinghofer A. 2001. The guanine nucleotide-binding switch in three dimensions. Science **294**(5545)**:**1299–1304.

Walker JE, Saraste M, Runswick MJ, Gay NJ. 1982. Distantly related sequences in the alpha- and beta-subunits of ATP synthase, myosin, kinases and other ATP-requiring enzymes and a common nucleotide binding fold. EMBO J. **1**(8)**:**945–951.

Wang W, Cho HS, Kim R, Jancarik J, Yokota H, Nguyen HH, Grigoriev IV, Wemmer DE, Kim S. 2002. Structural characterization of the reaction pathway in phosphoserine phosphatase: crystallographic "snapshots" of intermediate states. J. Mol. Biol. **319**(2)**:**421–431.

Wätzlich D, Bröcker MJ, Uliczka F, Ribbe M, Virus S, Jahn D, Moser J. 2009. Chimeric nitrogenase-like enzymes of (bacterio)chlorophyll biosynthesis. J. Biol. Chem. **284**(23)**:**15530–15540.

Wellington CL, Beatty JT. 1989. Promoter mapping and nucleotide sequence of the *bchC* bacteriochlorophyll biosynthesis gene from *Rhodobacter capsulatus.* Gene **83**(2)**:**251–261.

Wiethaus J, Busch, Andrea W U, Dammeyer T, Frankenberg-Dinkel N. 2010. Phycobiliproteins in *Prochlorococcus marinus*: biosynthesis of pigments and their assembly into proteins. Eur. J. Cell Biol. **89**(12)**:**1005–1010.

Wilks HM, Timko MP. 1995. A light-dependent complementation system for analysis of NADPH:protochlorophyllide oxidoreductase: identification and mutagenesis of two conserved residues that are essential for enzyme activity. Proc. Natl. Acad. Sci. U.S.A. **92**(3)**:**724–728.

Wlodawer A, Minor W, Dauter Z, Jaskolski M. 2008. Protein crystallography for non-crystallographers, or how to get the best (but not more) from published macromolecular structures. FEBS J. **275**(1)**:**1–21.

Xiong J. 2000. Molecular evidence for the early evolution of photosynthesis. Science **289**(5485)**:**1724–1730.

Yamamoto H, Kato M, Yamanashi K, Fujita Y. 2014. Reconstitution of a sequential reaction of two nitrogenase-like enzymes in the bacteriochlorophyll biosynthetic pathway of *Rhodobacter capsulatus.* Biochem. Biophys. Res. Commun. **448**(2)**:**200–205.

Yamamoto T, Yokomizo T, Nakao A, Izumi T, Shimizu T. 2001. Immunohistochemical localization of guinea-pig leukotriene B4 12-hydroxydehydrogenase/15-ketoprostaglandin 13-reductase. Eur. J. Biochem. **268**(23)**:**6105–6113.

Yamanashi K, Minamizaki K, Fujita Y. 2015. Identification of the chlE gene encoding oxygen-independent Mg-protoporphyrin IX monomethyl ester cyclase in cyanobacteria. Biochem. Biophys. Res. Commun. **463**(4)**:**1328–1333.

Yang ZM, Bauer CE. 1990. *Rhodobacter capsulatus* genes involved in early steps of the bacteriochlorophyll biosynthetic pathway. J. Bacteriol. **172**(9)**:**5001–5010.

Yen HC, Marrs B. 1976. Map of genes for carotenoid and bacteriochlorophyll biosynthesis in *Rhodopseudomonas capsulata.* J. Bacteriol. **126**(2)**:**619–629.

Ying X, Ma K. 2011. Characterization of a zinc-containing alcohol dehydrogenase with stereoselectivity from the hyperthermophilic archaeon *Thermococcus guaymasensis.* J. Bacteriol. **193**(12)**:**3009–3019.

Youn B, Camacho R, Moinuddin, Syed G A, Lee C, Davin LB, Lewis NG, Kang C. 2006a. Crystal structures and catalytic mechanism of the Arabidopsis cinnamyl alcohol dehydrogenases AtCAD5 and AtCAD4. Org. Biomol. Chem. **4**(9)**:**1687–1697.

Youn B, Kim S, Moinuddin SGA, Lee C, Bedgar DL, Harper AR, Davin LB, Lewis NG, Kang C. 2006b. Mechanistic and Structural Studies of Apoform, Binary, and Ternary Complexes of the Arabidopsis Alkenal Double Bond Reductase At5g16970. J. Biol. Chem. **281**(52)**:**40076–40088.

Young DA, Bauer CE, Williams JC, Marrs BL. 1989. Genetic evidence for superoperonal organization of genes for photosynthetic pigments and pigment-binding proteins in *Rhodobacter capsulatus.* Mol. Gen. Genet. **218**(1)**:**1–12.

Zdobnov EM, Apweiler R. 2001. InterProScan - an integration platform for the signature-recognition methods in InterPro. Bioinformatics **17**(9)**:**847–848.

Zsebo KM, Hearst JE. 1984. Genetic-physical mapping of a photosynthetic gene cluster from *R. capsulata.* Cell **37**(3)**:**937–947.

7 Appendix

7.1 Reservoir conditions for *P. marinus* DPOR crystal formation

Table 17: Conditions resulting in *P. marinus* DPOR crystals. The conditions highlighted in gray were chosen for further refinement experiments. n.a.: not available (no details of the appearance were recorded).

Well	Reservoir composition	Appearance of crystals / Remarks
PEG II Suite		
C1	0.1 M sodium acetate pH 4.6 4 % (w/v) PEG 4000	high number of small crystals
C2	8 % (w/v) PEG 4000	high number of small crystals, see Figure 9
C5	0.1 M sodium acetate 0.1 M HEPES pH 7.5 12 % (w/v) PEG 4000	high number of small crystals, similar to well C2
C6	0.1 M Tris pH 8.5 12 % (w/v) PEG 4000	high number of small crystals, similar to well C2
C7	0.2 M Lithium sulfate 0.1 M Tris pH 8.5 16 % (w/v) PEG 4000	small crystals
C8	0.2 M sodium acetate 0.1 M Tris pH 8.5 16 % (w/v) PEG 4000	n.a.
E2	10 % (w/v) PEG 4000 20 % (v/v) isopropanol	needles
E3	0.1 M tri-sodium citrate pH 5.6 10 % PEG 4000 10 % (v/v) isopropanol	low number of larger crystals with undefined shape
E4	0.1 M HEPES pH 7.5 10 % (w/v) PEG 4000 5 % (v/v) isopropanol	crystals with undefined shape, see Figure 9
E5	0.1 M HEPES pH 7.5 10 % (w/v) PEG 4000 20 % (v/v) isopropanol	small crystals
E9	0.2 M $AmSO_4$ 0.1 M HEPES pH 7.5 16 % (w/v) PEG 4000 10 % (v/v) isopropanol	small crystals
G3	0.1 M potassium chloride 0.1 M Tris pH 8.5 3 % (w/v) PEG 6000	low number of larger crystals with defined shape, suitable for data collection, see Figure 9
G4	0.01 M magnesium chloride 10 % (w/v) PEG 6000	small crystals
G6	10 % (w/v) PEG 6000 5 % glycerol	small crystals (needles)
G8	0.01 M tri-sodium citrate 16 % (w/v) PEG 6000	star-shaped crystals
H4	4 % (w/v) PEG 8000	small crystals (needles)
H6	0.1 M Tris pH 8.5 8 % (w/v) PEG 8000	high number of crystals
H11	0.1 M HEPES pH 7.5 10 % (w/v) PEG 8000 10 % ethylene glycol	pointed needles

Table 17, continued.

Well	Reservoir composition	Appearance of crystals / Remarks
PEG I Suite		
G7	0.2 M lithium sulfate 20 % (w/v) PEG 3350	high number of small crystals
G10	0.2 M potassium sulfate 20 % (w/v) PEG 3350	high number of small crystals
G12	0.2 M di-sodium tartrate 20 % (w/v) PEG 3350	small crystals
H9	0.2 M tri-lithium citrate 20 % (w/v) PEG 3350	small crystals
H10	0.2 M tri-sodium citrate 20 % (w/v) PEG 3350	low number of larger crystals with defined shape, reflections were measured in initial scattering experiments
H11	0.2 M tri-potassium citrate 20 % (w/v) PEG 3350	low number of larger crystals with defined shape, reflections were measured in initial scattering experiments
PACT Suite		
E11	0.2 M sodium citrate 20 % (w/v) PEG 3350	high number of small crystals
G11	0.2 M sodium citrate 0.1 M Bis-tris propane pH 7.5 20 % (w/v) PEG 3350	high number of small crystals
JCSG Core I Suite		
A7	0.2 M tri-potassium citrate 20 % (w/v) PEG 3350	n.a.
B3	0.1 M HEPES pH 7.5 10 % (w/v) PEG 8000	low number of larger crystals with defined shape, reflections were measured in initial scattering experiments, see Figure 9
B7	0.2 M di-sodium tartrate 20 % (w/v) PEG 3350	n.a.
B10	0.2 M potassium sodium tartrate 20 % (w/v) PEG 3350	n.a.
D8	0.2 M sodium sulfate 20 % (w/v) PEG 3350	n.a.
E6	0.1 M MES pH 60 5 % (w/v) PEG 3000 30 % (v/v) PEG 200	small crystals
E9	0.2 M ammonium sulfate 20 % (w/v) PEG 3350	small crystals
F1	0.1 M MES pH 5.0 10 % (w/v) PEG 6000 final pH 6.0	low number of larger crystals with undefined shape
MPD Suite		
no crystals observed		

7.2 Contacts between MgADP•AlF_3 and L_2

Table 18: Key contacts between MgADP•AlF_3 and the peptide chains of L_2. Analysis was performed with UCSF Chimera (section 2.6.11) on the ligand bound to chain A of L_2. Amino acid residues belonging to the second L protomer are marked by asterisks (*). For relevant water molecules that form hydrogen bonds with the nucleotide or coordinate Mg^{2+} and AlF_3, their additional hydrogen bonding partners, as well as the bond distances, are listed.

Interacting Atom	Residue (interacting atom)	Distance [Å]	Additional hydrogen bonding partner	Distance [Å]
Base				
N7	Asn-209 ($N_{\delta 2}$)	3.1		
N6	Asn-209 ($O_{\delta 1}$)	3.0		
N6	Arg-233 (O)	3.1		
N3	H_2O No. 1	3.1		
N1	Val-235 (N)	3.0		
Ribose				
O2'	Asp-178* ($O_{\delta 2}$)	3.3		
O2'	H_2O No. 2	3.0		
O3'	Asp-180* ($O_{\delta 2}$)	2.7		
O3'	H_2O No. 2	3.1		
O5'	Thr-44 ($O_{\gamma 1}$)	3.3		
Phosphate				
O1A	Lys-37* (N_ζ)	2.9		
O1A	H_2O No. 3	2.6	Asp-70 ($O_{\delta 1}$)	3.8
O2A	Thr-44 (N)	2.6		
O2A	Thr-44 ($O_{\gamma 1}$)	2.8		
O1B	Ser-43 (O_γ)	3.1		
O1B	Ser-43 (N)	2.7		
O1B	H_2O No. 3	2.9		
O1B	H_2O No. 4	3.0	Asp-151 ($O_{\delta 1}$); Val-152 (O)	2.5; 3.8
O2B	Lys-37* (N_ζ)	2.9		
O2B	H_2O No. 3	3.5		
O3B	Gly-41 (N)	3.0		
O3B	Lys-42 (N_ζ)	2.5		
O3B	Lys-42 (N)	2.7		
PB	AlF_3 (F_1/F_2)	3.3/3.7		
Mg^{2+}				
	Ser-43 (O_γ)	2.0		
	AlF_3 (F_1)	1.9		
	ADP (O1B)	2.2		
	H_2O No. 3	2.1		
	H_2O No. 4	2.1		
	H_2O No. 5	2.0	Asp-70 ($O_{\delta 1}$); Asp-66 ($O_{\delta 2}$)	2.8; 2.9
AlF_3				
	Lys-37* (N_ζ)	2.6		
	Gly-39 (N)	3.1		
	Lys-42 (N_ζ)	2.7		
	Lys-68 (N_ζ)	3.0		
	Gly-154 (N)	3.2		
	H_2O No. 3	2.9		
	H_2O No. 4	2.8		
	H_2O No. 5	2.7		
	H_2O No. 6	2.8	Asp-155* ($O_{\delta 1}$/$O_{\delta 2}$)	2.8/3.0

7.3 Residues of the docking interfaces of DPOR and nitrogenase complexes

Residues of the octameric DPOR complex and the MgADP•AlF_4^--stabilized nitrogenase complex from *A. vinelandii* (PDB ID 1M34) participating in intersubunit contacts were analyzed using the PISA server (section 2.6.11). This tool identifies residues located at the interface of two protein subunits and detects hydrogen bonds and salt bridges between individual residues. A detailed list of all residues involved in the interaction of the DPOR and nitrogenase subunits of the aluminum fluoride stabilized complexes is given.

Table 19: Residues of L (NifH) involved in NB (NifD/NifK) docking. Bold: residues interacting with N (NifD). Italic: residues interacting with B (NifK). Bold/italic: residues interacting with both N and B (NifD and NifK). H: hydrogen bond, S: salt bridge.

L_2 chain A	Type of interaction	$NifH_2$ chain F	Type of interaction	L_2 chain B	Type of interaction	$NifH_2$ chain E	Type of interaction
Ile84		**Met58**		*Ile84*		*Met58*	
Asp85		**Glu59**		*Asp85*		*Glu59*	
Glu88	HS	**Ala62**		*Glu88*	HS	*Ala61*	
Asp91	HS	*Ala64*		**Val90**		***Ala62***	
Phe92		**Gly65**		***Asp91***	HS	***Gly65***	
His93		*Thr66*		***Phe92***		***Thr66***	
Glu95		**Val67**		**His93**	HS	*Val67*	
Gly117		*Glu68*		**Ser94**	H	**Glu68**	
Pro118		*Asp69*	HS	**Glu95**	H	*Gly90*	
Pro119		**Gly90**		**Glu96**	H	*Pro91*	
Thr122		**Pro91**		*Gly117*		*Val95*	
Gly123		**Gly94**		*Pro118*		*Gly96*	
Cys124	H	**Val95**		*Pro119*		***Cys97***	H to NifK
Gly126		**Gly96**		*Gly121*		**Gly99**	
Tyr127	H	***Cys97***	H to NifD	*Thr122*	H	***Arg100***	HS
Val128		**Ala98**		*Gly123*	H	*Gly101*	
Gly130		*Gly99*		***Cys124***	H to B	**Ile103**	
Gln131		***Arg100***	HS	**Gly126**		*Thr104*	H
Lys134		**Gly101**		***Tyr127***	H to N	**Glu111**	
Cys158		*Ile103*		*Val128*		**Cys132**	
Gly159		**Thr104**	H	**Gly130**		**Gly133**	
Gly160	H	*Glu111*	H	**Gln131**	H	**Gly134**	H
Ala163		*Cys132*		**Lys134**		**Arg140**	HS
Gln166	H	*Gly133*		**Glu138**		**Glu141**	S
Ala194		*Gly134*		**His140**		**Lys170**	HS
Lys195		*Arg140*	HS	**Cys158**		**Tyr171**	
Lys197		*Glu141*		**Gly159**		**Ser174**	
Asn198	H	*Asn142*		**Gly160**			
Tyr199	H	*Lys170*	H	**Ala163**			
		Tyr171		**Gln166**			
		Asn173	H	**Ala194**			
		Ser174		**Lys197**			
				Asn198	H		
				Tyr199	H		

Table 20: Residues of N (NifD) and B (NifK) interacting with L_2 ($NifH_2$). Bold: residues interacting with chain A of L_2 (chain F of $NifH_2$). Italic: residues interacting with chain B of L_2 (chain E of $NifH_2$). Bold/italic: residues interacting with both L (NifH) protomers. H: hydrogen bond, S: salt bridge, ch.: chain.

N	Type of interaction	NifD	Type of interaction	B	Type of interaction	NifK	Type of interaction
Lys8	HS	*Lys51*		*Ala62*		*Glu120*	HS
Glu67	H	**Glu120**	HS	*Arg63*	HS	*Asp121*	
Arg68	HS	**Lys121**		*Leu65*	H	*Ala123*	H
Asp69		**Ile123**	H	*Gly66*		*Val124*	H
Leu70	H	**Val124**	H	*Gly67*		*Phe125*	
Ala71		**Phe125**		***Asp68***		*Gly126*	
Gly72		**Gly126**		*Thr69*	H	***Gln128***	
Leu73		***Asp128***	HS to ch. E	***Ala70***	H to ch. B	**Glu156**	HS
Asp75		*Gly157*	H	**Glu71**		***Val157***	
His77		*Leu158*		**Lys74**		***Ile158***	
Glu78		***Ile159***	H to ch. E	**Glu98**		**Gly159**	H
Glu106		***Gly160***	H to ch. E	**Leu99**	H	***Asp160***	
Val107		***Asp161***	H to ch. E	***Ile100***	H to ch. A	**Asp161**	S
Ile108		*Asp162*	S	***Gln101***	H to ch. A	**Asn163**	
Lys109		*Glu164*		***Asp102***	H to ch. B	**Ala164**	
Asp111	H	*Ser165*		**Gln103**	H	***Phe165***	
Arg114	H	*Lys168*	S	**Ser106**	H	**Asn167**	
Arg118	H	*Val169*		**Leu107**	H	**Asn168**	H
Ile137		*Arg182*		**Gly110**	H	**Lys171**	H
Glu138	H	*Glu184*	HS	**Met111**		**His185**	
Lys150		*Phe186*		**Glu121**		**Pro187**	
Thr218		*Arg187*		**Pro123**		**Phe189**	
Asp219		*Gly188*		**Tyr125**		**Val190**	
Arg222	H	*Val189*		**Ser126**		**Arg206**	
Asp226		*Leu193*		**Lys127**		**Leu210**	
Tyr319	H	*His196*				**Glu299**	
Leu320						**Lys300**	
Asn321						**Lys303**	H
Arg322							
Glu323							
Glu340	HS						

Table 21: Hydrogen bonds (italic) and salt bridges (bold) between individual residues of DPOR subunits.

N	L chain A	B	L chain A	N	L chain B	B	L chain B
Arg68 (NH1)	*Asp91 (OD1)*	*Ser106 (OG)*	*Gln166 (OE1)*	*Lys8 (NZ)*	*Asp91 (OD2)*	*Arg63 (NH1)*	*Asp91 (OD1)*
Arg68 (NH2)	*Asp91 (OD1)*	*Ser106 (OG)*	*Tyr199 (OH)*	*Arg222 (NH2)*	*Ser94 (OG)*	*Arg63 (NH1)*	*Asp91 (O)*
Arg68 (NH2)	*Glu88 (OE2)*	*Leu107 (N)*	*Tyr199 (OH)*	*Arg222 (NH1)*	*Ser94 (OG)*	*Arg63 (NH2)*	*Glu88 (OE1)*
Arg68 (NH2)	*Glu88 (O)*	*Leu99 (O)*	*Cys124 (SG)*	*Tyr319 (OH)*	*Glu95 (OE2)*	*Arg63 (NH2)*	*Glu88 (OE2)*
Glu67 (OE1)	*Tyr127 (OH)*	*Leu99 (O)*	*Tyr127 (N)*	*Arg118 (NH1)*	*Asn198 (OD1)*	*Arg63 (NH2)*	*Asp91 (OD1)*
Leu70 (O)	*Cys124 (N)*	*Ile100 (O)*	*Gly160 (N)*	*Arg114 (NE)*	*Asn198 (OD1)*	*Thr69 (N)*	*Thr122 (OG1)*
Arg68 (NE1)	**Glu88 (OE2)**	*Gln101 (O)*	*Gly160 (N)*	*Arg114 (NE)*	*Asn198 (O)*	*Thr69 (OG1)*	*Thr122 (OG1)*
Arg68 (NH1)	**Asp91 (OD1)**	*Gly110 (O)*	*Asn198 (ND2)*	*Glu340 (OE2)*	*His93 (NE2)*	*Ala70 (N)*	*Thr122 (OG1)*
Arg68 (NH2)	**Asp91 (OD1)**	*Gln103 (O)*	*Tyr199 (OH)*	*Tyr319 (OH)*	*Ser94 (N)*	*Asp102 (OD1)*	*Thr122 (OG1)*
Arg68 (NH2)	**Glu88 (OE2)**			*Glu138 (OE1)*	*Tyr127 (OH)*	*Thr69 (OG1)*	*Gly123 (N)*
				Glu138 (OE1)	*Gln131 (NE2)*	*Leu65 (O)*	*Cys124 (N)*
				Asp111 (OD2)	*Tyr199 (OH)*	**Arg63 (NH1)**	**Asp91 (OD1)**
				Lys8 (NZ)	**Asp91 (OD2)**	**Arg63 (NH2)**	**Glu88 (OE1)**
				Glu340 (OE1)	**His93 (NE2)**	**Arg63 (NH2)**	**Glu88 (OE2)**
				Glu340 (OE2)	**His93 (NE2)**	**Arg63 (NH2)**	**Asp91 (OD1)**

Table 22: Hydrogen bonds (italic) and salt bridges (bold) between individual residues of nitrogenase subunits.

NifD chain A	NifH chain F	NifK chain B	NifH chain F	NifD chain A	NifH chain E	NifK chain B	NifH chain E
Glu120 (OE2)	*Arg100 (NE)*	*Glu156 (O)*	*Arg100 (NH1)*	*Gly157 (O)*	*Arg100 (NH1)*	*Glu120 (OE1)*	*Arg100 (NE)*
Glu120 (OE2)	*Thr104 (OG1)*	*Glu156 (OE1)*	*Arg100 (NH1)*	*Glu184 (OE1)*	*Arg100 (NH1)*	*Glu120 (OE2)*	*Thr104 (OG1)*
Ile123 (O)	*Cys97 (N)*	*Gly159 (O)*	*Arg140 (NH2)*	*Glu184 (OE1)*	*Arg100 (NH2)*	*Glu120 (OE2)*	*Arg100 (NH2)*
Val124 (O)	*Cys97 (N)*	*Lys400 (NZ)*	*Asp69 (OD1)*	*Ile159 (O)*	*Gly134 (N)*	*Ala123 (O)*	*Cys97 (N)*
Glu120 (OE2)	**Arg100 (NE)**	*Lys303 (NZ)*	*Glu111 (O)*	*Gly160 (O)*	*Arg140 (NH2)*	*Val124 (O)*	*Cys97 (N)*
Glu120 (OE2)	**Arg100 (NH2)**	*Asn168 (ND2)*	*Lys170 (O)*	*Asp161 (O)*	*Arg140 (NH2)*	**Glu120 (OE1)**	**Arg100 (NE)**
		Lys171 (NZ)	*Asn173 (O)*	*Asp128 (OD2)*	*Lys170 (NZ)*	**Glu120 (OE1)**	**Arg100 (NH2)**
		Glu156 (OE1)	**Arg100 (NH1)**	**Glu184 (OE1)**	**Arg100 (NH1)**	**Glu120 (OE2)**	**Arg100 (NE)**
		Asp161 (OD2)	**Arg140 (NE)**	**Glu184 (OE1)**	**Arg100 (NH2)**	**Glu120 (OE2)**	**Arg100 (NH2)**
		Lys400 (NZ)	**Asp69 (OD1)**	**Asp162 (OD1)**	**Arg140 (NE)**		
		Lys400 (NZ)	**Asp69 (OD2)**	**Asp162 (OD2)**	**Arg140 (NE)**		
				Asp128 (OD2)	**Lys170 (NZ)**		
				Lys168 (NZ)	**Glu141 (OE1)**		
				Lys168 (NZ)	**Glu141 (OE2)**		

7.4 Structure-based sequence alignments of DPOR subuntis N and B

Structure-based amino acid sequence alignment of the *P. marinus* DPOR subunits N and B with the respective subunits from *R. capsulatus*, *T. elongatus* and the related nitrogenase subunits were created (section 2.6.11) to visualize differences and similarities between the proteins.

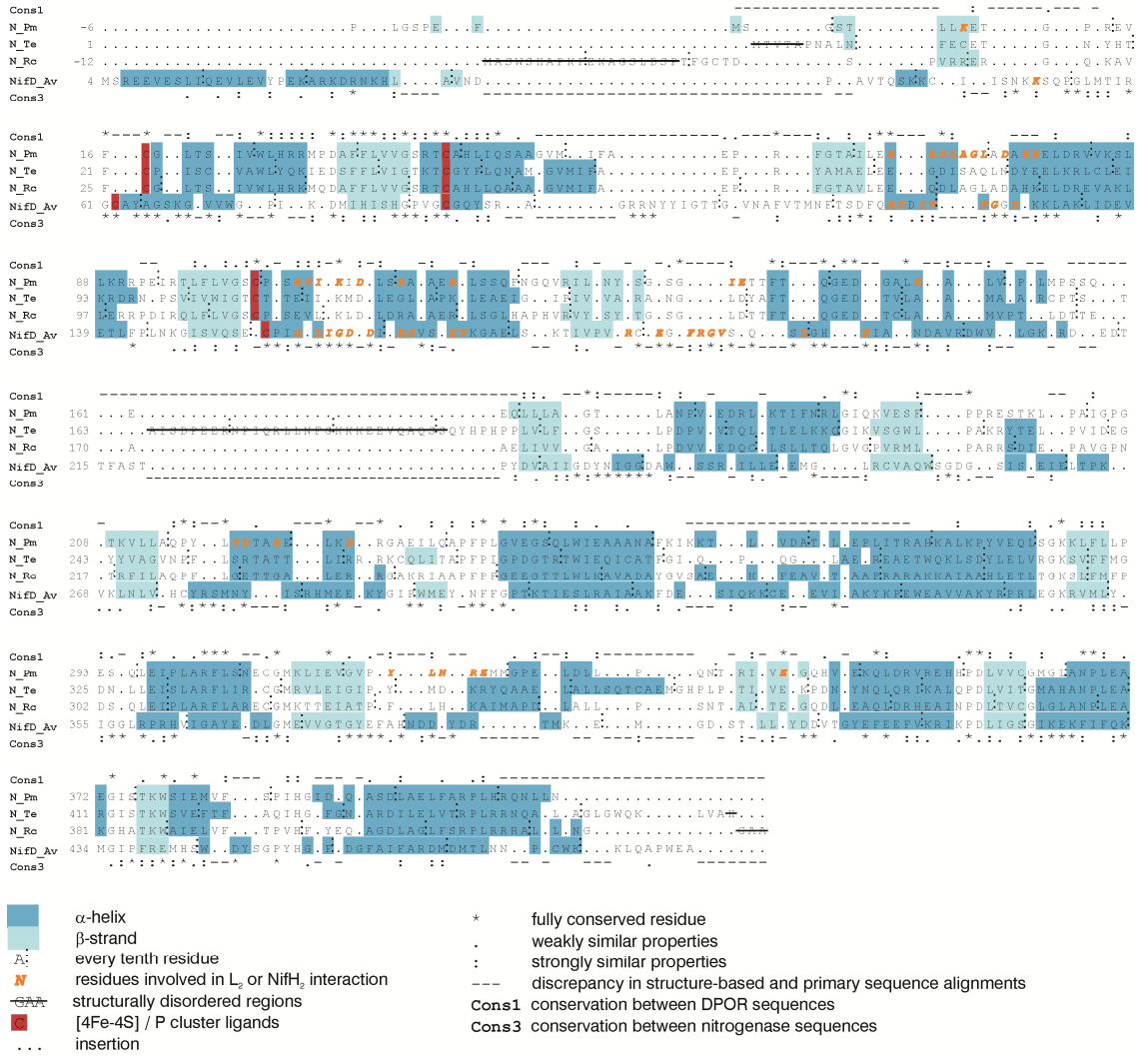

Figure 27: Structure-based amino acid sequence alignment of DPOR N subunits and nitrogenase NifD. Helices (blue) and β-strands (light-blue) are highlighted. The conservation patterns derived from primary amino acid sequence alignments (not shown) of 15 N sequences (Cons1) and 16 NifD sequences (Cons3) were manually added to the structure-based amino acid sequence alignment. Dashes (—) indicate structural incongruities, which are *inter alia* caused by conformational changes. Orange font indicates residues involved in protein-protein interactions between L_2 and $(NB)_2$ or $NifH_2$ and $(NifD/NifK)_2$, respectively. All interface residues were identified using the PISA server (section 2.6.11). Ligands of the metalloclusters are highlighted by red shading. Asterisks (*) indicate fully conserved residues, colons (:) mark residues with strongly similar properties, residues with weakly similar properties are indicated by a period (.). The structure-based alignment was generated using UCSF Chimera (section 2.6.11). Primary amino acid sequence alignments were generated using ClustalW (section 2.6.11). Av, *A. vinelandii*; Pm, *P. marinus*; Rc, *R. capsulatus*; Te, *T. elongatus*.

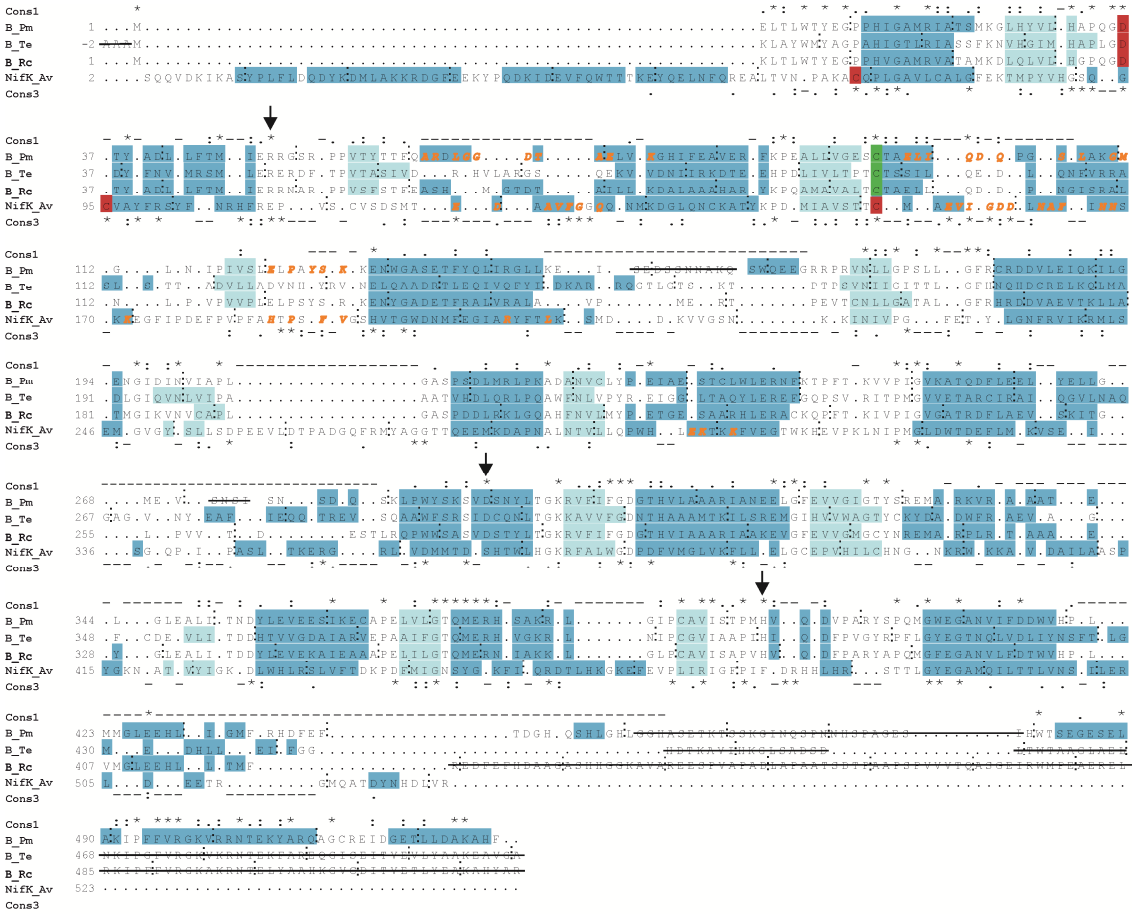

Figure 28: Structure-based amino acid sequence alignment of DPOR B subunits and nitrogenase NifK. Helices (blue) and β-strands (light-blue) are highlighted. The conservation patterns derived from primary amino acid sequence alignments (not shown) of 14 B sequences (Cons1) and 16 NifK sequences (Cons3) were manually added to the structure-based amino acid sequence alignment. Dashes (—) indicate structural incongruities, which are *inter alia* caused by conformational changes. Orange font indicates residues involved in protein-protein interactions between L_2 and $(NB)_2$ or $NifH_2$ and $(NifD/NifK)_2$, respectively. All interface residues were identified using the PISA server (section 2.6.11). Ligands of the metalloclusters are highlighted by red shading. Asterisks (*) indicate fully conserved residues, colons (:) mark residues with strongly similar properties, residues with weakly similar properties are indicated by a period (.). Arrows indicate *P. marinus* B residues which were mutagenized in the present study. The structurally disordered C-terminal regions of the *R. capsulatus* and *T. elongatus* B subunits were aligned by their primary sequences only because no structural information was available. The structure-based alignment was generated using UCSF Chimera (section 2.6.11). Primary amino acid sequence alignments were generated using ClustalW (section 2.6.11). Av, *A. vinelandii*; Pm, *P. marinus*; Rc, *R. capsulatus*; Te, *T. elongatus*.

7.5 Amino acid sequence alignments of BchC and zinc-containing MDRs

Individual amino acid sequence alignments of 19 BchC sequences and 11 zinc-containing MDRs were created (section 2.6.11). The conservation patterns of these alignments were also implemented in Figure 25.

```
Cphae      ------------------MKAKAIVFTGVRQIEVKNVTLKP-VLSTDVMIETYWSSIST 40
Paes       ------------------MKHAKAIVFTGVRQIEVKKVTLKS-MSSTDVLVETYWSSIST 41
Clut       ------------------MKSKAIVFTGVRQIELREVTLKP-LSSTDVLVETWWSSIST 40
Cpha       ------------------MKTKAIVFTGIRQIEVSEVQLKP-LGSTDVLVETYWSSIST 40
Ppha       ------------------MKAKAIVFSGVRQIELCEVTLKS-LSSTDVLVETWWSSIST 40
Clim       ------------------MKSKAIVFSGVRQISLCEVTLKQ-LSSTDVLVETYWSSIST 40
Ctep       ----------------MEAKKSKAIVFSGVNQIELREVTLKP-VSSTDVLVETWWSSIST 43
Cpar       ----------------MEAKKSKAIVFSGVRQIELRDVTLKP-ISSTDVLVETWWSSIST 43
Amul       ------------------MLDSLAIIIERPFDLSLRRVRLDA-PAATDVVVEVAWSGVST 41
Rden       ------------------MDTTAVLLKGPKDLDVDTLQLHV-PGDGDLVVEIEHSGIST 40
Rsph       ------------------MRTTAVILSGPRDLGLQTIQLNE-PAPGDIVVEITHSGIST 40
Dshi       ------------------MHATAVVLTGPKALGLQDVAVSD-PTATDIVVRIDHSGIST 40
Jann       ------------------MHTTAVILEGPKALGLGQVDLCA-PSDGDLVIDVSHSGIST 40
Boli       ------------------MDAIAVVLGRPRELSLQRLLLAD--AQDCLTVDIECSAIST 39
Hhal       MSDPSPASSVDPGGPGSGPRSARAVVFEAPERLALQDVALID-PGPGDVVVDIEFSGIST 59
Rpal       ------------------METIAVVLKQPKNVEISRLPLTP-PTAEDVVVDVAWSGVST 40
Tmob       ------------------MNAIAVVLEQPERLALSRLDLSPPPGDEDVVVDIDWSGIST 41
Rpho       ------------------MDTLAVVIEKPQSLGLKRLPLTP-PTEADVVVAIEWSGIST 40
Tvio       ----------MNPDTPTLEALAVVLEQPERLSLQRLALTP-PGDADVVVDIEWSGIST 47
                              : *:::     : :  : :        : :    *.:**

Cphae      GTEKMAFEGLIPS-PPFIFPFIPGYETVGKITKVGAHVNDNLIGKYAYIAGS-FGY---- 94
Paes       GTEKMAFNGLIPS-PPFIFPFIPGYETVGKITKVGDHVNDSLLGKYAYIAGS-FGY---- 95
Clut       GTEKMAFNGLIPS-PPFIYPFIPGYETVGKITEVGAHVNRELIGRYAYIAGS-FGY---- 94
Cpha       GTEKMAYNGLIPS-PPFIFPFIPGYETVGKITEVGDHVKESLIGKFAYIAGS-FGY---- 94
Ppha       GTEKMAYNGLIPS-WPFIFPFIPGYETVGKIIQAGDHVNQSLIGKFAYVAGS-FGY---- 94
Clim       GTEKMAYNGLIPS-PPFIFPFIPGYETVGRIIEAGDHVNQSLIGKFAYVAGS-FGY---- 94
Ctep       GTEKMALNGLIPS-PPFIFPFIPGYETVGRIVEAGDHVNQGLIGKFAYVAGS-FGY---- 97
Cpar       GTEKMALNGLIPS-PPFIFPFIPGYETVGRIVEAGDHVNQDLIGKFAYVAGS-FGY---- 97
Amul       GTEKLIFTGEMPPFPGMGYPLVPGYEATGTIVETGREVRGR-LGETVFVPGA-RCF---- 95
Rden       GTEKLFWSGEMPPFPGMGYPLVPGYEAVGEVVEADRATGFK-VGERVFVPGA-NCY---- 94
Rsph       GTEKLFYTGQMPPFPGMGYPLVPGYEAAGEVVEAAPDTGFR-PGDRVFVPGS-NCFAPTD 98
Dshi       GTEKLFWSGKMPPFPGFSFPLVPGYEAAGEVVEAGADTSYK-PGDRVFVPGA-NCY---- 94
Jann       GTEKLFWSGQMPPFPGMGYPLVPGYEAAGEVVEAAANTGFK-PGDRVFVPGA-NCY---- 94
Boli       GTERLLYEGRMPPFPGMGYPLVPGYEAVGRVAHAAPHSGFR-KGERVFVPGAARCF---- 94
Hhal       GTERLLWKGTMPQFPGLAYPLVPGYESVGRVVTAGAESGRR-EGEVVFVPGA-RCY---- 113
Rpal       GTERLLWSGRMPAFPGMGYPLVPGYESVGEVVEAGSATDLR-PGQMVFVPGA-KCF---- 94
Tmob       GTERLLWSGRMPHFPGMGYPLVPGYESVGRIVSAGPGSGRE-EGQRVFVPGA-RCF---- 95
Rpho       GTERLLWSGRMPPFPGLGYPLVPGYESVGRVIEAGAASGRA-VGERVFVPGA-TCY---- 94
Tvio       GTERLLWSGRMPDFPGMGYPLVPGYESVGRVIFAGLQAGLT-VGQRVFVPGA-RCY---- 101
           ***::   * :*    : :*::****:.* :  .         *  .:: *:   :
```

Figure 29: Amino acid sequence alignment of BchC sequences. BchC sequences from the following organisms were used: *Acidiphilum multivorum* (Amul), *Bradyrhizobium oligotrophicum* (Boli), *Chlorobaculum parvum* (Cpar), *C. tepidum* (Ctep), *Chlorobium limicola* (Clim), *Chlorobium luteolum* (Clut), *Chlorobium phaeobacteroides* (Cphae), *Chlorobium phaeovibrioides* (Cpha), *D. shibae* (Dshi), *Halorhodospira halophila* (Hhal), *Jannaschia sp.* (Jann), *Prosthecochloris aestuarii* (Paes), *Pelodictyon phaeoclathratiforme* (Ppha), *R. sphaeroides* (Rsph), *Rhodopseudomonas palustris* (Rpal), *Rhodospirillum photometricum* (Rpho), *R. denitrificans* (Rden), *Thioflavicoccus mobilis* (Tmob), *Thiocystis violascens* (Tvio). The conservation pattern of this alignment was implemented in Figure 25. The alignment was prepared with Clustal Omega (section 2.6.11).

```
Cphae      -EDVNAAFGGASQFVVCPVESITVLDGIDDPKCGIALPLGATALHFMDLGDVQGRKVLVL 153
Paes       -TDVNAAFGGASEYVVCPVESITILDGIADPQCGIALPLGATALHFMDLAEIKDKKVLVL 154
Clut       -EGVNAAFGGASQFVACPVESLTVLEGIENPQCGIALPLGATALHIVDLAAVKGKKVLVL 153
Cpha       -EGVNAAFGGASQFVACPVDSITILDGIENPQYGIALPLGATALHIVDLAEVKNKKILIL 153
Ppha       -EGVNAAFGGASEYIACPVESITVLDNIENPKCGIALPLGATALHIVDLAQVENKKVLVL 153
Clim       -IDVNAAFGGASQYIVCPVDSITLLDSIANPQCGIALPLGATALHIIDLAAVENRKVLIL 153
Ctep       -EDVNAAFGGASQFIVCPVESLTVLDGIANPQCGIALPLGATALHIVDLAEVKNRKVLVL 156
Cpar       -EDVNAAFGGASQFIVCPVESLTVLDGIANPQCGIALPLGATALHIVDLAEVKNRKVLVL 156
Amul       -GEMRALFGADSRHLVVPAERAVRVPAAL-GANATLLALAATARHAIRVA--GGAPELIV 151
Rden       -DGAFGLFGGAASRVVTASDRVTRIDAGH-GASGALLALAATARHSMAGLN-KSVPDLIV 151
Rsph       AGPIRGLFGAATKRLVTPAHRAVRIDPAL-EAEGALLALAATARHALAGLN-HVLPDLIV 156
Dshi       -GDVRGLFGGASNLLVSKADRVVRIDESL-KAEGALLALAATARHAMAGLN-KSVPDLIV 151
Jann       -GDVKGLFGGASARLVSAADRVVRIDPAL-KAEGALLALAATARHAMAGMD-KQLPELIV 151
Boli       -GEVKSLFGAAASRLNVPPQRLVALDDSI-GERGVLLALAATAYHALAIGG-DGRAECVV 151
Hhal       -QEVSGLFGGAASRVVVSGERVIPLPDGL-GERGVLLALAATAWHAVAE----APPDLVV 167
Rpal       -GEVRGLFGASASRLVVAAKRVIPLDQEL-GERGILLALAATAYHAIAAHD-GRAPECIV 151
Tmob       -GDVRGLFGGAASRLVVPGSRVVPIPDDL-AERGILLALAATAYHAVAACS-AGCPELVV 152
Rpho       -GEVRGLFGGAAAKVVVPGARVVPLPEGM-DETGTLFALAATAHHAVTLPG-SALPDLII 151
Tvio       -GEVRGLFGGAASRVVAPGSRMVPVDEKF-GEQSVLMALAATAYHAIAGPA-SPHVELIV 158
                 . **. :  :         :        .  : *.*** * :           ::

Cphae      GQGAVGILAVQLAKHMGASLVAATEPHQNRLNYS--SADLKVNPSCQDVSAELAGNEFDV 211
Paes       GQGAVGILAVQLAKYMGAKLVAATEPYQNRLNYS--EADLCINPNVQDVSASLAGHEFDI 212
Clut       GQGAVGLLAAELAKLMGAALVAATEPSQNRLRHS--PADIRINPDTEDVMAALAGHEFDV 211
Cpha       GQGAVGILAAELSKLMGAKLVAATEPHPKRLKFS--PADIRINPEKEDVSAALAGHEFDV 211
Ppha       GQGAVGILAAELAKLMGAKLVAATEPNKKRLQLS--SADLKVNPETEDVAAALAGHEFDV 211
Clim       GQGAVGILASELARHMGARLIAVTEPYQNRLRFS--SADLKVNPDNEDVSAALAGHEFDV 211
Ctep       GQGAVGILAAELAKRFGASLVAVTEPHQRRLDIS--TSDIKVNPEKQDVSVALAGHEFDV 214
Cpar       GQGAVGILAAELAKHMGASLVAVTEPHQNRLDIS--TADIKVNPDKQDVSAALAGHEFDV 214
Amul       GHGVLGRLIARLATL-DGGAPVVWETRAARFAGA--RGYEVRAAAD------DSRRDYRT 202
Rden       GHGVLGRLLARLTIAAGAPAPMVWEIDESRRKGA--QGYEVIAPED------DPRRDYTS 203
Rsph       GHGTLGRLLARLTIAAGGEPPVVWETKAERRRHA--EGYEVIDPAT------DQRRDYRS 208
Dshi       GHGVLGRLLARLTIAAGAPAPTVWEISEDRAKGA--TGYQVIHPDA------DTRRDYRS 203
Jann       GHGVFGRLLARLTIAAGGKAPTVWEIDADRAQGA--TGYEVLHPDA------DDRKDYSC 203
Boli       GHGVLGRLLARLIVAMGGDPPVVWESNPERASGA--MGYCVIDPAE------DSKRDYRL 203
Hhal       GHGVLGRLIARIGVL-VDHPPTVWETNADRRAGA--EGYTVVDPDS------DERHDYPR 218
Rpal       GHGVLGRLLARIAVALGNPPPVVWEKNPVRASGA--VGYAVVDPAE------DQKRDYKS 203
Tmob       GHGVLGRLIARLTVAKCSKAPTVWERNPIRATGG--EGYQVVDPQD------DPRVDYRS 204
Rpho       GHGVLGRLVARVV-VALGGRPVVWEKNPARCDGA--LGYEVVDPDA------DGRKDYTS 202
Tvio       GHGVLGRLLARIAALGEGTRPVVWETNPERRQGAEGYGYEVLAPDD------DPRRDYRS 212
           *:*..* *  .:          . *    *   .   .                  ::
```

Figure 29, continued.

```
Cphae      MIDSTGVMSAIETGLRFLKFHGKVIFGGYYQ-RMNIDYSQAFDKELSFVAARQWAKGDLL 270
Paes       MIDSTGVMSAIETGLRFLKFHGKVIFGGYYQ-RMNIDYSQAFDKELSFMAAKQWAKGDLL 271
Clut       LIDSTGIMSAIDTGLRFLKFHGQVIFGGYYQ-RMNIDYSQAFQKELSFIAAKQWAKGDLE 270
Cpha       LIDSTGIMAAIDTGLRFLKFHGTVIFGGYYQ-RMNIDYSQAFQKELSFIAAKQWAQGDLE 270
Ppha       LIDSTGIMSAIDTGLRFLKFQGTVIFGGYYQ-RINIDYSQAFQKELSFIAAKQWAKGDLE 270
Clim       LIDSTGIMSAIDTGLRFLKFHGVVIFGGYYQ-RMNIDYSQAFQKELSFIAAKQWAHGDLE 270
Ctep       LIDSTGIMSAIETGLRFLKFHGKVIFGGYYQ-RMNIDYSQAFNKELSFIAARQWAKGDLH 273
Cpar       LIDSTGIMSAIDTGLRFVKFHGKVIFGGYYQ-RINIDYSQAFNKELSFIAARQWAKGDLR 273
Amul       IIDASGDSAILDRLIGRLAPGGMITLAGFYAAPLGFAFPPAFMREARIAIAAQWQPEDLA 262
Rden       VYDASGSVEVLNDLVGRLAKGGEIVLAGFYTTAISFAFPPAFMKEARFRVAAEWTHDDLA 263
Rsph       IYDASGDPKLIDSLVMRLAKGGEIVLAGFYTEPVAFTFVPAFMKEARLRIAAEWQPEDMV 268
Dshi       IYDASGNAELISSLIMRIQKGGEIVLAGFYD-QITFPFPPAFMKEARLRIAAEWDRDDLI 262
Jann       IYDASGQSDLLNTLIARLKKGGEIVLAGFYPEPLTFAFPPAFMREARMRIAAEWTRDDLI 263
Boli       IFDASGDTGLLDSLIARLAPRGEIILAGFYSAPLTFSYPPAFMREAAIRVAAEWKHEDLL 263
Hhal       ICDVSGDAGLLDTLIGRLGHGGEVVLAGFYSDRLSFAFPSAFMREARLRVAAEWQRSDLE 278
Rpal       IYDVSGDPTLLDSLISRIAPSGEVVLAGFYSEPLSFTFPPAFMREARIRVAAEWQQPDIA 263
Tmob       ICDVSGDSTVLDGLIARLAGGGEVVLAGFYDEPLAFSFPPAFMREARIRVAAEWAEADLI 264
Rpho       ICDVSGDAGLLDTLIARLAPQGEIVLAGFYEAPLSFTFPPAFMREARLRVAAQWKPADVA 262
Tvio       ICDMSGDSAILDSLIARLARGGEIILGGFYSQPVAFTFPPAFMREARFRIAAEFQPADLA 272
           : * :*    :.  :  :   * : :.*:*   : : :  ** :*  :  * ::   *:

Cphae      RVKELIKNNTLQAKKIFTHSHPVNADLAEAYHQAFNDPDCLKMVLNWKPENENTD----- 325
Paes       RVRELIRNGNLHAEKIFTHSHAVDQNLEEAYQQAFNDPDCLKMILNWKKT---------- 321
Clut       RVRKLIAEGRLNTEKIFTHHHPVDDAITDAYMQAFNDPDCMKMILTWKKEAEEGGTPCHT 330
Cpha       RVRALIAERRLNAEKIFTHQSPVDESITETYLKAFGDPDCLKMILNWKSEGKEANGSCYL 330
Ppha       RVRELIAQQKLNAARIFTHQHTVEEDITEAYLQAFTNPDCMKMILLWKTGTQQEEAGCPI 330
Clim       RVRDLIAAKKLNAEKIFTHQCQVDDNITSVYMQAFGDPDCLKMILHWKTDAEEQERACYL 330
Ctep       RVRELIAAGKINAEKIFTHQCTVDDNLMEAYMQAFSDSDCLKMIIHWKHGNEAGE--HFP 331
Cpar       RVRDLIANGKINAEKIFTHQCSLEDNLMEAYMQAFDDPDCLKMIIHWQDGSEAEKDGGMA 333
Amul       DVAARVAAGRLDLSGLVTHRVPAA-DAAQAYPAAFNDDSCLKLLIDWRDMT--------- 312
Rden       ATRALVEGGSLSLENLITHQASHL-NARAAYAQAFTDPDCLKMILNWKDVA--------- 313
Rsph       ATRALIESGALSLANLITHTRPAS-EAAEAYATAFSDPDCLKMILDWRATA--------- 318
Dshi       ATRALIDSGALSLEELITHTTQAA-DCANAYQTAFEDPSCLKMILDWSATA--------- 312
Jann       ATRDLIDHGALSLDDLITHTRNSD-QAAEAYQTAFEDAACLKMILNWAPSSREATGRNGE 322
Boli       AVRNLVDTGRLSLDGLITHHADAR-SAENAYRIAFDDPSCLKMVLDWRAAA--------- 313
Hhal       AVTGKIETGALSLDGLITHCLDAA-EAASAYRIAFGDPDCLKMVLDWRNS---------- 327
Rpal       ATKDLIESGRLSLDGLITHHHDAK-SAPDAYRIAFEDAACLKMVLNWRLS---------- 312
Tmob       AVKEMVEAGHLSLDGLITHRQDAA-QAEAAYQTAFTDPTCLKMVLDWRDVA--------- 314
Rpho       GILALLGDGRLSLAGLITHHARPE-EADAAYRTAFGDPACLKMILDWRSAS--------- 312
Tvio       AVRALLDSGRLSLDGLITHRLPAT-EAHAAYRTAFGDPSCLKMILDWRNLS--------- 322
                :    :    :.**          .*  ** :  *:*::: *

Cphae      ------       325
Paes       ------       321
Clut       APKP--       334
Cpha       TGKP--       334
Ppha       TAKS--       334
Clim       TSET--       334
Ctep       TCNTAN       337
Cpar       TCNMGR       339
Amul       ------       312
Rden       ------       313
Rsph       ------       318
Dshi       ------       312
Jann       TVQ---       325
Boli       ------       313
Hhal       ------       327
Rpal       ------       312
Tmob       ------       314
Rpho       ------       312
Tvio       ------       322
```

Figure 29, continued.

```
ADH_Sc          --MSIPE---TQ-KGVIFYESHGKLEYKDI--------PVPKPK-ANELLINVKYSGVCH      45
CAD_At          --MGIMEAERKT-TGWAARDPSGILSPYTY--------TLRETG-PEDVNIRIICCGICH      48
LADH_Ec         -----MSTAGKV-----IKCKAAVLWEEKKPFSIEEV-EVAPPK-AHEVRIKMVATGICR      48
LArDH_Nc        -----MASSASKTNIGVFTNPQHDLWISEASPSLESVQKGEELK-EGEVTVAVRSTGICG      54
SDH_Hs          -----MAAAAKPNNLSLVVHGPGDLRLENY--------PIPEPG-PNEVLLRMHSVGICG      46
SDH_Ba          ---------MASDNLSAVLYKQNDLRLEQR--------PIPEPK-EDEVLLQMAYVGICG      42
GPDH_Eco        -----MKSVVND-------TDGI-VRVAES--------VIPEIKHQDEVRVKIASSGLCG      39
TDH_Ec          -----MKALSKL-------KAEEGIWMTDV--------PVPELG-HNDLLIKIRKTAICG      39
TDH_Bs          MQSGKMKALMKK-------DGAFGAVLTEV--------PIPEID-KHEVLIKVKAASICG      44
TDH_Ph          -MSEKMVAIMKT-------KPGYGAELVEV--------DVPKPG-PGEVLIKVLATSICG      43
TDH_Tk          -MAEKMQAIMKT-------KPAYGAELVEV--------DVPKPG-PGEVLIKVLATSICG      43
                                                        :: : :   .:*

ADH_Sc          TDLHAWH-GDW-PLPVKLPLVGGHEGAGVVVGMGENVKGWKIGDYAGIKWLNGSCMACEY      103
CAD_At          TDLHQTK-NDL-GMS-NYPMVPGHEVVGEVVEVGSDVSKFTVGDIVGVGCLVGCCGGCSP      105
LADH_Ec         SDDHVVS----GTLVTPLPVIAGHEAAGIVESIGEGVTTVRPGDKVIPLFTP-QCGKCRV      103
LArDH_Nc        SDVHFWKHGCIGPMIVECDHVLGHESAGEVIAVHPSVKSIKVGDRVAIEPQV-ICNACEP      113
SDH_Hs          SDVHYWEYGRIGNFIVKKPMVLGHEASGTVEKVGSSVKHLKPGDRVAIEPGA-PRENDEF      105
SDH_Ba          SDVHYYEHGRIADFIVKDPMVIGHEASGTVVKVGKNVKHLKKGDRVAVEPGV-PCRRCQF      101
GPDH_Eco        SDLPRIF----KNGAHYYPITLGHEFSGYIDAVGSGVDDLHPGDAVACVPLL-PCFTCPE      94
TDH_Ec          TDVHIYNWDEWSQKTIPVPMVVGHEYVGEVVGIGQEVKGFKIGDRVSGEGHI-TCGHCRN      98
TDH_Bs          TDVHIYNWDQWARQRIKTPYVFGHEFSGIVEGVGENVSSVKVGEYVSAETHI-VCGECVP      103
TDH_Ph          TDLHIYEWNEWAQSRIKPPQIMGHEVAGEVVEIGPGVEGIEVGDYVSVETHI-VCGKCYA      102
TDH_Tk          TDLHIYEWNEWAQSRIKPPQIMGHEVAGEVVEVGPGVEDLQVGDYISVETHI-VCGKCYA      102
                :*                   ***  * :  :   *     *:

ADH_Sc          CELGNESNCPHADL----------------------SGYTHDGSFQQYATADAVQAAHIPQ      142
CAD_At          CERDLEQYCPKKIWSYNDV----------------YINGQPTQGGFAKATVVHQKFVVKIPE      151
LADH_Ec         CKHPEGNFCLKNDLSMPRGTMQDGTSRFTCRGKPIHHFLGTSTFSQYTVVDEISVAKIDA      163
LArDH_Nc        CLTGRYNGCERVDFLSTPP----------------------VPGLLRRYVNHPAVWCHKI-G      152
SDH_Hs          CKMGRYNLSPSIFFCATPP----------------------DDGNLCRFYKHNAAFCYKLPD      145
SDH_Ba          CKEGKYNLCPDLTFCATPP----------------------DDGNLARYYVHAADFCHKLPD      141
GPDH_Eco        CLKGFYSQCAKYDFIGSR-----------------------RDGGFAEYIVVKRKNVFALPT      133
TDH_Ec          CRGGRTHLCRNTIGVGVN-----------------------RPGCFAEYLVIPAFNAFKIPD      137
TDH_Bs          CLTGKSHVCTNTAIIGVD-----------------------TAGCFAEYVKVPADNIWRNPA      142
TDH_Ph          CRRGQYHVCQNTKIFGVD-----------------------TDGVFAEYAVVPAQNIWKNPK      141
TDH_Tk          CKHNRYHVCQNTKIFGVD-----------------------MDGVFAHYAIVPAKNAWKNPK      141
                *       .                                . : .
```

Figure 30: Amino acid sequence alignment of zinc-containing MDRs. The following sequences were used: liver alcohol dehydrogenase *Equus caballus* (LADH_Ec), alcohol dehydrogenase 1 *S. cerevisiae* (ADH_Sc), L-threonine dehydrogenase *Pyrococcus horikoshii* (TDH_Ph), L-threonine dehydrogenase *Thermcoccus kodakaraensis* (TDH_Tk), sorbitol dehydrogenase *Homo sapiens* (SDH_Hs), sorbitol dehydrogenase *Bemisia argentifolii* (SDH_Ba), L-arabinitol 4-dehydrogenase *Neurospora crassa* (LArDH_Nc), galactitol-1-phosphat dehydrogenase *E. coli* (GPDH_Ec), cinnamyl alcohol dehydrogenase 5 *Arabidopsis thaliana* (CAD_At), L-threonine dehydrogenase *E. coli* (TDH_Ec), L-threonine dehydrogenase *Bacillus subtilis* (TDH_Bs). The conservation pattern of this alignment was implemented in Figure 25. The alignment was prepared with Clustal Omega (section 2.6.11). Asterisks (*) indicate fully conserved residues, colons (:) mark residues with strongly similar properties, residues with weakly similar properties are indicated by a period (.).

```
ADH_Sc      GTDLAQVAPILC-AGITVYKALKSANLMAGHWVAISGAAGGLGSLAVQYAKAMGYRVLGI      201
CAD_At      GMAVEQAAPLLC-AGVTVYSPLSHFGLKQPGLRGGILGLGGVGHMGVKIAKAMGHHVTVI      210
LADH_Ec     ASPLEKVCLIGCGFSTGYGSAVKVAKVTQGSTC-AVFGLGGVGLSVIMGCKAAGAARIIG      222
LArDH_Nc    NMSYENGAMLEP-LSVA-LAGLQRAGVRLGDPV-LICGAGPIGLITMLCAKAAGACPLVI      209
SDH_Hs      NVTFEEGALIEP-LSVG-IHACRRGGVTLGHKV-LVCGAGPIGMVTLLVAKAMGAAQVVV      202
SDH_Ba      NVSLEEGALLEP-LSVG-VHACRRAGVQLGTTV-LVIGAGPIGLVSVLAAKAYGAFVV-C      197
GPDH_Eco    DMPIEDGAFIEP-ITVG-LHAFHLAQGCENKNV-IIIGAGTIGLLAIQCAVALGAKSVTA      190
TDH_Ec      NISDDLAAIFDP-FGNA-VHTA-LSFDLVGEDV-LVSGAGPIGIMAAAVAKHVGARNVVI      193
TDH_Bs      DMDPSIASIQEP-LGNA-VHTV-LESQPAGGTT-AVIGCGPIGLMAVAVAKAAGASQVIA      198
TDH_Ph      SIPPEYATLQEP-LGNA-VDTV-LAGPISGKSV-LITGAGPLGLLGIAVAKASGAYPVIV      197
TDH_Tk      DMPPEYAALQEP-LGNA-VDTV-LAGPIAGRST-LITGAGPLGLLGIAVAKASGAYPVIV      197
                                              . * :*      .   *

ADH_Sc      DGGEG-KEELFRSIGGEVFIDFTKEKDIV----GAVLKATDGGAHGVINVSVSEAAIEAS      256
CAD_At      SSSNKKREEALQDLGADDYVIGSDQAKMS---------ELADSLDYVIDTVPVHHALEPY      261
LADH_Ec     VDINKDKFAKAKEVGATECVNPQDYKKPIQEV---LTEMSNGGVDFSFEVIGRLDTMVTA      279
LArDH_Nc    TDIDEGRLKFAKEICPEVVTHKVERLSAEESAKKIVESFGGIEPAVALECTGVESSIAAA      269
SDH_Hs      TDLSATRLSKAKEIGADLVLQ--ISKESPQEIARKVEGQLGCKPEVTIECTGAEASIQAG      260
SDH_Ba      TARSPRRLEVAKNCGADVTLVVDPAKEEESSIIERIRSAIGDLPNVTIDCSGNEKCITIG      257
GPDH_Eco    IDISSEKLALAKSFGAMQTFN--SSEMSAPQM--QSVLRELRFNQLILETAGVPQTVELA      246
TDH_Ec      TDVNEYRLELARKMGITRAVN--VAKENLNDV--MAELGMTEGFDVGLEMSGAPPAFRTM      249
TDH_Bs      IDKNEYRLRLAKQMGATCTVS--IEKEDPLKI--VSALTSGEGADLVCEMSGHPSAIAQG      254
TDH_Ph      SEPSDFRRELAKKVGADYVIN--PFEEDVVKE--VMDITDGNGVDVFLEFSGAPKALEQG      253
TDH_Tk      SEPSEFRRKLAKKVGADYVVN--PFEEDPVKF--VMDITDGAGVEVFLEFSGAPKALEQG      253
               .  :    :.                                  :       .

ADH_Sc      TRYV-RANGTTVLVGMPAGAKCCSDV--FNQVVKSISIVGSY--VGNRA--DT-REALDF      308
CAD_At      LSLL-KLDGKLILMGVINNPLQFLTP---LLMLGRKVITGSF--IGSMK--ET-EEMLEF      312
LADH_Ec     LSCCQEAYGVSVIVGVPPDSQNLSMN--PMLLLSGRTWKGAI--FGGFKSKDSVPKLVAD      335
LArDH_Nc    IWAV-KFGGKVFVIGVGKNEIQIPFM--R-ASVREVDLQFQY------RYCNTWPRAIRL      319
SDH_Hs      IYAT-RSGGNLVLVGLGSEMTTVPLL--H-AAIREVDIKGVF------RYCNTWPVAISM      310
SDH_Ba      INIT-RTGGTLMLVGMGSQMVTVPLV--N-ACAREIDIKSVF------RYCNDYPIALEM      307
GPDH_Eco    VEIA-GPHAQLALVGTLHQDLHLTSATFGKILRKELTVIGSWMNYSSPWPGQEWETASRL      305
TDH_Ec      LDTM-NHGGRIAMLGIPPSDMSIDWT--K-VIFKGLFIKGIY----GREMFETWYKMAAL      301
TDH_Bs      LAMA-ANGGRFHILSLPEHPVTIDLT--NKVVFKGLTIQGIT----GRKMFSTWRQVSQL      307
TDH_Ph      LQAV-TPAGRVSLLGLYPGKVTIDFN--NLIIFKALTIYGIT----GRHLWETWYTVSRL      306
TDH_Tk      LKAV-TPGGRVSLLGLFPREVTIDFN--NLIIFKALEVHGIT----GRHLWETWYTVSSL      306
                      .   ::.                                  .

ADH_Sc      FARGLV-KSPI--KVVG-LSTLPEIY-EKMEKGQIVGRYVVDTS--K-----      348
CAD_At      CKEKGL-SSII--EVVK-MDYVNTAF-ERLEKNDVRYRFVVDVE--GSNLDA      357
LADH_Ec     FMAKKFALDPLITHVLP-FEKINEGF-DLLRSGE-SIRTILTF----------      375
LArDH_Nc    VENGLVDLTRLVTHRFP-LEDALKAF-ETASDPK-TGAIKVQIQSLE-----      363
SDH_Hs      LASKSVNVKPLVTHRFP-LEKALEAF-ETFKKGL---GLKIMLKCDPSDQNP      357
SDH_Ba      VASGRCNVKQLVTHSFK-LEQTVDAF-EAARKKA-DNTIKVMISCRQG----      352
GPDH_Eco    LTERKLSLEPLIAHRGS-FESFAQAVRDIARNAM-PGKVLLIP----------      346
TDH_Ec      IQSG-LDLSPIITHRFS-IDDFQKGF-DAMRSGQ-SGKVILSWD---------      341
TDH_Bs      ISSNMIDLAPVITHQFP-LEEFEKGF-ELMRSGQ-CGKVILIP----------      347
TDH_Ph      LQSGKLNLDPIITHKYKGFDKYEEAF-ELMRAGK-TGKVVFMLK---------      348
TDH_Tk      IQSGKLNLDPIITHKYKGFDKFEEAF-ELMRAGK-TGKVVFFPH--KG----      350
                       :  .    :.       :            .
```

Figure 30, continued.

Danksagung

Viele Personen haben zum Gelingen dieser Arbeit beigetragen, indem sie mich während der Promotionszeit auf verschiedenste Weise unterstützt haben:

Zunächst gilt mein Dank meinem Doktorvater Professor Dr. Dieter Jahn - vielen Dank dafür, dass ich in Deinem Arbeitskreis auf dem Chlorophyll-Thema arbeiten, mich mit den schönen Tetrapyrrolen beschäftigen konnte und außerdem Konferenzen in Bremen, Berlin und Canterbury besuchen durfte.

Ich danke Herrn Professor Dr. Wulf Blankenfeldt für die Übernahme der Aufgaben des zweiten Referenten und Fachprüfers im Rahmen meiner Promotion.

Mein Dank gilt ebenso Herrn Professor Dr. Ralf-Rainer Mendel für die Übernahme des Prüfungsvorsitzes bei meiner Disputation.

Ein großer Dank gilt meinem Arbeitsgruppenleiter Dr. Jürgen Moser - vielen Dank, dass Du immer „erreichbar“ und zum Diskutieren oder zum Beantworten von Fragen bereit warst. Ebenso danke ich Dir für Deine unerschütterliche Zuversicht und dass ich von Dir viel über Tetrapyrrole, Proteinkristallisation und Röntgenstrukturanalyse lernen konnte.

Mein Dank gilt Herrn Professor Dr. Dirk Heinz sowie Dr. Jörn Krauße vom HZI für die sehr gute Kooperation im Rahmen der DPOR-Strukturaufklärung. Dr. Jörn Krauße sei insbesondere gedankt für die Aufnahme des Datensatzes und die Lösung der DPOR-Struktur sowie die gemeinsame Arbeit an der Struktur und dem Paper, für viele Erklärungen zum Thema Kristallisation und Strukturanalyse sowie zahlreiche Hilfestellungen bei der Arbeit mit PyMOL, Chimera und dem PISA-Server. Beate Jaschok-Kentner (HZI) danke ich für die Durchführung der N-terminalen Sequenzierungen.

Ich danke Herrn Professor Dr. Hugo Scheer für die Bereitstellung der artifiziellen Substrate.

Ein großer Dank gilt den aktuellen und ehemaligen Mitgliedern der AG Moser - Dr. Wiebke Arendt, Maike Groenewold, Dr. Stefanie Hebecker, Svenja Kiesel, Sabine Peters, Janis Rabe und Simone Virus, sowie zahlreichen Bachelor- und Materstudenten und Praktikanten - vielen Dank dafür, dass ihr in der Arbeitsgruppe so eine freundschaftliche Atmosphäre geschaffen habt, man euch alles Mögliche fragen konnte, ihr immer hilfsbereit wart, in zahlreichen Diskussionen viele Anregungen zum Thema gegeben habt und mich auch noch unterstützt habt, als ich schon nicht mehr im Labor war. Ich danke außerdem insbesondere Simone für die Anleitung der erfolgreichen DPOR-Kristallisationsexperimente, als ich selbst noch ganz am Anfang meiner Arbeit stand. Außerdem danke ich Dir für die Vorarbeiten zum BchF/BchC-Thema, die Durchführung der HPLC-Läufe, die Proteinreinigung für die ICP-MS-Analyse und die Chlide-Präparation, sowie für die Durchführung der zusätzlichen Experimente für das BchC-Paper (insbesondere der Bestimmung der spezifischen Aktivitäten von BchC mit verschiedenen Substraten). Auch Sabine danke ich für ihre Arbeiten zu BchC im Rahmen ihrer Diplomarbeit und Sabine und Simone für die Weiterleitung der BchF-Probe zur N-terminalen

Sequenzierung. Wiebke danke ich außerdem vielmals für das Korrekturlesen eines großen Teils dieser Arbeit! Ich bedanke mich auch ganz herzlich bei Johannes Rebelein und Marion Schwietering, die im Rahmen ihres Praktikums die erfolgreiche DPOR-Kristallisation bewirkt haben sowie bei Timm Reichelt und David Brötje für die Generierung der BchC-Mutanten im Rahmen ihres Praktikums.

Ein besonderer Dank gilt Constanze Finger - vielen Dank für Deine Hilfsbereitschaft und Unterstützung, sowohl bei arbeitsbezogenen als auch bei vielen anderen Angelegenheiten!

Der mittlerweile nach Leipzig umgezogenen Arbeitsgruppe von Professor Dr. Gunhild Layer und der Arbeitsgruppe von Dr. Martina Jahn danke ich ebenfalls für viele Hilfestellungen, Anregungen und Anteilnahme während der Freitagsseminare und auch sonst. Mela, Vera, Dagmar und Julia: danke für die schöne Reise nach Canterbury!

Rebekka, Tanja und Ida danke ich für die gemeinsame Bürozeit und dass ihr mich durch viel guten Zuspruch unterstützt und ermutigt habt.

Ein großes Dankeschön geht auch an alle anderen Mitglieder des Instituts für Mikrobiologie für die gute Zusammenarbeit, von der mir die allseits anzutreffende Hilfsbereitschaft und Freundlichkeit, die gute Atmosphäre innerhalb der Doktorandeninitiative und die Retreats in Erinnerung bleiben werden. Christina, Daniela, Bernd Hoppe, Barbara und Dagmar danke ich für viel Geduld und Unterstützung bei der Bearbeitung vieler nichtwissenschaftlicher Angelegenheiten und die andauernde Unterstützung des Laboralltags.

Ich danke auch meinen lieben Freunden aus der Hannover-Zeit - ich bin sehr froh, dass wir auch fünf Jahre nach Ende des Studiums noch so guten Kontakt haben. Danke für eure Freundschaft, Unterstützung und Anteilnahme! Außerdem: vielen Dank, liebe Anna, für das Korrekturlesen eines großen Teils dieser Arbeit!

Ohne die Unterstützung und Ermutigung seitens meiner Familie - meiner Eltern, meiner Geschwister und meiner Tante - wäre diese Arbeit wohl nicht zustande gekommen - vielen Dank hierfür!

Schließlich gilt ein besonderer Dank meinem Freund Alexander, der diese Arbeit vier Jahre lang begleitet und die Aufs und Abs dieser Zeit miterlebt und abgefangen hat. Ich danke Dir für Deine andauernde Unterstützung, Dein Verständnis und Deine Geduld!